Doctoral Dissertation

HIGH-VALENT METAL SPECIES PRODUCED BY THE FENTON-LIKE REACTIONS AT NEUTRAL PH FOR OXIDATIVE DEGRADATION OF ORGANIC CONTAMINANTS

Hak-Hyeon Kim

Department of Urban and Environmental Engineering
(Environmental Science and Engineering)

Graduate School of UNIST

2019

HIGH-VALENT METAL SPECIES PRODUCED BY THE FENTON-LIKE REACTIONS AT NEUTRAL PH FOR OXIDATIVE DEGRADATION OF ORGANIC CONTAMINANTS

Hak-Hyeon Kim

Department of Urban and Environmental Engineering
(Environmental Science and Engineering)

Graduate School of UNIST

High-valent metal species produced by Fenton-like reactions at neutral pH for oxidative degradation of organic contaminants

A dissertation
submitted to the Graduate School of UNIST
in partial fulfillment of the
requirements for the degree of
Doctor of Philosophy

Hak-Hyeon Kim

01/10/2019 of submission

Approved by

Advisor
Kyung Hwa Cho

High-valent metal species produced by Fenton-like reactions at neutral pH for oxidative degradation of organic contaminants

Hak-Hyeon Kim

This certifies that the dissertation of Hak-Hyeon Kim is approved.

01/10/2019 of submission

signature

Advisor: Kyung Hwa Cho

signature

Changha Lee

signature

Young-Nam Kwon

signature

Changsoo Lee

signature

Kangwoo Cho

ABSTRACT

For decades, advanced oxidation processes (AOPs) collectively utilizing hydroxyl radical ($^{\bullet}OH$) and sulfate radical ($SO_4^{\bullet-}$) have been extensively studied for oxidatively degrading a broad spectrum of recalcitrant organic contaminants due to their non-selective reactivities. However, those properties cause indiscriminate usage of reagents because most produced radical species were consumed by undesirable reactions with natural background materials (e.g. chloride, bicarbonate, and natural organic matters). For dealing with this dilemma on AOPs, in recent studies, high-valent metal species which exhibit target-specific reactivities produced in Fenton(-like) reactions have been developed for elevating system efficacies. In this dissertation, several approaches were further attempted to enhance the production of reactive oxidants likely high-valent metal species for oxidative degradation of organic contaminants at neutral pH.

Firstly, the production of reactive oxidants from nanoparticulate zero-valent iron (nZVI) and ferrous ion (Fe(II)) in the presence of oxygen was greatly enhanced by the addition of tetrapolyphosphate (TPP) as an iron-chelating agent. Compared to other ligands, TPP exhibited superior activity in improving the oxidant yields. The nZVI/TPP/O_2 and the Fe(II)/TPP/O_2 systems showed similar oxidant yields with respect to the iron consumed, indicating that nZVI only serves as a source of Fe(II). The degradation efficacies of selected organic compounds were also similar in the two systems. It appeared that both hydroxyl radical ($^{\bullet}OH$) and ferryl ion (Fe(IV)) are produced, and $^{\bullet}OH$ dominates at acidic pH. However, at pH > 6, little occurrence of hydroxylated oxidation products suggests that Fe(IV) is a dominant oxidant. The degradation rates of selected organic compounds by the Fe(II)/TPP/O_2 system had two optimum points at pH 6 and 9, and these pH-dependent trends are likely attributed to the speciation of Fe(IV) with different reactivities.

Secondly, the copper-catalyzed Fenton-like reaction in the presence of bicarbonate (i.e., the Cu(II)/HCO_3^-/H_2O_2 system) was examined for the phenol degradation. The rate of phenol degradation by the copper-catalyzed Fenton-like reaction ($[Cu(II)]_0$ = 0.1 mM, $[H_2O_2]_0$ = 10 mM, pH = 10) was accelerated by 17-fold in the presence of 50 mM HCO_3^-. The rate of phenol degradation by the Cu(II)/HCO_3^-/H_2O_2 system increased with increasing doses of Cu(II) and HCO_3^-, but showed an optimal value for the H_2O_2 dose and pH at 5 mM and 10, respectively. The Cu(II)/HCO_3^-/H_2O_2 system was selective in degrading phenolic compounds; benzoic acid was resistant to degradation. Cu(III) species (likely complexed forms with carbonate) are believed to be the reactive oxidants responsible for the phenol degradation by the Cu(II)/HCO_3^-/H_2O_2 system. Meanwhile, aerating CO_2 gas successfully accelerated the phenol degradation by the copper-catalyzed Fenton-like reaction,

implying that CO_2 aeration can be a practical option to supply bicarbonate when implementing the Cu(II)/HCO_3^-/H_2O_2 system.

Lastly, nickel oxide-nickel carbide (NiO-NiC) nanocomposite (denoted as NiOC) have been found to activate peroxydisulfate (PDS), accelerating the oxidation of aqueous organic compounds. The NiOC-activated PDS effectively degraded select phenolic compounds and pharmaceuticals. The degradation rate of 4-chlorophenol by the NiOC coupled with PDS was more than 100-folds higher than that by the combination of commercial microparticulate nickel oxide and PDS. Notably, the PDS utilization efficiency, expressed by the ratio of degraded organic compound to decomposed PDS, was close to 90% at certain experimental conditions. The NiOCs were also found to exhibit magnetic properties that can facilitate the separation of those materials after water treatment. Further, the size and crystallinity of the NiOC significantly affect to degradation capability of the NiOC/PDS system. A nonradical mechanism is believed to act on the PDS activation by the NiOC, and it appears that generated high-valent nickel species (likely Ni(IV)) on the NiOC surface is responsible for dominant reactive species. Different approaches including electrochemical analysis, electron paramagnetic resonance (EPR) spectroscopy, and X-ray absorption near edge structure (XANES) analysis were used to elucidate the mechanisms through which organic compounds are oxidized on the NiOC in the presence of PDS.

CONTENTS

List of Figures

List of Tables

List of Schemes

Chapter 1. Introduction

1.1. Research background

1.1.1. Emerging organic contaminants as potential hazardous substances

For decades, industrial growth and human activity have been lead to be needed the production of new artificial materials and inevitably cause discharge of refractory organic compounds as byproducts to the aquatic system [1]. Those organic compounds are considered as potential pollutants to the ecosystem known as emerging contaminants and also commonly appeared non-biodegradable and persistent properties in water [2]. Among them, the use of pharmaceuticals and personal care products (PPCPs) has increased tremendously with increasing concerns about hygiene and health care with population growth [1]. Phenol and its derivatives have been widely used as essential precursors in the manufacturing of PPCPs [2]. PPCPs and phenolic compounds are known to be not effectively degraded by conventional water treatment (e.g. biodegradation). Trace amounts (a few ng/L) of these compounds are frequently detected in even surface water [3, 4], causing concerns about potential contamination of drinking water. And also, in Korea, specific organic contaminants which exhibited potentially harmful (in)directly affected the ecosystems have been regulated strictly in industrial drainages and effluents (Table 1.1) [5, 6]. For these reasons, novel water treatment technologies are necessary for the efficient control of those organic contaminants and also several processes have been developed successfully for operating practically in water and wastewater treatment plants [7].

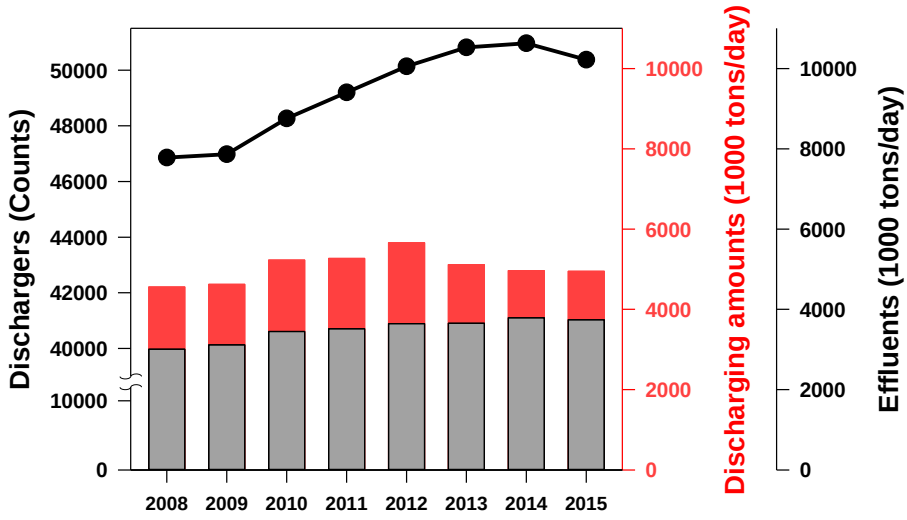

Figure 1.1. Statistics of annual industrial wastewater discharge in Korea.

Table 1.1. Regulation of specific water-quality hazardous substances including emerging organic contaminants in Korea.

Specific water-quality hazardous substances (Criteria on 01. 01. 2019)		
Contaminants	Criteria (mg/L)	Enacted year
Polychlorinated biphenyls (PCBs)	-	1978
Phenolic compounds	1	1991
Perchloroethylene (PCE)	0.02	
Trichloroethylene (TCE)	0.06	
Benzene	0.01	1999
Carbon tetrachloride	0.004	
1,1-Dichloroethylene	0.03	
Dichloromethane	0.02	
Chloroform	0.08	2006
1,2-Dichloroethane	0.03	
Acrylonitrile	0.01	2009
Bromoform	0.03	
Diethylhexyl phthalate	0.02	
1,4-Dioxane	0.05	
Vinyl chloride	0.01	
Acrylamide	0.015	2016
Bis(2-ethylhexyl) adipate	0.2	
Epichlorohydrin	0.03	
Formaldehyde	0.5	
Naphthalene	0.05	
Pentachlorophenol	0.001	
Phenol	0.1	
Styrene	0.02	

1.1.2. Fenton(-like) process as a conventional AOP

For decades, advanced oxidation processes (AOPs) which utilizing hydroxyl radical (•OH ($E°$[•OH/H_2O]] = 2.81 V_{NHE} [8]) were successfully developed for oxidatively degrading non-biodegradable organic contaminants. In order to generate •OH, various precursors (e.g., hydrogen peroxide (H_2O_2), ozone (O_3), oxygen (O_2), and directly produced from water) have been used for dissociation by supply of external energy sources (e.g. UV irradiation, γ-radiolysis, ultrasound, electron beam, high-voltage discharge, etc.) or additional injection of transition metals as catalysts [9].

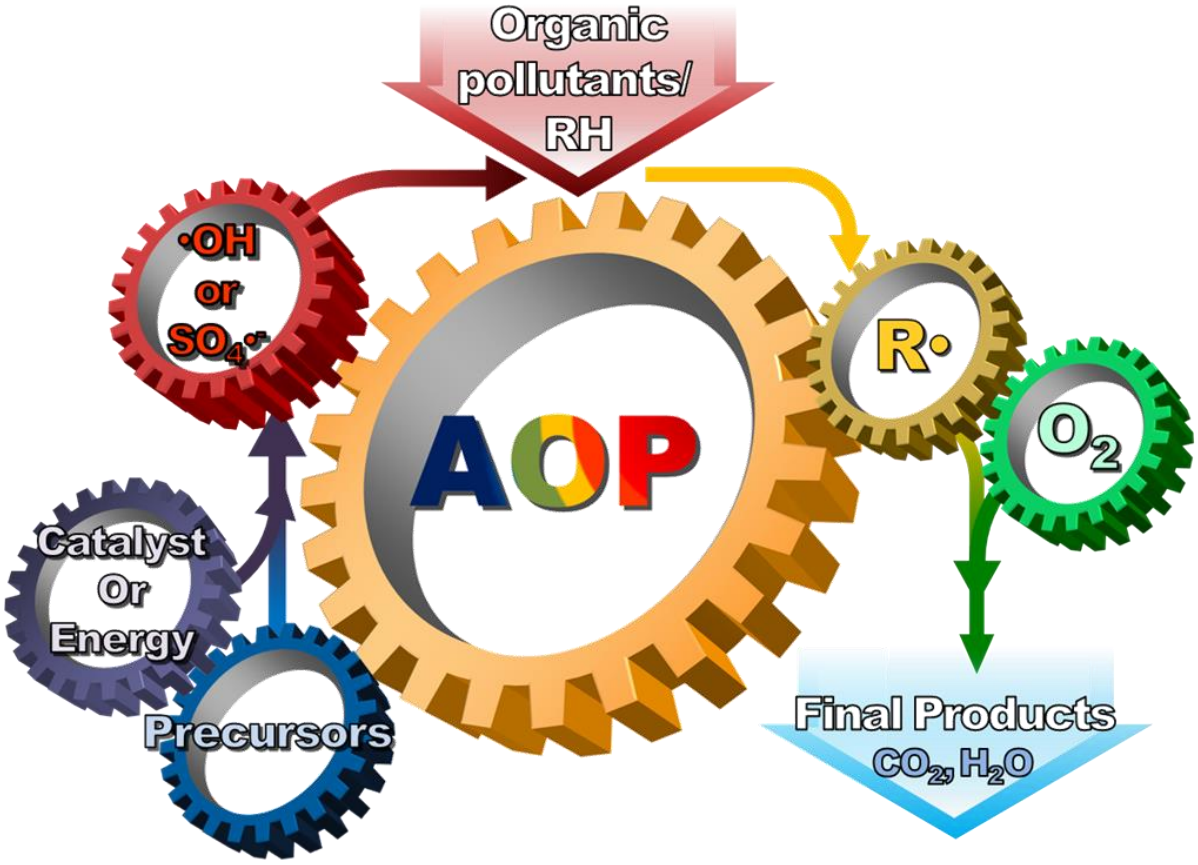

Scheme 1.1. Depicted diagram of AOPs for oxidatively degradation of organic contaminants.

Among them, the aforementioned processes utilizing transition metals are known as Fenton and Fenton-like reactions which have been extensively studied as effective tools to degrade recalcitrant organic compounds in wastewater [7]. Specifically, conventional Fenton system generates •OH via the 1-electron transfer reaction of ferrous ion (Fe(II)) and H_2O_2 at acidic pH, and subsequently ferric ion (Fe(III)) is reduced by H_2O_2. The iron species are act like catalyst in Fenton(-like) reactions (reaction 1.1 & 1.2). However, the reaction 2 is believed to the rate-determining step which leads to the

accumulation of Fe(III) [10].

$$Fe(II) + H_2O_2 \rightarrow Fe(III) + {}^{\bullet}OH + OH^- \text{ (fast) } (k_1 = 63\ M^{-1}s^{-1}) \quad (1.1)$$

$$Fe(III) + H_2O_2 \rightarrow Fe(II) + O_2^{\bullet-} + 2H^+ \text{ (slow) } (k_2 = 0.01\ M^{-1}s^{-1}) \quad (1.2)$$

On the other hands, in neutral pH region, the efficacy of Fenton system is drastically decreased by precipitation of ferric species (low solubility) and relatively weak oxidant (likely Fe(IV)) produced [11].

$$Fe(II) + H_2O_2 \rightarrow Fe(IV) + H_2O \quad (1.3)$$

Further, zero-valent iron (ZVI) which is known as in situ Fenton's reagent generator has been believed to produce reactive oxidants such as hydroxyl radical ($^{\bullet}OH$) and ferryl ion (Fe(IV)) when corroded by oxygen (detailed mechanism on ZVI corrosion is described in chapter 2). The oxidative degradation of herbicides, aromatic compounds, alcohols, and arsenic has been demonstrated in aqueous solution containing nanoparticulate ZVI (nZVI) (or granular ZVI) in the presence of oxygen [12-16]. The reaction of ferrous ion (Fe(II)) with oxygen also produces reactive oxidants under neutral pH conditions, leading to the oxidation of organic compounds [11]. nZVI and Fe(II) with a supply of oxygen (i.e., the nZVI/O_2 and the Fe(II)/O_2 systems) have been proposed as potential agents for in situ chemical oxidation (ISCO) to rapidly oxidize refractory organic compounds in groundwater.

However, a major limitation of the nZVI/O_2 and the Fe(II)/O_2 systems was the low yield of reactive oxidants. The oxidant yields were only less than 10% with respect to nZVI and Fe(II) added [11]. The yields from nZVI were no greater than those from Fe(II), indicating that the oxidant production from nZVI is mainly due to the oxidation of Fe(II) released from nZVI. The four-electron transfer from nZVI to oxygen (involving the direct conversion of oxygen to water) and the iron precipitation at neutral pH were responsible for the low oxidant yields.

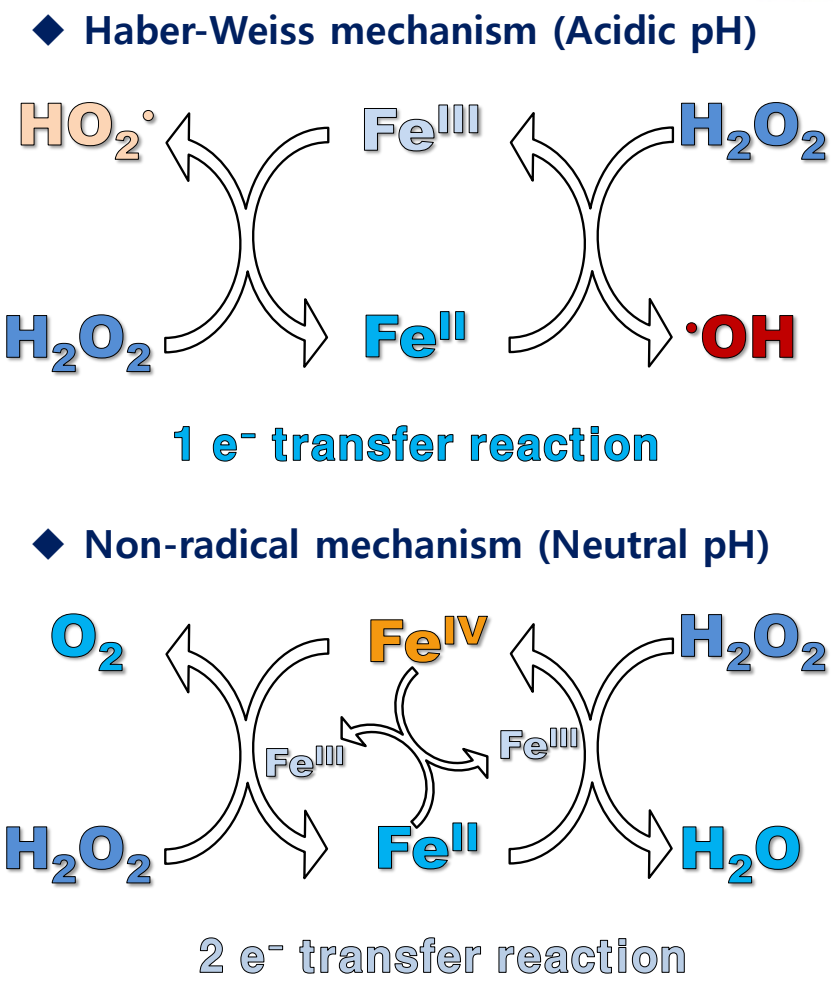

Scheme 1.2. Oxidants production by iron-based Fenton(-like) systems

On the other hands, persulfates comprehensively indicating peroxydisulfate (PDS) and peroxymonosulfate (PMS) have been extensively studied for oxidatively degrading aqueous organic contaminants [17-21]. Persulfates themselves have been known as strong oxidizing capability via two-electron transfer reaction ($E°[S_2O_8^{2-}/SO_4^{2-}]$ = 1.96 V_{NHE} for PDS [8] and $E°[HSO_5^{-}/SO_4^{2-}]$ = 1.75 V_{NHE} for PMS [22]). However, in past studies, it has been found that persulfates could be activated with external energy source or catalyst, generate more reactive radical species (i.e., sulfate radical anion, $SO_4^{\bullet-}$ ($E°[SO_4^{\bullet-}/SO_4^{2-}]$ = 2.5-3.1 V_{NHE} [23]) and hydroxyl radical) by homolytic or heterolytic cleavage of peroxide bond in persulfates. Due to the powerful oxidizing capability of $SO_4^{\bullet-}$ which could be applicable to oxidatively degrading a board spectrum of organic contaminants [18, 24-26], research focus on persulfate activation and sulfate radical-based advanced oxidation processes (SR-AOPs) has been tremendously increased as an alternative oxidation system to H_2O_2-based advanced oxidation processes (AOPs).

Several approaches have been developed for persulfate activation which is more readily than H_2O_2 activation by O-O bond dissociation (92 kJ mol^{-1} for PDS; 213 kJ mol^{-1} for H_2O_2 [5]) to produce radical species supplying external energy (e.g., heating [27] and UV irradiation [27, 28]). Further, electron accepting capability of persulfates which means more vulnerable to reductive cleavage of peroxide bond is superior to that of H_2O_2, which enables applying diverse activators (e.g., adding bases [29], organic compounds [30, 31], and transition metals [18, 19]). Among them, transition metals have been considered to the most sustainable and simple to activate persulfates due to their catalytic properties without additional energy or continuous chemical consumption. More specifically, the catalytic activation of persulfate by transition metals is believed to proceed analogously via the mechanism of Fenton-like reaction, where persulfates are reductively/oxidatively decomposed into radical species through redox cycle of the metal ion (reaction 1.4 and 1.5). It has been found that persulfates are decomposed by catalytic reaction with several metal ions (e.g. cobalt, vanadium, iron, manganese, silver , titanium [18, 19], and copper [32]).

$$M^{n+} + S_2O_8^{2-} \text{ (or } HSO_5^-) \rightarrow M^{(n+1)+} + SO_4^{\bullet-} + SO_4^{2-} \text{ (or } SO_4^{\bullet-} + OH^-) \quad (1.4)$$

$$M^{(n+1)+} + S_2O_8^{2-} \text{ (or } HSO_5^-) \rightarrow M^{n+} + S_2O_8^{\bullet-} \text{ (or } SO_5^{\bullet-} + H^+) \quad (1.5)$$

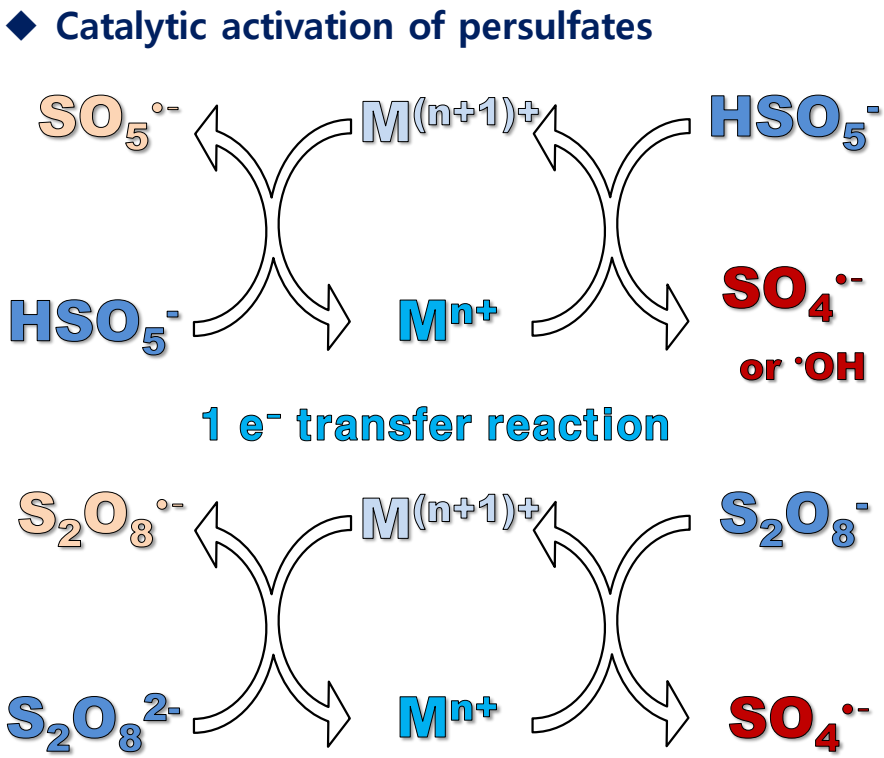

Scheme 1.3. Oxidants production by metal-catalyzed activation of persulfate systems.

1.1.3. Dilemma of conventional AOPs

However, aforementioned non-selective reactivities of hydroxyl radical or sulfate radical cause indiscriminate usage of reagents because most produced radical species were consumed by undesirable reactions with natural background materials (e.g. chloride (Cl^-), bicarbonate (HCO_3^-), and natural organic matters (NOMs)). For example, carbonate radical ($CO_3^{\bullet-}$, $E°[CO_3^{\bullet-}/CO_3^{2-}]$ = 1.6 V_{NHE} [8]) which is a produced intermediate from the reaction between $^{\bullet}OH$ and HCO_3^- narrows spectrum of oxidizing capacity (increasing selectivity) due to relatively low reactivity compared with that of $^{\bullet}OH$. In other words, both reactivity and selectivity on the degradation of organic contaminants are incompatible in the conventional AOPs (depicted in Figure 1.2) [8, 22, 33-39].

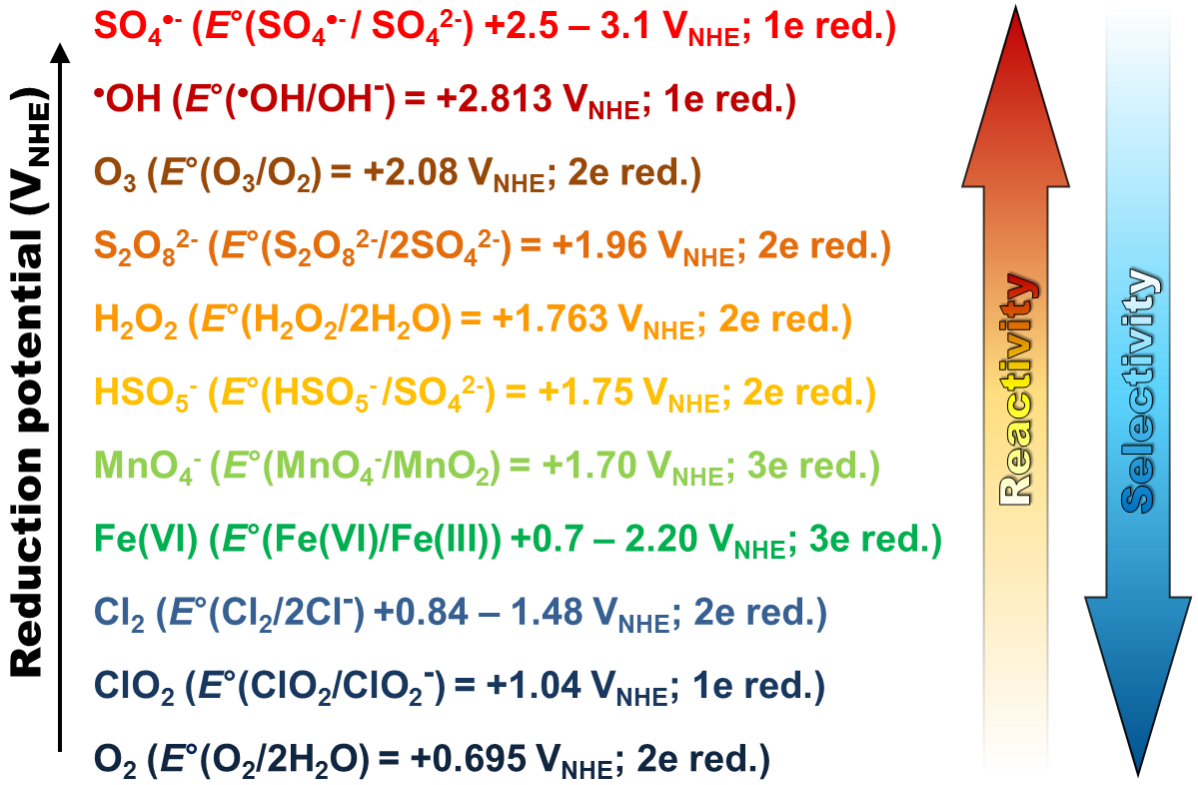

Figure 1.2. Standard reduction potentials of various oxidants and related radical species.

For dealing with this dilemma of AOPs, in recent studies, high-valent metal species which exhibit target-specific reactivities produced in Fenton(-like) reactions have been developed for elevating system efficacies [11, 40]. With those research interests, several approaching ways are considered as key parameters to be potential solutions to overcome the dilemma of AOPs, which are (i) to explore metal-chelating agents to enhance the production of reactive oxidant and also to minimize the effects of natural background materials, (ii) complexation with those materials initially, and (iii) to develop

the limitation way of reaction sites without the adsorption of those materials on the catalyst surface.

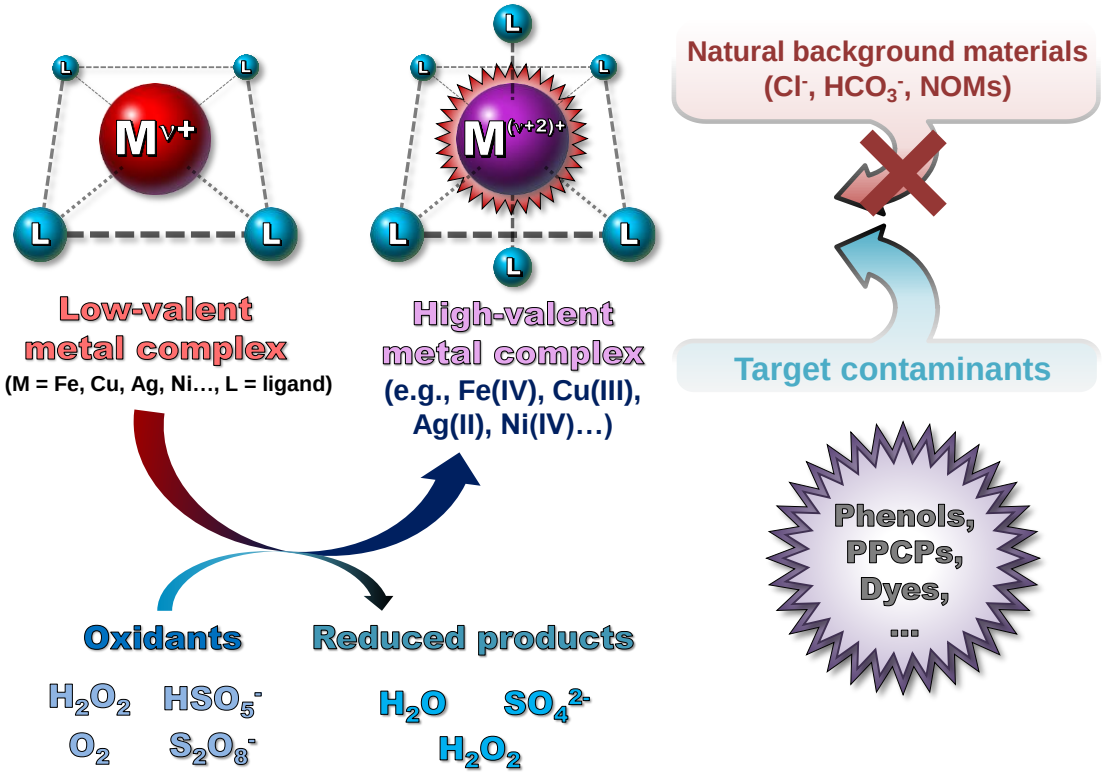

Figure 1.3. Potential approaches for dealing with dilemma of conventional AOPs.

1.1.4. Alternative oxidation systems

In the past studies, it has been reported that the addition of iron-chelating agents such as oxalate, ethylenediaminetetraacetic acid (EDTA), and nitrilotriacetic acid (NTA) enhanced the oxidant production from nZVI and Fe(II) by increasing the iron solubility [41-43]. In addition, the coordination of Fe(II) with these ligands appeared to alter the mechanism of the Fenton reaction to favor the production of •OH relative to Fe(IV). Polyoxometalate (POM) such as polyoxotungstate, polyoxosilicate, and polyoxomolybdate also increased the oxidant yields in the nZVI/O_2 and the Fe(II)/O_2 systems by mediating the electron transfer from nZVI to oxygen (i.e., changing the four-electron transfer to a two-electron transfer) as well as by forming soluble complexes with iron at neutral pH [44]. However, the use of organic ligands is problematic with chemical oxidation applications due to issues such as the scavenging of oxidants and the subsequent self-destruction by oxidation. POM, as an inorganic compound, is resistant to oxidation, but is known to undergo hydrolysis at neutral pH. The stability issue remains unresolved [44-46].

It was recently reported that tetrapolyphosphate (TPP) is a stable inorganic ligand that improves oxidant production from Fe(II) and nZVI [47, 48]. Effective degradation of atrazine and

pentachlorophenol was demonstrated in nZVI/O_2 and Fe(II)/O_2 systems with TPP. In particular, atrazine degradation by the nZVI/O_2 system was dramatically enhanced in the presence of TPP, which could not be explained by the role of the released Fe(II)-TPP complexes. Therefore, it was suggested that TPP promotes electron transfer from the nZVI core to the surface-bound Fe(II), increasing the electron density available for oxygen activation [48]. In spite of these studies, the oxidant yields have not been quantified in TPP-enhanced nZVI/O_2 and Fe(II)/O_2 systems. The quantitative measurement of oxidant yields can provide new insight into the mechanism of oxidant production. In addition, there has been little discussion on the nature of oxidants produced by those systems (especially, the possible generation of Fe(IV) species).

On the other hands, copper-catalyzed Fenton-like reactions (i.e., the Cu(II)/H_2O_2 system and its modifications) have been shown to degrade organic compounds under neutral and basic pH conditions [40, 49, 50]. These systems also have been suggested as effective methods to inactivate microorganisms [51, 52] and control membrane biofouling [53]. The cupryl (Cu(III)) species were proposed as the reactive oxidants dominantly produced by the copper-catalyzed Fenton-like reactions [50].

Meanwhile, several recent studies have reported that copper-catalyzed Fenton-like reactions can be enhanced in by the presence of bicarbonate (HCO_3^-), demonstrating successful degradation of organic compounds, such as dyes [54] and an antimicrobial agent [55]. The enhanced reactions in the presence of HCO_3^- are believed to result because Cu(II)-carbonate complexes are more reactive in the catalytic decomposition of H_2O_2 into reactive oxidants than the Cu(II) species without H_2O_2 (e.g., Cu(II)-hydroxo complexes or Cu(II) oxide). Cu(III) species [54] and hydroxyl radical ($^{\bullet}OH$) [55] were suggested as major oxidants responsible for the degradation of organic compounds. However, despite these references [54, 55], little information is available for the Cu(II)/HCO_3^-/H_2O_2 system. Phenolic compounds have not been examined as target contaminants in the Cu(II)/HCO_3^-/H_2O_2 system. In addition, information about factors such as pH and doses of reagents (Cu(II), HCO_3^-, and H_2O_2), as well as the efficiency of H_2O_2 use, have not been clearly reported. Moreover, further discussion is needed on the major oxidant produced by the Cu(II)/HCO_3^-/H_2O_2 system; the reactive oxidants suggested by the two previous studies contradict each other [54, 55].

Lastly, in a recent study, PDS coupling with copper oxide (CuO) was proposed as an alternative activating way through nonradical mechanism, where electron rearrangement in PDS molecule occurs at the CuO surface and increases the oxidizing capacity of PDS subsequently [56]. Carbonaceous materials (e.g., carbon nanotubes (CNTs) [57, 58], reduced graphene oxide (rGO) [59], mesoporous carbon (CMK-8) [60], biochar [61], and graphitized nanodiamonds (G-NDs) [62, 63]) have been proposed as a new class of non-metallic persulfate activator. In general, it is believe that the combination of persulfates and carbon-based materials produces reactive species which shows

efficient degrading capability of organic compounds. Despite of those prevailing evidences, there are contradictory interpretations including the nature of produced reactive species and the mechanism of persulfate activation (i.e., radical versus nonradical mechanisms).

1.2. Objectives of the study

In this dissertation, several approaches were attempted to enhance the production of reactive oxidants likely high-valent metal species for oxidative degradation of organic contaminants at neutral pH. Specific objectives in respective chapters were described as follows.

Firstly, the primary objectives of chapter 2 were to quantify the oxidant yields from nZVI/O_2 and Fe(II)/O_2 systems with TPP and to explore the nature of oxidants produced by the systems. For these purposes, excess probe compounds were employed, and the formation of their oxidation products was quantified. In addition, the oxidative degradation of selected organic compounds at low concentrations was examined under different conditions. To test the practical applicability, some of the experiments were conducted in natural water and the possible effects of water constituents on the efficiency of the system are discussed.

Secondly, the objectives of chapter 3 are (i) to assess the potential of the Cu(II)/HCO_3^-/H_2O_2 system for degrading phenol by investigating factors that affect the phenol degradation rate, and (ii) to discuss the reactive oxidants mainly responsible for the phenol degradation by the Cu(II)/HCO_3^-/H_2O_2 system. For these purposes, various levels of pH and doses of reagents were examined for effects on the phenol degradation in the Cu(II)/HCO_3^-/H_2O_2 system. The Cu(II)/H_2O_2/HCO_3^- system was compared to the Co(II)/HCO_3^-/H_2O_2 system, a similar Fenton-like system enhanced by HCO_3^- [14–16]. The degradation of several other organic compounds, such as benzoic acid, bisphenol A, and 4-chlorophenol, was also examined. To gain insight into the reactive oxidants produced by the system, experiments using scavengers and a probe compound of reactive oxidants were performed. In addition, aerating CO_2 gas was tested as a means of supplying HCO_3^- to the Cu(II)/H_2O_2 system.

Lastly, in chapter 4, nickel oxide-nickel carbide (NiO-NiC) nanocomposite (denoted as NiOC) as a magnetically recoverable activator of persulfates is newly reported, which can efficiently degrade and mineralize the selected organic compounds at neutral pH. The NiOC was synthesized by a simple ligand-assisted method only using Ni(II) precursor and citrate as a chelating agent, and sintering temperature on the NiOC synthesis was also optimized. In order to benchmark catalytic performance of NiOC, degradation kinetics of organic compound and PDS utilization efficiency were compared with commercialized micro and nanoparticulate nickel oxides (denoted as micro NiO and nano NiO,

respectively). We further discuss a unique mechanism involved with nonradical activation of persulfate. High-valent nickel species (likely Ni(IV) species) is elucidated to the dominant oxidant species during persulfate activation combined with NiOC based on the evidences from experiments using radical scavenger, linear sweep voltammetry (LSV), electron paramagnetic resonance (EPR), and X-ray absorption near edge structure (XANES).

Chapter 2. Polyphosphate-enhanced production of reactive oxidants by nanoparticulate zero-valent iron and ferrous ion in the presence of oxygen: Yield and nature of oxidants

2.1. Materials and Methods

2.1.1. Materials

All chemicals were of reagent grade and were used as received without further purification except for 2,4-dinitrophenyl hydrazine (DNPH). DNPH was purified three times by recrystallization in acetonitrile. Chemicals used in this study include methanol, formaldehyde (HCHO), DNPH, benzoic acid, *para*-hydroxybenzoic acid (*p*-HBA), coumarin, 7-hydroxycoumarin (7-HC), cimetidine (CMT), acetaminophen (AAP), carbamazepine (CBZ), Reactive Black 5 (RB5), oxalic acid, EDTA, NTA, sodium polyoxotungstate (used as POM), sodium hexametaphosphate (HMP), ferric perchlorate, ferrous sulfate, hydrogen peroxide, sodium chloride, sodium bicarbonate, sodium hydroxide, perchloric acid, hydrochloric acid (all from Sigma-Aldrich Co.), acetonitrile (J.T. Baker Co.), Suwannee river humic acid (International Humic Substances Society), and sodium tetrapolyphosphate (International Laboratory Co.). All stock solutions were prepared in deionized water (18 MΩ·cm Milli-Q water from a Millipore system). nZVI was synthesized by the aqueous-phase reduction of ferrous sulfate solution using sodium borohydride as a reducing agent; nZVI so produced forms aggregates of spherical single nanoparticles (10–80 nm). The detailed synthetic procedure is described elsewhere [64]. Stock solutions of nZVI and Fe(II) were freshly prepared prior to the experiments.

2.1.2. Experimental setup and procedure

All experiments were performed with 100 mL solutions (in 125 mL of Erlenmeyer flasks) open to the atmosphere at room temperature (22 ± 2°C). The solution pH was initially adjusted using 1 N $HClO_4$ and 1 N NaOH solutions, and the pH variations were less than 0.1 units during the reaction for all experiments (polyphosphates partially serve as pH buffers). The reaction was initiated by adding an aliquot of nZVI or Fe(II) stock solution to a pH-adjusted reaction solution containing all other compounds (probe compounds, target organic compounds, iron-chelating agents including TPP, etc. depending on the experiment). The amount of nZVI and Fe(II) used was typically 0.168 mM as Fe (10 mg/L for nZVI). Samples were withdrawn using a 1 mL plastic syringe or a 10 mL glass syringe at predetermined timed intervals, and were immediately filtered with a 0.2-μm hydrophilic polytetrafluoroethylene syringe filter. For experiments needing deaeration, ultrapure nitrogen gas was bubbled through the reaction solution with a needle-type diffuser for 30 min prior to initiation and throughout the entire reaction.

In experiments to quantify oxidant yields, methanol was introduced as a probe compound to capture reactive oxidants (both •OH and Fe(IV)), and its oxidized product (HCHO) was analyzed [11]. Typically, an excess amount of methanol (200 mM) was used to ensure that all oxidants were scavenged. Benzoic acid (10 mM) and coumarin (1 mM) were used as probe compounds for •OH, and their hydroxylated products (*p*-HBA and 7-HC, respectively) were analyzed [14, 65].

For experiments using natural water, raw water was obtained from the Nak-Dong river (ND river water) and from an aquifer in the Jeon-Buk province (JB groundwater). The quality parameters of the natural water samples are summarized in the supplementary data, Table 2.1. The natural water samples were filtered with a 0.45-μm filter within 24 h after sampling and stored at 4°C until use.

Table 2.1. Quality parameters of natural water samples

ND river water		JB groundwater	
pH	7.73	pH	7.48
Alkalinity (mg/L as $CaCO_3$)	38	Alkalinity (mg/L as $CaCO_3$)	40
DOC (mg/L)	4.055	DOC (mg/L)	0.3096
DTN (mg/L)	2.89	DTN (mg/L)	1.36
Na^+ (mg/L)	7.53	Na^+ (mg/L)	10.71
K^+ (mg/L)	2.85	K^+ (mg/L)	0.52
Mg^{2+} (mg/L)	2.22	Mg^{2+} (mg/L)	15.80
Ca^{2+} (mg/L)	11.97	Ca^{2+} (mg/L)	3.17
Cl^- (mg/L)	9.08	Cl^- (mg/L)	7.67
NO_3^- (mg/L)	6.69	NO_3^- (mg/L)	3.90
SO_4^{2-} (mg/L)	14.39	SO_4^{2-} (mg/L)	18.74
PO_4^{3-} (mg/L)	0.12	PO_4^{3-} (mg/L)	0.03

2.1.3. Analytical methods

The concentration of HCHO was measured by DNPH derivatization and subsequent HPLC analysis (UV absorbance detection at 350 nm) [66]. *p*-HBA, 7-HC, CMT, AAP, and CBZ were also analyzed by HPLC with UV detection at 270, 320, 230, 241, and 285 nm, respectively. Separation was performed on an Agilent - Eclipse XDB C18 column (150 mm × 4.6 mm, 3.5 μm) using a binary mixture of 0.1% (w/w) aqueous phosphoric acid and neat acetonitrile as the eluent at a flow rate of 1.5 mL/min. RB5 was spectrophotometrically analyzed by measuring visible light absorbance at 597 nm. Total dissolved iron was analyzed by atomic absorption spectroscopy at 248.3 nm (AAnalyst 700, Perkin-Elmer Co.). The concentration of dissolved Fe(II) was quantified by the 1,10-phenanthroline method [67].

2.2. Results

2.2.1. Oxidative transformation of methanol and benzoic acid

Methanol and BA were used as probe compounds for detecting reactive oxidants. To ensure that all of the oxidants were scavenged by the probe compound, an excess of probe compound was employed, and the major oxidized product was quantified. The production of HCHO and *p*-HBA (by the oxidation of methanol and BA, respectively) was monitored in the nZVI/O_2 and Fe(II)/O_2 systems with and without TPP at neutral pH (Figure 2.1a and 2.1b). The concentrations of HCHO and *p*-HBA increased instantaneously in the initial stage of the reaction, and the increase gradually slowed over time. The nZVI/O_2 and the Fe(II)/O_2 systems without TPP produced 18–23 μM HCHO in 4 h (Figure 2.1a). In the presence of TPP, the HCHO production was significantly enhanced; the concentrations of HCHO after 4 h of reaction time were 87 and 127 μM for the nZVI/O_2 and Fe(II)/O_2 systems, respectively. In the nZVI/O_2 system with TPP, the concentration of dissolved iron released from nZVI was 114 μM in 4 h, which accounts for 68% of the nZVI added (Figure 2.2).

The production of *p*-HBA by the BA oxidation was negligible in the nZVI/O_2 and Fe(II)/O_2 systems without TPP (Figure 2.1b), which was consistent with previous observations [11]. In the presence of TPP, a small amount of *p*-HBA was detected (i.e., 3.6 and 4.9 μM for the nZVI/O_2 and Fe(II)/O_2 systems, respectively). Coumarin also marginally yielded its hydroxylated product (7-HC) by the oxidation in the systems with TPP (Figure 2.3).

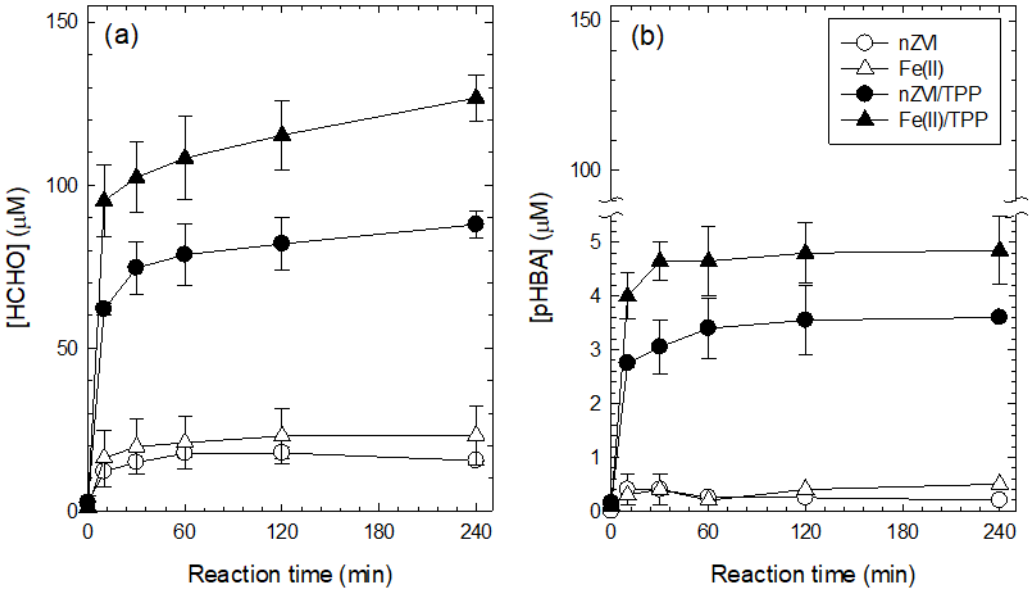

Figure 2.1. Effect of TPP on the production of HCHO (a) and *p*-HBA (b) by the nZVI/O_2 and the Fe(II)/O_2 systems ([Methanol]$_0$ = 200 mM; [Benzoic acid]$_0$ = 10 mM; [nZVI]$_0$ = 10 mg/L (0.168 mM as Fe); [Fe(II)]$_0$ = 0.168 mM; [TPP]$_0$ = 1 mM; pH = 7.0).

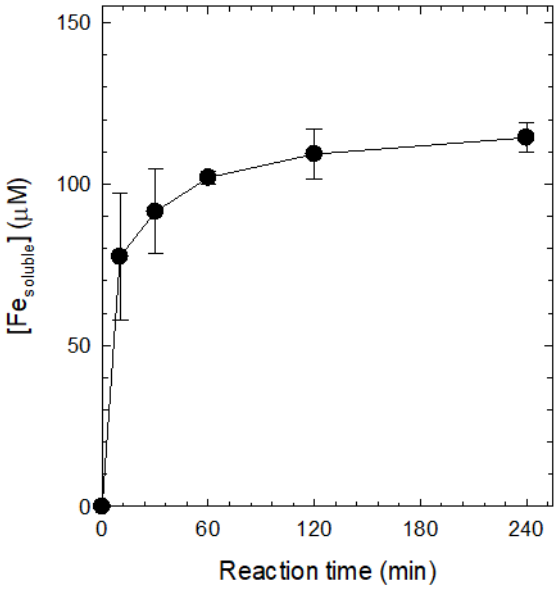

Figure 2.2. Dissolved iron concentration in the nZVI/TPP/O_2 system ([Methanol]$_0$ = 200 mM; [nZVI]$_0$ = 10 mg/L (0.168 mM as Fe); [TPP]$_0$ = 1 mM; pH = 7.0).

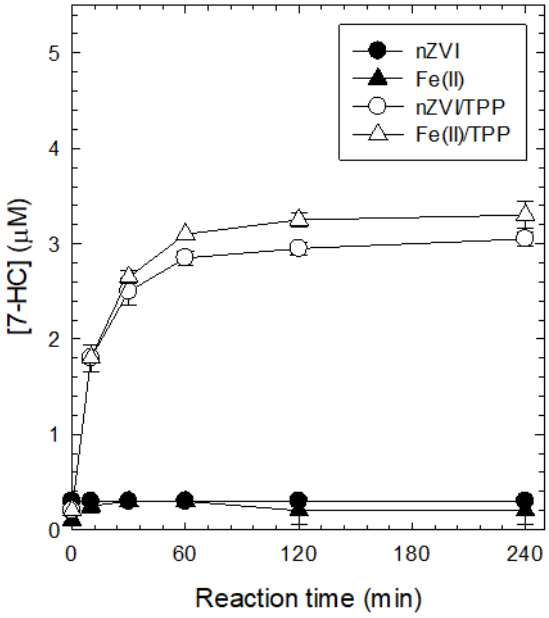

Figure 2.3. Effect of TPP on the production of 7-HC by the nZVI/O_2 and Fe(II)/O_2 systems ($[Coumarin]_0$ = 1 mM; $[nZVI]_0$ = 10 mg/L (0.168 mM as Fe); $[Fe(II)]_0$ = 0.168 mM; $[TPP]_0$ = 1 mM; pH = 7.0).

2.2.2. Effects of different ligands

The production of HCHO was monitored in the nZVI/O_2 and Fe(II)/O_2 systems with different iron-chelating agents such as oxalate, EDTA, POM, HMP, and TPP (Figure 2.4a and 2.4b). For both systems, the oxidant yield was significantly enhanced by the addition of iron-chelating agents. The results with EDTA and oxalate were consistent with those in a previous study [42]. TPP exhibited the highest activity to enhance the oxidant yield. In particular, the HCHO concentration produced by the Fe(II)/TPP/O_2 system was higher than that by the nZVI/TPP/O_2 system.

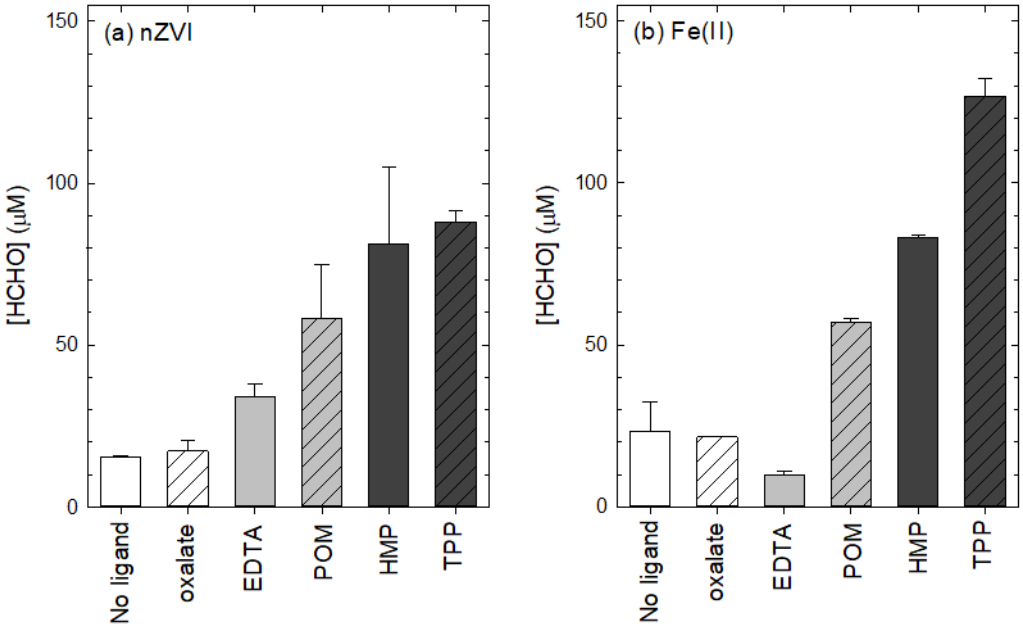

Figure 2.4. Effects of oxalate, EDTA, POM, HMP, and TPP on the production of HCHO by the nZVI/O_2 (a) and Fe(II)/O_2 (b) systems. ($[Methanol]_0$ = 200 mM; $[nZVI]_0$ = 10 mg/L (0.168 mM as Fe); $[Fe(II)]_0$ = 0.168 mM; $[oxalate]_0$ = $[EDTA]_0$ = $[POM]_0$ = $[TPP]_0$ = $[HMP]_0$ = 1 mM; pH_0 = 7.0; reaction time = 4 h).

2.2.3. Oxidative degradation of organic compounds

The degradation of selected pharmaceutical compounds (i.e., CMT, AAP, and CBZ) was investigated in the nZVI/TPP/O_2 and Fe(II)/TPP/O_2 systems (Figure 2.5a and 2.5b). The pharmaceuticals were degraded following pseudo first-order kinetics. Both systems exhibited similar activity for the degradation of pharmaceuticals, and the degradation efficacy was in the order of CBZ > AAP > CMT. Under deaerated conditions (by bubbling ultrapure N_2 gas), no significant degradation of pharmaceuticals were observed (data not shown).

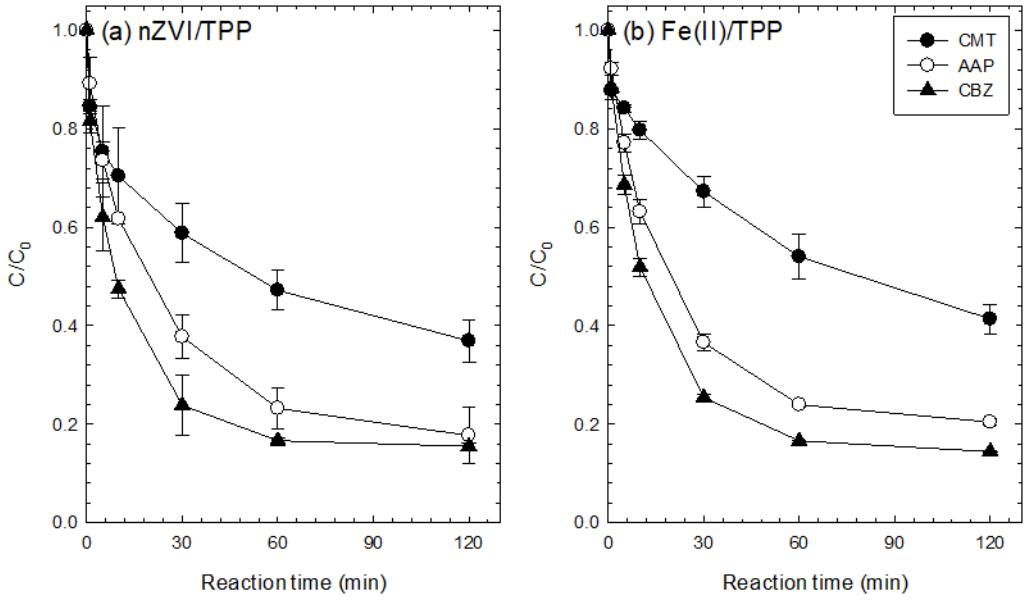

Figure 2.5. Oxidative degradation of selected pharmaceuticals by the nZVI/O_2 (a) and the Fe(II)/O_2 (b) systems ($[CMT]_0 = [AAP]_0 = [CBZ]_0 = 10$ μM; $[nZVI]_0 = 10$ mg/L (0.168 mM as Fe); $[Fe(II)]_0 = 0.168$ mM; $[TPP]_0 = 1$ mM; pH = 7.0).

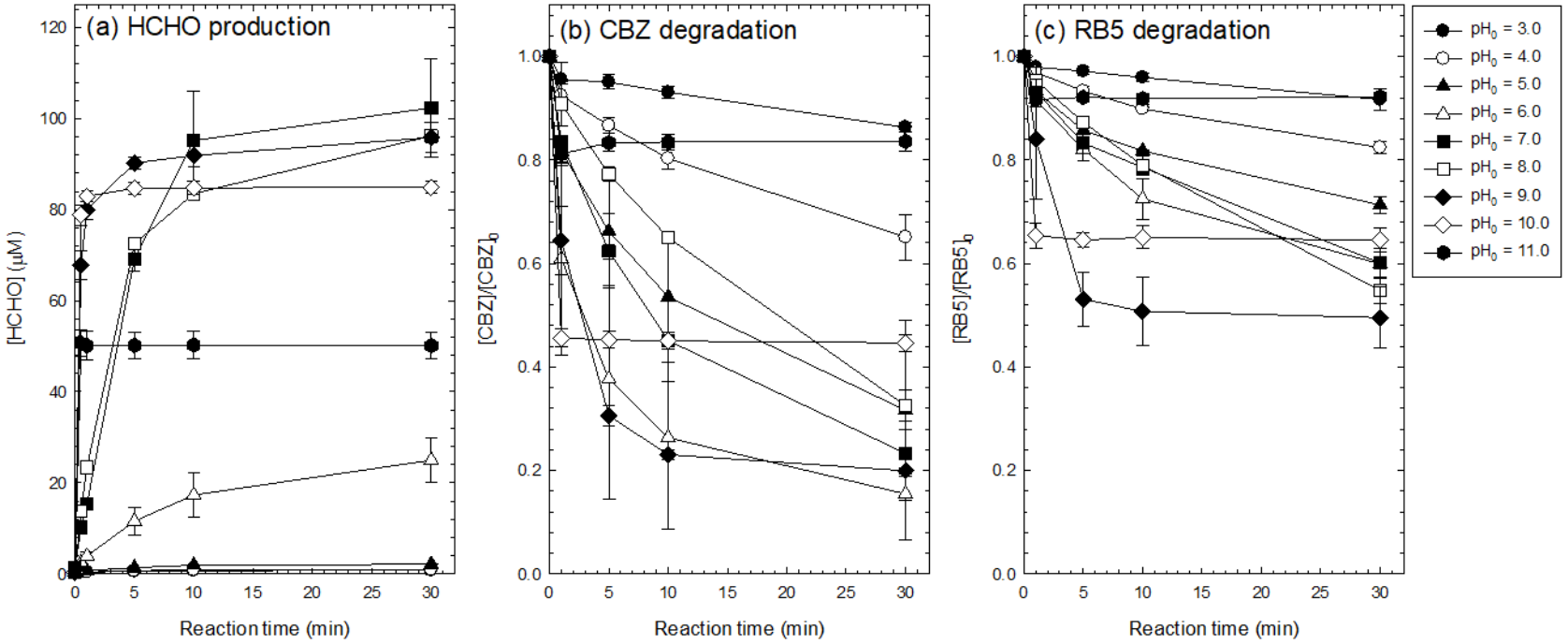

Figure 2.6. Production of HCHO (a) and degradation of CBZ (b) and RB5 (c) by the Fe(II)/TPP/O_2 system at different pH values ($[Methanol]_0$ = 200 mM; $[CBZ]_0$ = 10 μM; $[RB5]_0$ = 10 mg/L; $[Fe(II)]_0$ = 0.168 mM; $[TPP]_0$ = 1 mM).

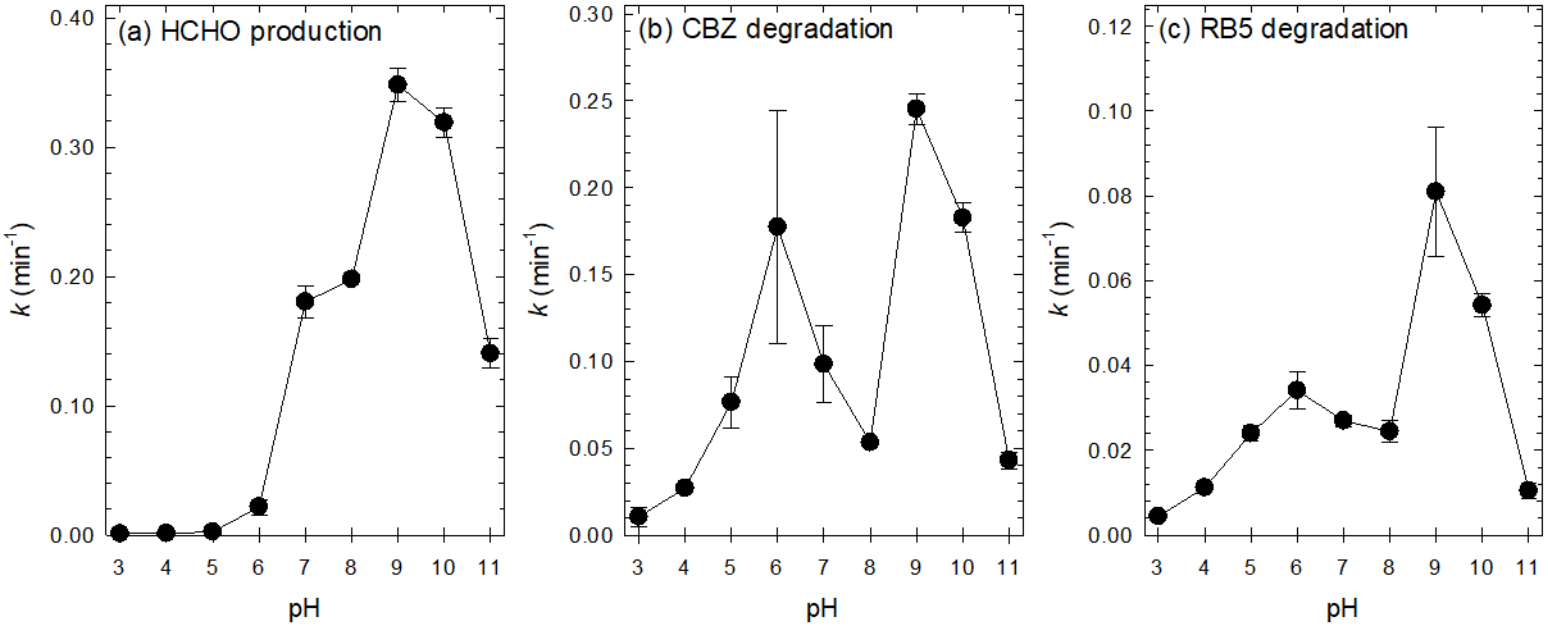

Figure 2.7. Pseudo first-order rate constants for the production of HCHO (a) and degradation of CBZ (b) and RB5 (c) by the Fe(II)/TPP/O_2 system as a function of pH ($[Methanol]_0$ = 200 mM; $[CBZ]_0$ = 10 μM; $[RB5]_0$ = 10 mg/L; $[Fe(II)]_0$ = 0.168 mM; $[TPP]_0$ = 1 mM).

2.2.4. Effect of pH

Experiments for the production of HCHO and the degradation of CMZ and RB5 in the Fe(II)/TPP/O_2 system were performed at different pH values between 3 and 11. The time-concentration profiles were obtained under each condition (Figure 2.6), and the calculated pseudo first-order rate constants (using the datapoints within 10 min) are depicted as functions of pH (Figure 2.7a–2.7c). The production of HCHO was significantly accelerated at pH values above 5 with a maximum at pH 9 (Figure 2.7a), which is attributed to the accelerated oxidation of Fe(II)-TPP at higher pH values (Figure 2.8). However, interestingly, the degradation rate of CBZ showed two distinct optima at pH 6 and 9 (Figure 2.7b). RB5 degradation was also optimized at the same pH values (Figure 2.7c), though the first optimum at pH 6 appeared to be somewhat lower compared to CBZ.

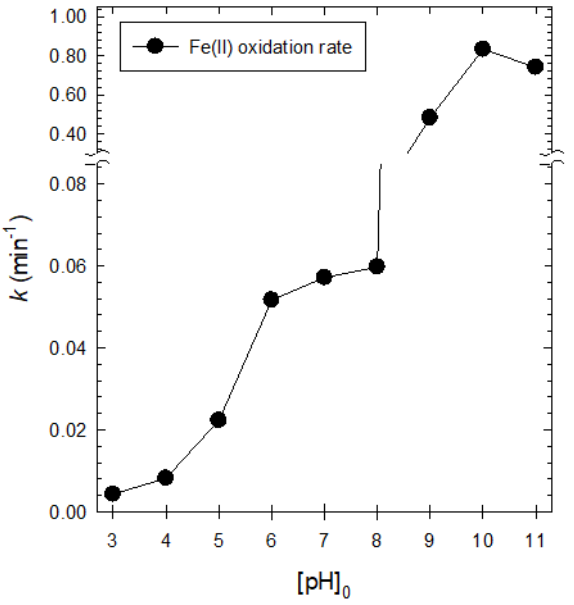

Figure 2.8. Rates of Fe(II) oxidation (pseudo first-order rate constants) in the Fe(II)/TPP/O_2 system as a function of pH ($[Fe(II)]_0$ = 0.168 mM; $[TPP]_0$ = 1 mM).

2.2.5. Oxidative degradation of CBZ in natural water samples

The degradation of CBZ by the Fe(II)/TPP/O_2 system was evaluated in natural water (Figure 2.9). Compared to deionized water, CBZ was slightly less degraded in natural water, possibly due to the oxidant-scavenging effect of water constituents. The CBZ degradation was marginally more inhibited in ND river water, which contains higher concentrations of organic substances than JB groundwater (Table 2.1). The addition of humic acid decreased the degradation rate of CBZ by the Fe(II)/TPP/O_2 system in deionized water (Figure 2.10a), confirming the inhibitory effect of organic substances. Inorganic substances such as bicarbonate and chloride were also found to inhibit the CBZ degradation (Figure 2.10b).

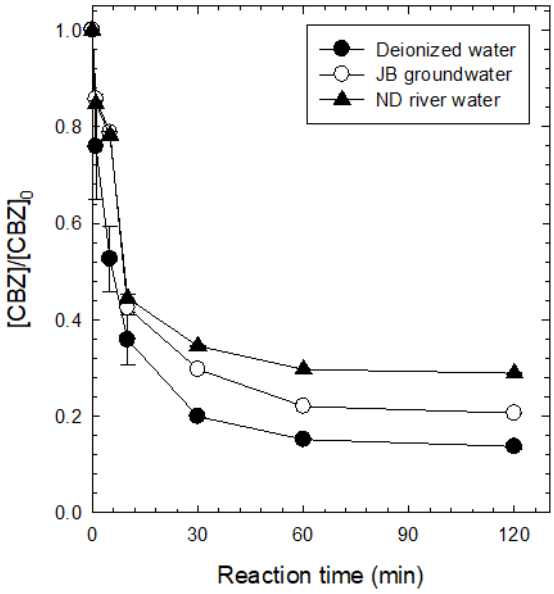

Figure 2.9. Oxidative degradation of CBZ by the Fe(II)/TPP/O_2 system in natural water samples ($[CBZ]_0$ = 10 μM; $[Fe(II)]_0$ = 0.168 mM; $[TPP]_0$ = 1 mM; pH = 7.0).

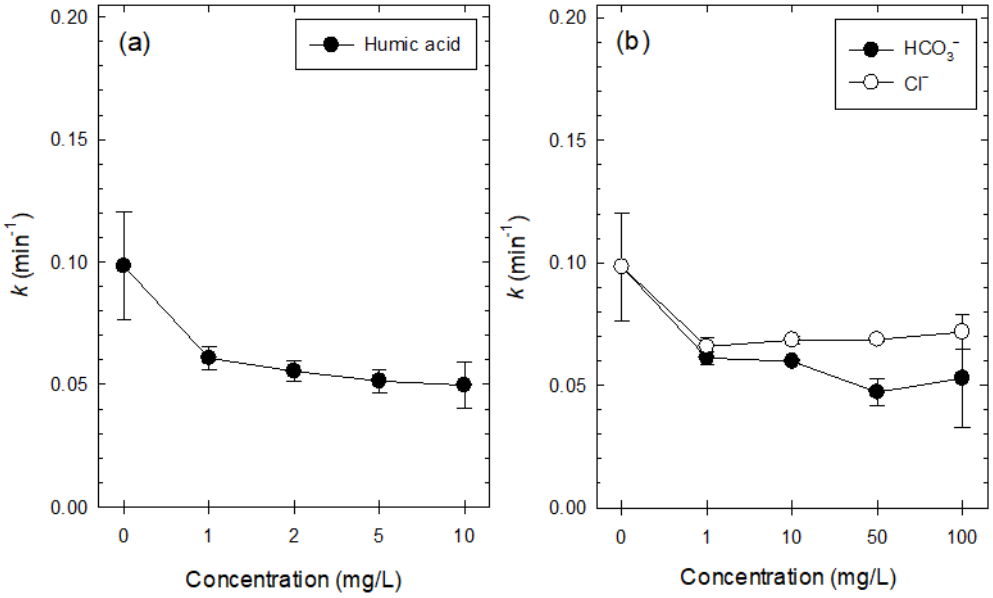

Figure 2.10. Effects of humic acid (a) and HCO_3^- and Cl^- (b) on the degradation of CBZ by the Fe(II)/TPP/O_2 system ($[CBZ]_0$ = 10 μM; $[Fe(II)]_0$ = 0.168 mM; $[TPP]_0$ = 1 mM; pH = 7.0).

2.3. Discussion

2.3.1. Oxidant production from nZVI and Fe(II) in the presence of oxygen

The corrosion of nZVI by dissolved oxygen produces H_2O_2 via a two-electron transfer reaction (reaction 2.1; [68, 69]). The H_2O_2 so produced is mainly reduced to water by another two-electron transfer reaction (reactions 2.2), providing minimal opportunities for conversion into reactive oxidants (i.e., $^{\bullet}OH$ or Fe(IV)) by the Fenton reaction (reactions 2.3). As a result, nZVI merely serves as the source of Fe(II). This four-electron transfer mechanism (reactions 2.1 & 2.2) is primarily responsible for the low oxidant yield (Δ[Oxidant]/Δ[Fe^0] < 10%) from the nZVI oxidation by oxygen [11].

$$Fe^0_{(s)} + O_2 + 2H^+ \rightarrow Fe(II) + H_2O_2 \quad (2.1)$$

$$Fe^0_{(s)} + H_2O_2 + 2H^+ \rightarrow Fe(II) + 2H_2O \quad (2.2)$$

$$Fe(II) + H_2O_2 \rightarrow Fe(III) + {}^{\bullet}OH + OH^- \text{ (or } Fe(IV) + H_2O) \quad (2.3)$$

Under neutral pH conditions, Fe(II) is oxidized by oxygen via a series of one-electron transfer reactions to produce reactive oxidants (reactions 2.4, 2.5 and 2.3) [70-72].

$$Fe(II) + O_2 \rightarrow Fe(III) + O_2^{\bullet-} \quad (2.4)$$

$$Fe(II) + O_2^{\bullet-} + 2H^+ \rightarrow Fe(III) + H_2O_2 \quad (2.5)$$

According to reactions 2.3–2.5, the theoretical oxidant yield (Δ[Oxidant]/Δ[Fe(II)]) from the Fe(II) oxidation by oxygen should be 33% because three molar equivalents of Fe(II) are consumed to produce one equivalent of the oxidant. However, iron precipitation decreases the oxidant yield; the formation of Fe(III)-oxyhydoroxides can cause the Fe(II)-Fe(III) co-precipitation to limit the Fe(II) availability [11], and the precipitate surfaces can accelerate the scavenging of Fe(IV) (i.e., the dominant oxidant at neutral pH) by adjacent Fe(II) [73].

2.3.2. Roles of TPP

The primary role of polyphosphates in enhancing oxidant production in the nZVI/O_2 and Fe(II)/O_2 systems is iron-chelation, which prevents the formation of iron precipitates at neutral pH. The complexation of Fe(III) with TPP was verified by the UV-visible absorption spectra, and the Fe(III)-TPP complexes were soluble (filterable) and colorless (Figure 2.11). As described earlier, the formation of soluble iron increases Fe(II) availability by preventing Fe(II)-Fe(III) co-precipitation and mitigates the undesired consumption of Fe(IV) by the reaction with Fe(II) in precipitate surfaces, eventually enhancing the oxidant yield. In addition, the complexation of Fe(II) with TPP can affect the kinetics and mechanism of the Fenton reaction.

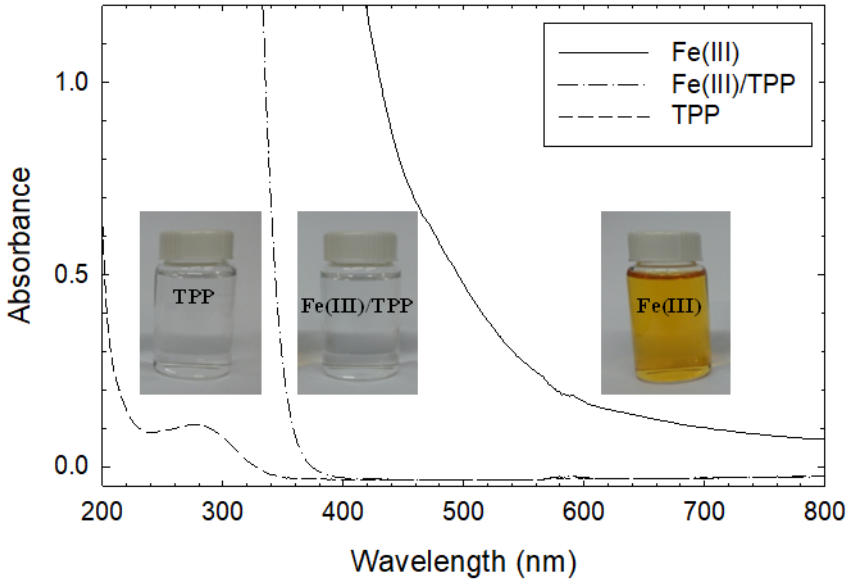

Figure 2.11. UV/Vis absorption spectra of Fe(III), TPP, and Fe(III)-TPP ($[Fe(III)]_0$ = 2 mM; $[TPP]_0$ = 10 mM; pH = 7.0).

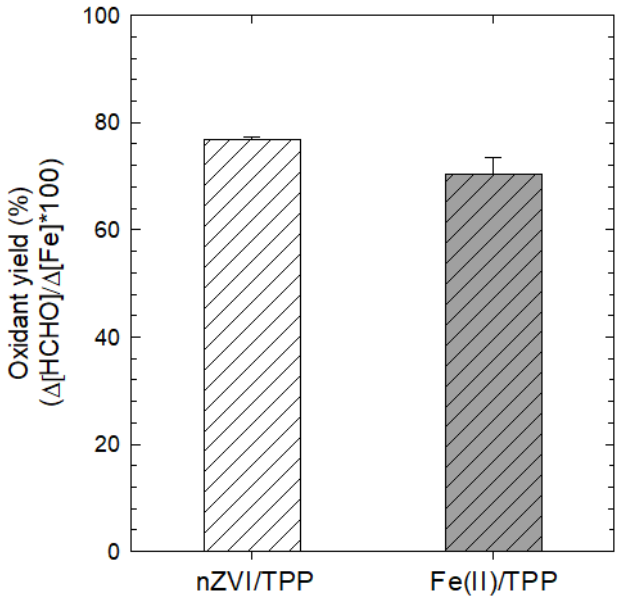

Figure 2.12. Oxidant yields from the nZVI/TPP/O_2 and Fe(II)/TPP/O_2 systems ($[Methanol]_0$ = 200 mM; $[nZVI]_0$ = 10 mg/L (0.168 mM as Fe); $[Fe(II)]_0$ = 0.168 mM; $[TPP]_0$ = 1 mM; pH_0 = 7.0; reaction time = 4 h; the dissolved iron concentration in Figure 2.2 was used as Δ[Fe] for nZVI).

Meanwhile, a notable observation is that the nZVI/TPP/O_2 system produced less HCHO than the Fe(II)/TPP/O_2 system (Figure 2.1a). Considering the concentration of nZVI consumed in the nZVI/TPP/O_2 system (i.e., the dissolved iron concentration; Figure 2.2), the oxidant yields of the two systems were similar (Figure 2.12), indicating that nZVI has no roles other than as the source of Fe(II). In addition, the nZVI/TPP/O_2 system was not more superior in the degradation of pharmaceuticals compared to the Fe(II)/TPP/O_2 system (Figure 2.5). These observations are inconsistent with the earlier study [48] in which the degradation of atrazine by nZVI with TPP was only partially attributed to the reactions of released Fe(II)-TPP. The results of the study suggested that nZVI transfers electrons to Fe(III)-TPP (both surface-bound and soluble Fe(III) species) to regenerate Fe(II)-TPP, which subsequently promotes the Fe(II)-mediated oxygen activation by a series of one-electron transfer reactions. However, such phenomena did not seem to occur in our systems based on the observations in Figures 2.1 and 2.5. There is no clear explanation for this discrepancy, but the differences in the nZVI material and the oxidation conditions may be responsible; Fe@Fe_2O_3 core-shell nanowires were used in the other study, and the nZVI dose was relatively high (20 mM, excess to dissolved oxygen). Fe@Fe_2O_3 core-shell nanowires may be more resistant to oxidation than the nZVI used in this study (chain-shaped aggregates of spherical nanoparticles) due to the rigid network structure.

Another noteworthy observation is that the oxidant yields (Δ[HCHO]/Δ[Fe(II)]) reached almost 70% in the Fe(II)/TPP/O_2 system (Figure 2.12), which is much higher than the theoretical yield (33%) based on the known mechanism (reactions 2.3–2.5). In fact, the use of methanol can somewhat increase the oxidant yield by producing additional $O_2^{\bullet-}$ during the oxidation process (reactions 2.6 & 2.7).

$$^{\bullet}OH \text{ (or Fe(IV))} + CH_3OH \rightarrow {}^{\bullet}CH_2OH + H_2O \text{ (or Fe(III))} \quad (2.6)$$

$$^{\bullet}CH_2OH + O_2 \rightarrow HCHO + H^+ + O_2^{\bullet-} \quad (2.7)$$

The resultant $O_2^{\bullet-}$ participates in chain reactions (reactions 2.5, 2.3, 2.6, 2.7, and their repetition), accelerating the oxidation of methanol into HCHO. When these chain reactions are taken into account, the theoretical maximum of the HCHO yield (Δ[HCHO]/Δ[Fe(II)]) approaches 50% as the kinetic chain length increases. However, the HCHO yield observed in the Fe(II)/TPP/O_2 system (70%) exceeded this maximum value, which suggests the presence of unknown pathways for producing reactive oxidants with higher oxidant yields. A possible pathway may be the two-electron oxidation of Fe(II)-TPP by oxygen to directly produce the reactive oxidant, Fe(IV) species (reaction 2.8 or 2.9), in which the oxidant yield reaches 100% with respect to Fe(II) added. It has been proposed that Fe(IV)-oxo complexes can be produced via oxygen activation by Fe(II)-EDTA at a stoichiometry equivalent to reaction 9 [74].

$$\text{Fe(II)-TPP} + O_2 + 2H^+ \rightarrow \text{Fe(IV)-TPP} + H_2O_2 \quad (2.8)$$

$$2\text{Fe(II)-TPP} + O_2 \rightarrow 2\text{Fe(IV)-O-TPP (oxo complexes)} \quad (2.9)$$

The partial contribution of these pathways may explain the high oxidant yield in the Fe(II)/TPP/O_2 system, but further study is needed to elucidate the detailed mechanisms.

2.3.3. Nature of oxidants

According to previous studies [11, 75], Fe(IV) (rather than •OH) is the dominant product of the Fenton reaction at neutral pH. However, the complexation of Fe(II) with ligands can alter the mechanism of the Fenton reaction, shifting the major oxidant from Fe(IV) to •OH. It has been suggested that the nZVI/O_2 system produces •OH in the presence of oxalate, NTA, and POM, and a mixture of •OH and Fe(IV) in the presence of EDTA [42, 44].

In the Fe(II)/TPP/O_2 system, the production of *p*-HBA by the BA oxidation was monitored at different pH values from 3−11, and was compared to the yields of HCHO (data from Figure 2.6) (Figure 2.13). As shown in Figure 2.13a, the *p*-HBA concentration was less than 7 μM in the entire pH range. However, the calculated ratios of [*p*-HBA]/[HCHO] (Figure 2.13a) were very high at pH < 5, suggesting that •OH may dominate at acidic pH. On the other hand, at pH > 6, the ratios of [*p*-HBA]/[HCHO] drastically decreased, indicating the shift from •OH to Fe(IV).

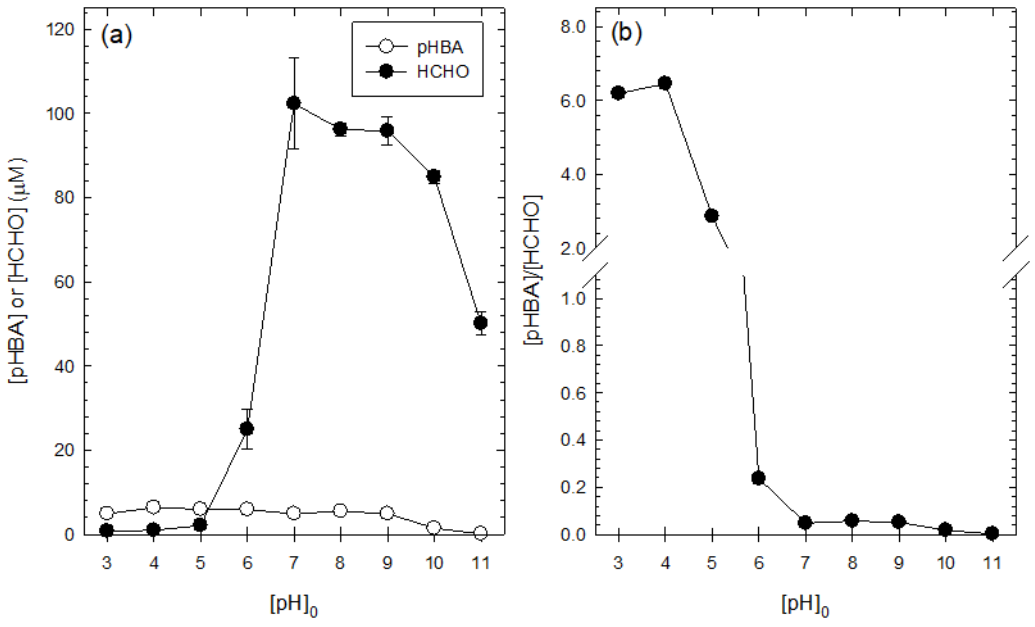

Figure 2.13. Production of *p*-HBA and HCHO (a) and ratios of produced pHBA to HCHO (b) by the Fe(II)/TPP/O_2 system as a function of pH ([Benzoic acid]$_0$ = 10 mM; [Methanol]$_0$ = 200 mM; [Fe(II)]$_0$ = 0.168 mM; [TPP]$_0$ = 1 mM; reaction time = 30 min).

At pH 7, the nZVI/TPP/O_2 and Fe(II)/TPP/O_2 systems still produced *p*-HBA, a hydroxylated oxidation product of BA (Figure 2.1b), implying that those systems produced $^{\bullet}OH$ as well. The formation of 7-HC from coumarin also supported the production of $^{\bullet}OH$ (Figure 2.3). However, the yields of the hydroxylated products were very low. The ratios of *p*-HBA to HCHO (Δ[*p*-HBA]/Δ[HCHO]) were 4.0 and 4.4% for the nZVI/TPP/O_2 and Fe(II)/TPP/O_2 systems, respectively (calculated from the values at 4 h in Figures 2.1a and 2.1b). Calculating the total HBA yield (including isomers) using the reported product ratio (i.e., *ortho*-HBA:*meta*-HBA:*para*-HBA = 1.7:2.3:1.2; [76]), the production of HBA accounted for 20.6 and 22.6% of the HCHO production in the nZVI/TPP/O_2 and Fe(II)/TPP/O_2 systems, respectively. These values were much lower than those reported for other ligand-enhanced systems in which $^{\bullet}OH$ is suggested to be a dominant oxidant (59 and 53% with oxalate, 63 and 129% with NTA, 54 and 53% with POM; values for the nZVI/ligand/O_2 and Fe(II)/ligand/O_2 systems, respectively (pH 7) calculated using data from previous studies [11, 42, 44]. As a result, we assumed that the production of Fe(IV) species was dominant in the systems with TPP.

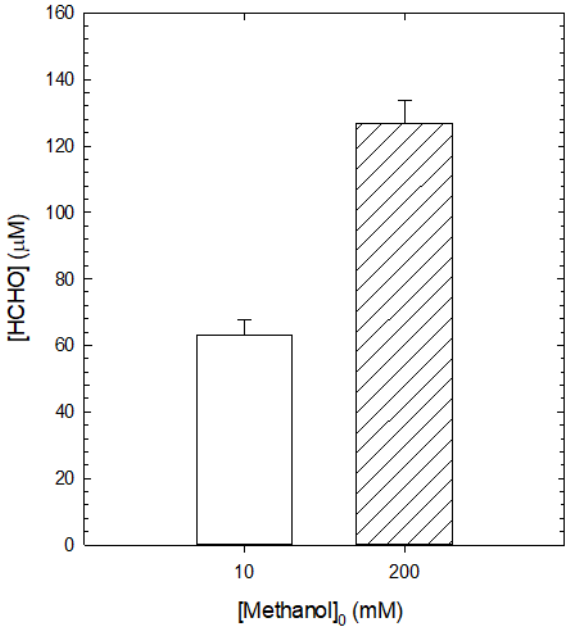

Figure 2.14. Production of HCHO by the Fe(II)/TPP/O_2 system at different methanol concentrations ([Methanol]$_0$ = 10 and 200 mM; [Fe(II)]$_0$ = 0.168 mM; [TPP]$_0$ = 1 mM; pH = 7.0; reaction time = 4 h).

Another evidence for the dominant occurrence of Fe(IV) species was the poor oxidant-scavenging efficacy of methanol at a lower concentration. The HCHO yield decreased by almost 50% when the amount of methanol added initially was reduced to 10 mM (Figure 2.14), which could not be explained by the behavior of •OH. In the Fe(II)/TPP/O_2 system, Fe(II)-TPP was the major oxidant scavenger competing with methanol. In order for Fe(II)-TPP (0.168 mM) to compete equally with methanol (10 mM) for the oxidant, the rate constant for the reaction of Fe(II)-TPP with the oxidant should be 60 times higher than that of methanol ($k = 1 \times 10^9$ M^{-1} s^{-1}; [77]). In fact, since the Fe(II)-TPP concentration decreases over time, the difference between the two rate constants should be even greater, which is unreasonable considering the nonselective reactivity of •OH. However, Fe(IV) can be more selective to the reaction with Fe(II) (reaction 2.10). For example, the Fe(IV) species formed by the ozonation of Fe(II) (i.e., ferryl-oxo complex, $Fe=O^{2+}$) exhibited 75 fold higher reactivity with Fe(II) than methanol [78].

Fe(IV)-TPP + Fe(II)-TPP → 2Fe(III)-TPP (2.10)

There are multiple Fe(IV) species with different reactivities [40, 43, 79]. The Fe(IV) species produced by the nZVI/TPP/O_2 and Fe(II)/TPP/O_2 systems are likely complexed forms with TPP (also with oxo or hydroxo group), which should undergo speciation as a function of pH. The unique trends in pH dependence for the degradation of CBZ and RB5 (with two optimum values at pH 6 and 9; Figures 2.7b and 2.7c) may be attributed to the pH-dependent speciation of Fe(IV)-TPP complexes with different reactivities. The speciation of CBZ and RB5 does not explain the pH dependence of their degradation. The rates of Fe(II)-TPP oxidation (Figure 2.8) and HCHO formation (Figure 2.7a) continued to increase with increasing pH up to 9–10, exhibiting different trends from those of CBZ and RB5 degradation (Figures 2.7b and 2.7c); excess methanol was assumed to capture most of the reactive oxidants regardless of reactivity. This result indicates that the pH dependence of CBZ and RB5 degradation does not result from the change in the rate of oxidant production, but possibly from changes in the reactivity of the resultant oxidant.

Exploring the nature of the Fe(IV) species from the Fenton (-like) reactions (including issues on the distinguishment from •OH) has been a challenging task because these species are unstable and may have complicated coordination chemistry. Despite decades of extensive research, a substantial portion of the knowledge relies on hypothetical claims and indirect evidence. Continuous efforts need to be exerted to elucidate the chemistry of Fe(IV).

2.3.4. Potential applications

The Fe(II)/TPP/O_2 system can be used to oxidize refractory organic contaminants in water and wastewater with different purposes including the ISCO application for groundwater remediation. Organic and inorganic constituents in natural water can somewhat reduce the system's efficacy by

scavenging oxidants, but these inhibitory effects do not appear to be critical (Figures 2.9 and 2.10). To treat highly concentrated wastewater, a proper method to effectively regenerate Fe(II) may be needed. The addition of H_2O_2 can also be considered to enhance the production of reactive oxidants [80]. For the ISCO application, the nZVI/TPP/O_2 system has no advantage over the Fe(II)/TPP/O_2 system in terms of the oxidant yield. However, a potential application of nZVI involving the use of TPP and oxygen may be a sequential reduction-oxidation treatment for mediums contaminated by multiple organic pollutants; nZVI is first used as a reducing agent to treat reductively-degradable organics (e.g., chlorinated organic compounds), then the released Fe(II) (including residual nZVI) is used for the oxic treatment of other compounds upon the addition of TPP with aeration.

Chapter 3. Enhanced oxidation of phenol by copper-catalyzed Fenton-like reaction in the presence of bicarbonate

3.1. Materials and Methods

3.1.1. Reagents

All chemicals were of reagent grade and used without further purification. Acetonitrile and 2,9-dimethyl-1,10-phenanthroline (DMP, Neocuproine) were from J.T. Baker® (USA) and TCI Co. (Japan), respectively, and all the other chemicals were obtained from Sigma-Aldrich Co. (USA). 18.2 MΩ·cm Milli-Q water from a Millipore system was used to prepare solutions. $CuSO_4$ was used to prepare the Cu(II) stock solution (10 mM). The stock solution of sodium bicarbonate ($NaHCO_3$) (0.5 M) was prepared freshly prior to the experiment.

3.1.2. Experimental setup and procedure

All experiments were conducted in a 125 mL Erlenmeyer flask open to the atmosphere at room temperature (22 ± 2ºC). For some experiments, the solution was aerated with ultrapure CO_2 gas using a diffuser for saturation (for 30 min prior to the experiment). The solution pH was adjusted using a 1 N $HClO_4$ and 1 N NaOH solution. The solutions for pH 7 and 8 were buffered with 5 and 1 mM phosphate, respectively. In all experiments, pH variations were less than 0.3 units during the reaction. The reaction was initiated by adding hydrogen peroxide (H_2O_2) to the prepared solution containing Cu(II) and the organic compound (and HCO_3^-). Samples were withdrawn using a 10 mL glass syringe at predetermined times and filtered through a 0.2-μm hydrophilic PTFE filter. The possible reactions of Cu(II) in samples were immediately quenched by adding 20 μL of 200 mM ethylenediaminetetraacetic acid (EDTA). All experiments were carried out at least in triplicate, and the average values and standard deviations (error bars) were presented. Main experimental conditions include: $[Cu(II)]_0$ = 0.1 mM, $[HCO_3^-]_0$ = 50 mM, $[H_2O_2]_0$ = 10 mM, $[Phenol]_0$ = 0.1 mM, and pH = 10. For some experiments, the doses of Cu(II), HCO_3^-, H_2O_2, and pH were varied in the ranges of 0.001–0.1 mM, 1–100 mM, 1–100 mM, and 7–12, respectively. All the experimental conditions were summarized in Table 3.1.

Table 3.1. Summary of experimental conditions

No	Cu(II) (mM)	Co(II) (mM)	HCO_3^- (mM)	H_2O_2 (mM)	Organic compounds (mM)	Oxidant scavengers (mM)	pH	Figure
1	0.1	-	50	10	0.1 (Phenol)	-	10.0	Figure 3.1 (a, b)
2	-	0.1	50	10	0.1 (Phenol)	-	10.0	Figure 3.1 (c, d)
3	0.001, 0.005, 0.01, 0.02, 0.05, 0.1	-	50	10	0.1 (Phenol)	-	10.0	Figure 3.4
4	0.1	-	1, 5, 10, 20,50, 100	10	0.1 (Phenol)	-	10.0	Figure 3.4
5	0.1	-	10	1, 5,10, 20, 50, 100	0.1 (Phenol)	-	10.0	Figure 3.4
6	0.1	-	50	10	0.1 (Phenol)	-	7.0, 8.0, 9.0, 10.0, 11.0, 12.0	Figure 3.5 (a, b)
7	0.1	-	50	10	50 mg/L (RB5)	-	7.0, 8.0, 9.0, 10.0, 11.0, 12.0	Figure 3.5 (c)
8	0.1	-	50	10	0.1 (Benzoic acid, Phenol, Bisphenol A, 4-Chlorophenol)	-	10.0	Figure 3.6
9	0.1	-	50	10	0.1 (Phenol)	50, 200, 1000 (*tert*-Butanol, Methanol)	10.0	Figure 3.7
10	0.1	-	(CO_2 aeration)	10	0.1 (Phenol)	-	10.0	Figure 3.8

3.1.3. Analytical methods

The concentration of organic compounds was measured by high-performance liquid chromatography (HPLC; Dionex Ultimate 3000; Thermo Fisher Scientific Inc., USA) with UV absorbance detection (at 277, 230, 230, 227 nm for phenol, 4-chlorophenol, bisphenol A, and benzoic acid, respectively). Separation was performed on an Agilent - Eclipse XDB - C18 column (150 mm × 4.6 mm, 5 μm) using a binary mixture of 0.1 % (w/w) phosphoric acid solution and acetonitrile as an eluent at a flow rate of 1.5 mL/min. H_2O_2 was analyzed using the titanium sulfate method on a UV/Vis spectrophotometer (S-3100; Scinco Co., Korea) [81]. Reactive Black 5 (RB5) was analyzed by measuring the absorbance at 597 nm. Chemical oxygen demand (COD) was analyzed by the $KMnO_4$ method using a COD analysis kit (COD-Mn-L; Humas Co., Korea).

3.2. Results

3.2.1. Phenol degradation by the Cu(II)/HCO_3^-/H_2O_2 system:

Comparison to the Co(II)/HCO_3^-/H_2O_2 system

The Cu(II)/HCO_3^-/H_2O_2 system degraded phenol (approximately 90% degradation in 2 h) much better than the Cu(II)/H_2O_2 system (10% degradation in 2 h) (Figure 3.1a); the phenol degradation by Cu(II)/HCO_3^- and H_2O_2/HCO_3^- was negligible. The COD removal was 38% in 2 h during the phenol degradation (Figure 3.2) The decomposition of H_2O_2 was also greater in the Cu(II)/HCO_3^-/H_2O_2 system than in the Cu(II)/H_2O_2 system (Figure 3.1b), indicating that HCO_3^- accelerates the Cu(II)-catalyzed decomposition of H_2O_2 to increase the production of reactive oxidants that can degrade phenol.

The Co(II)/HCO_3^-/H_2O_2 system (a similar HCO_3^--enhanced Fenton-like system) led to 72% degradation of phenol under the same conditions (Figure 3.1c); phenol was not degraded by other combinations, such as Co(II)/HCO_3^-, Co(II)/H_2O_2, and H_2O_2/HCO_3^-. Like the Cu(II)-catalyzed systems, the Co(II)/HCO_3^-/H_2O_2 system exhibited greater H_2O_2 decomposition than the Co(II)/H_2O_2 system (Figure 3.1d).

Comparing the Cu(II)/HCO_3^-/H_2O_2 and Co(II)/HCO_3^-/H_2O_2 systems (Figure 3.1a and 3.1b versus Figure 3.1c and 3.1d), the rates of phenol degradation and H_2O_2 decomposition were higher in the Co(II)/HCO_3^-/H_2O_2 system than in the Cu(II)/HCO_3^-/H_2O_2 system. However, the degree of phenol degradation was greater in the Cu(II)/HCO_3^-/H_2O_2 system (90% degradation in 60 min) than in the Co(II)/HCO_3^-/H_2O_2 system (72% degradation in 30 min). As a result, the H_2O_2 use efficiencies (i.e., Δ[Phenol]/Δ[H_2O_2], calculated from the results of Figure 1) were higher in the Cu(II)/HCO_3^-/H_2O_2 system than in the Co(II)/HCO_3^-/H_2O_2 system (Figure 3.3).

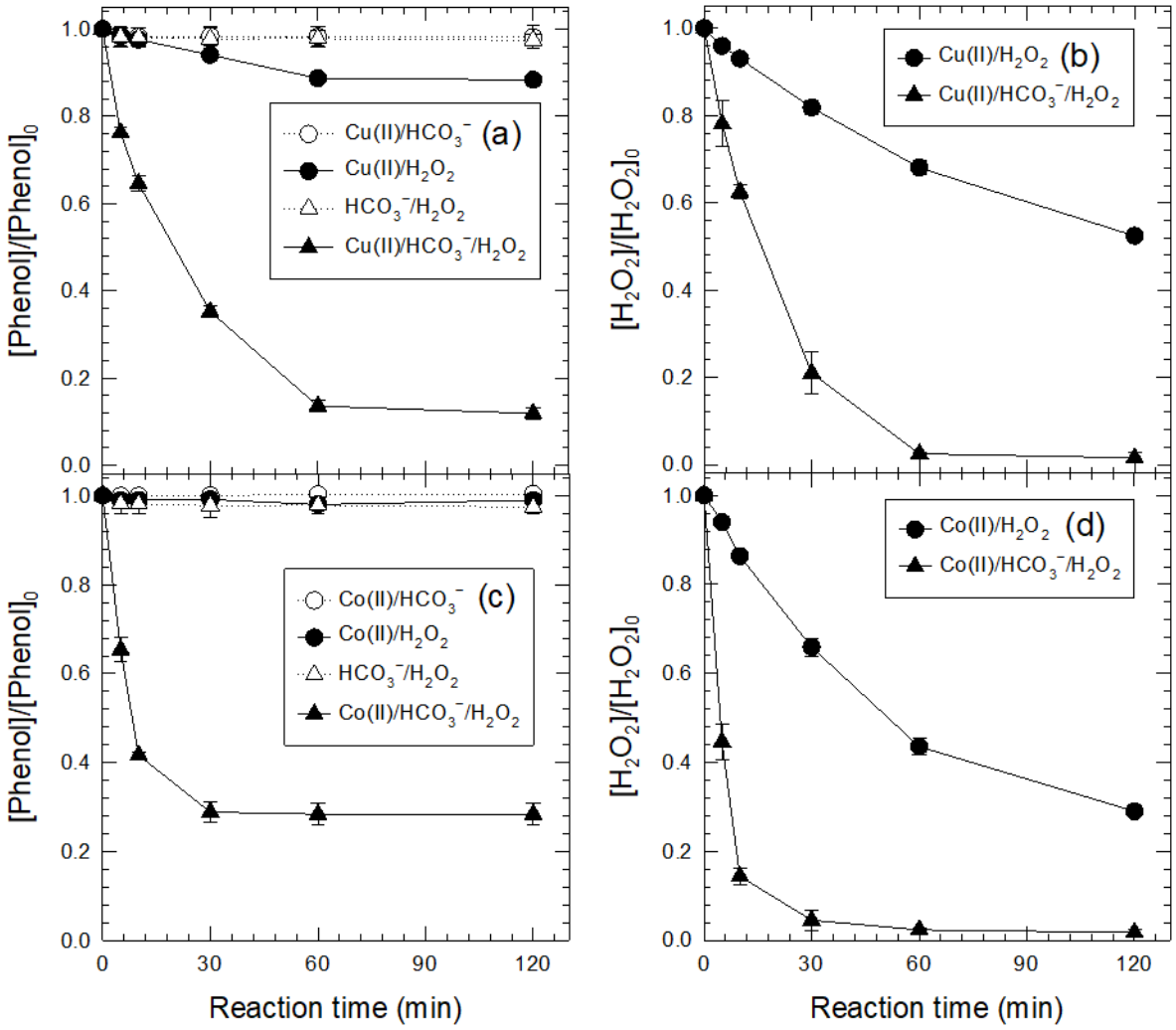

Figure 3.1. Degradation of phenol and decomposition of H_2O_2 by the Cu(II)/HCO_3^-/H_2O_2 system (a, b) and by the Co(II)/HCO_3^-/H_2O_2 system (c, d) ([Phenol]$_0$ = 0.1 mM; [Cu(II)]$_0$ = [Co(II)]$_0$ = 0.1 mM; [HCO_3^-]$_0$ = 50 mM; [H_2O_2]$_0$ = 10 mM; pH = 10.0).

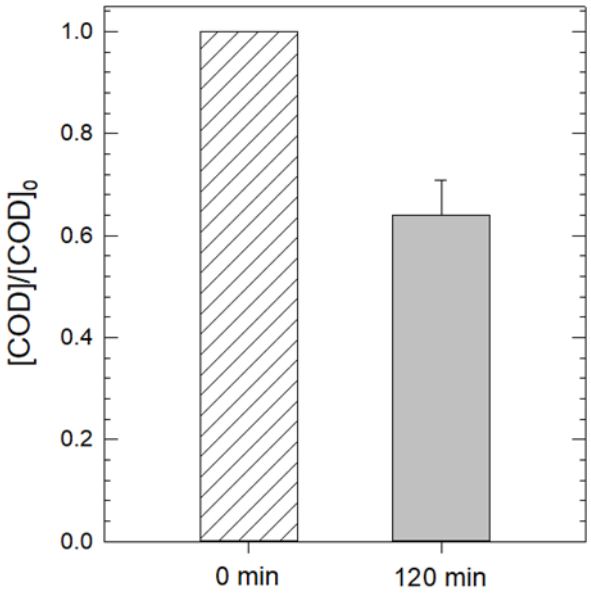

Figure 3.2. Removal of COD during the phenol degradation by the Cu(II)/HCO_3^-/H_2O_2 system ([Phenol]$_0$ = 0.1 mM; [Cu(II)]$_0$ = 0.1 mM; [HCO_3^-]$_0$ = 50 mM; [H_2O_2]$_0$ = 10 mM; pH = 10.0).

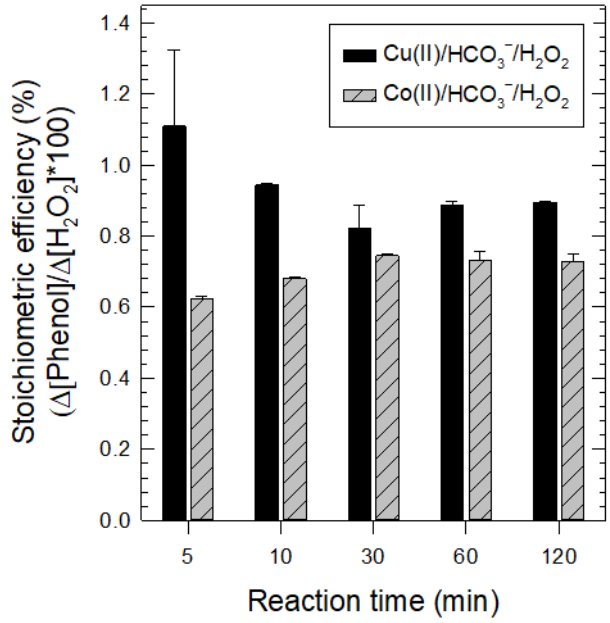

Figure 3.3. H_2O_2 use efficiency for phenol degradation by the Cu(II)/HCO_3^-/H_2O_2 and Co(II)/HCO_3^-/H_2O_2 systems (calculated from the data of Figure 1).

3.2.2. Effects of Cu(II), HCO_3^-, H_2O_2 doses, and solution pH

The effects of Cu(II), HCO_3^-, and H_2O_2 doses on the degradation of phenol were examined in the Cu(II)/HCO_3^-/H_2O_2 system (Figure 3.4). The rate of phenol degradation was presented by the pseudo-first order rate constant (k), which was determined using the data points for the phenol degradation of 50–70% ($R^2 > 0.9$). The k value increased with increasing doses of Cu(II) and HCO_3^-. However, when the H_2O_2 dose was adjusted, the optimal rate of phenol degradation was observed at 5 mM H_2O_2.

The phenol degradation by the Cu(II)/HCO_3^-/H_2O_2 system was optimal at pH 10 (Figure 3.5a); the k value increased with increasing pH from 7 to 10, then drastically decreased under alkaline pH conditions. However, the rate of H_2O_2 decomposition continued to increase with increasing pH from 7 to 12 (Figure 3.5b). In addition, when RB5 was employed as a target organic compound, it degraded faster with an alkaline pH (Figure 3.5c).

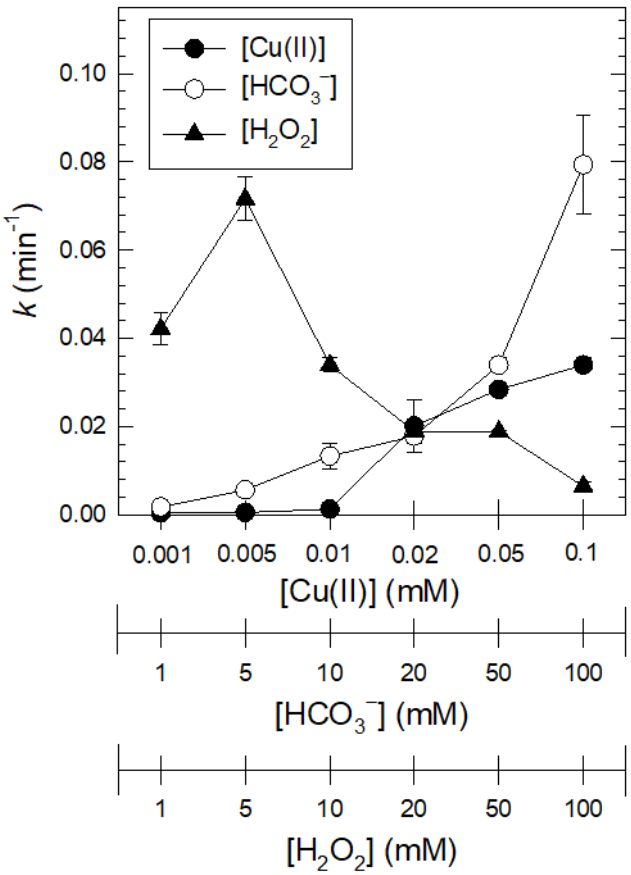

Figure 3.4. Effects of Cu(II), HCO_3^-, and H_2O_2 doses on the phenol degradation rate by the Cu(II)/HCO_3^-/H_2O_2 system ($[Phenol]_0 = 0.1$ mM; pH = 10.0; $[Cu(II)]_0 = 0.1$ mM for various doses of HCO_3^- and H_2O_2; $[HCO_3^-]_0 = 50$ mM for various doses of Cu(II) and H_2O_2; $[H_2O_2]_0 = 10$ mM for various doses of Cu(II) and HCO_3^-).

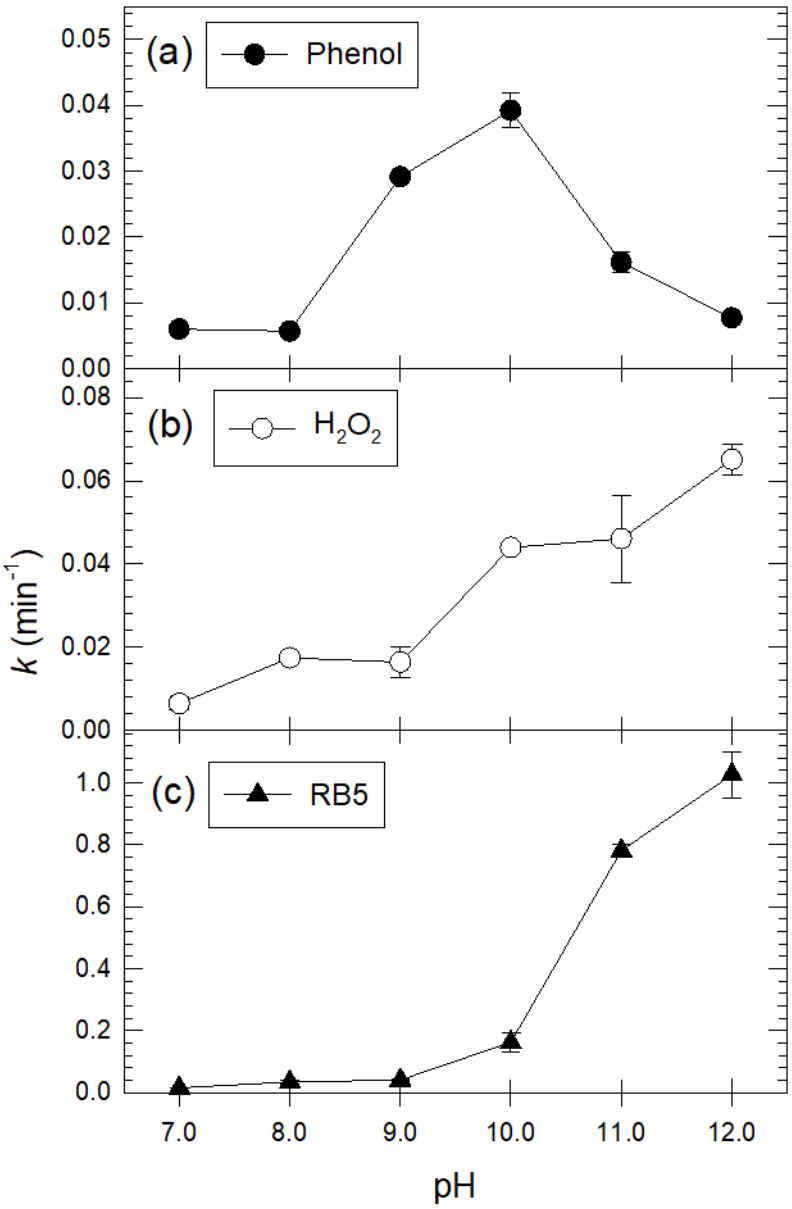

Figure 3.5. Rates of phenol degradation (a), H_2O_2 decomposition (b), and RB5 degradation (c) as a function of pH ($[Phenol]_0$ = 0.1 mM; $[H_2O_2]_0$ = 10 mM; $[RB5]_0$ = 50 mg/L; $[Cu(II)]_0$ = 0.1 mM; $[HCO_3^-]_0$ = 50 mM).

3.2.3. Degradation of selected organic compounds

Several organic compounds (benzoic acid, bisphenol A, and 4-chlorophenol) were also tested for degradation by the Cu(II)/HCO_3^-/H_2O_2 system (Figure 3.6). Benzoic acid was resistant to degradation, whereas the other compounds were successfully degraded, exhibiting degradation kinetics similar to that of phenol.

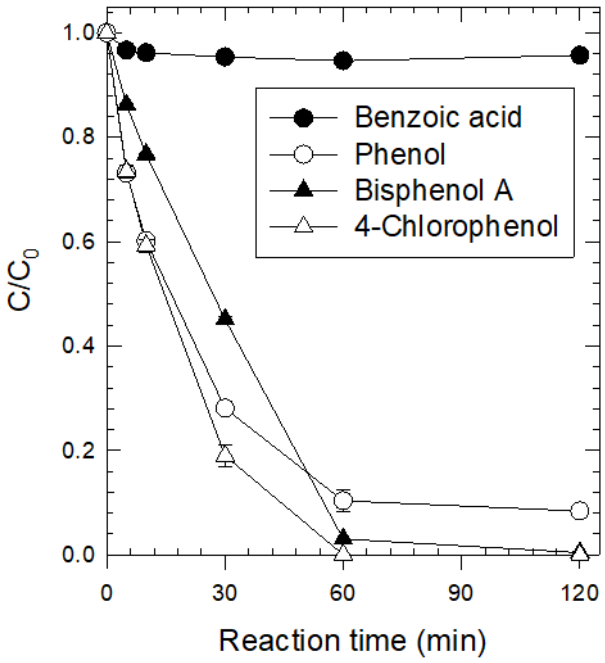

Figure 3.6. Degradation of several organic compounds by the Cu(II)/HCO_3^-/H_2O_2 system ([Benzoic acid]$_0$ = [Phenol]$_0$ = [Bisphenol A]$_0$ = [4-Chlorophenol]$_0$ = 0.1 mM; [Cu(II)]$_0$ = 0.1 mM; [HCO_3^-]$_0$ = 50 mM; [H_2O_2]$_0$ = 10 mM; pH = 10.0).

3.2.4. Effects of oxidant scavengers

Effects of oxidant scavengers (methanol and *tert*-butanol) on the rate of phenol degradation were examined in the Cu(II)/HCO_3^-/H_2O_2 system (Figure 3.7). The addition of methanol inhibited phenol degradation; the *k* value gradually decreased from 0.034 min^{-1} to 0.020 min^{-1} when the input concentration of methanol increased up to 1 M. On the other hand, *tert*-butanol did not inhibit the phenol degradation; in fact, the *k* value increased with the increasing concentration of *tert*-butanol.

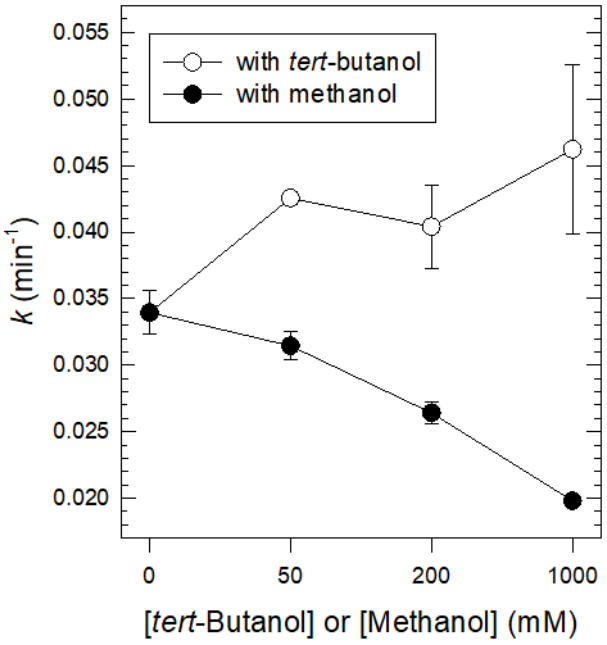

Figure 3.7. Effects of oxidant scavengers (*tert*-butanol and methanol) on the phenol degradation rate by the Cu(II)/HCO_3^-/H_2O_2 system ($[Phenol]_0$ = 0.1 mM; $[Cu(II)]_0$ = 0.1 mM; $[HCO_3^-]_0$ = 50 mM; $[H_2O_2]_0$ = 10 mM; pH = 10.0).

3.2.5. Aeration of CO_2 in the Cu(II)/H_2O_2 system

To explore the potential of CO_2 for supplying HCO_3^-, the phenol degradation by the Cu(II)/H_2O_2 system was examined by aerating CO_2 into the solution. As shown in Figure 3.8, the Cu(II)/H_2O_2 system with CO_2 aeration degraded phenol better than that without CO_2 aeration, indicating that CO_2 aeration is indeed effective in supplying HCO_3^- to the Cu(II)/H_2O_2 system. The measured alkalinity of the CO_2-aerated solution was equivalent to that of the 43.3 mM HCO_3^- solution.

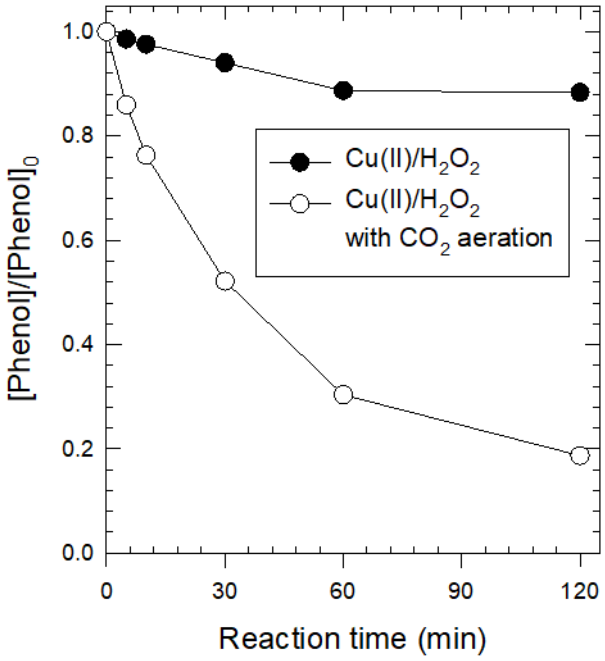

Figure 3.8. Degradation of phenol by the Cu(II)/H_2O_2 system with CO_2 aeration ($[Phenol]_0$ = 0.1 mM; $[Cu(II)]_0$ = 0.1 mM; $[H_2O_2]_0$ = 10 mM; pH_0 = 10.0).

3.3. Discussion

3.3.1. Production of reactive oxidants by the Cu(II)/HCO_3^-/H_2O_2 system

The Cu(II)/H_2O_2 system is known to produce reactive oxidants via the Fenton-like reaction mechanism [49, 82, 83]. Cu(II) is reduced to Cu(I) by the reaction with H_2O_2, producing superoxide radical anion ($O_2^{\bullet-}$) (reaction 3.1). Then, the reaction of Cu(I) with H_2O_2 produces reactive oxidants, i.e., $^{\bullet}OH$ and Cu(III) (reaction 3.2); $^{\bullet}OH$ and Cu(III) are produced by the one-electron and two-electron transfer reactions, respectively. Reaction 3.1 is believed to be slower than reaction 3.2, becoming the rate-determining step (RDS) for the production of reactive oxidants [49].

$$Cu(II) + H_2O_2 \rightarrow Cu(I) + O_2^{\bullet-} + 2H^+ \quad (3.1)$$

$$Cu(I) + H_2O_2 \rightarrow Cu(II) + {}^{\bullet}OH + OH^- \text{ or } Cu(III) + 2OH^- \quad (3.2)$$

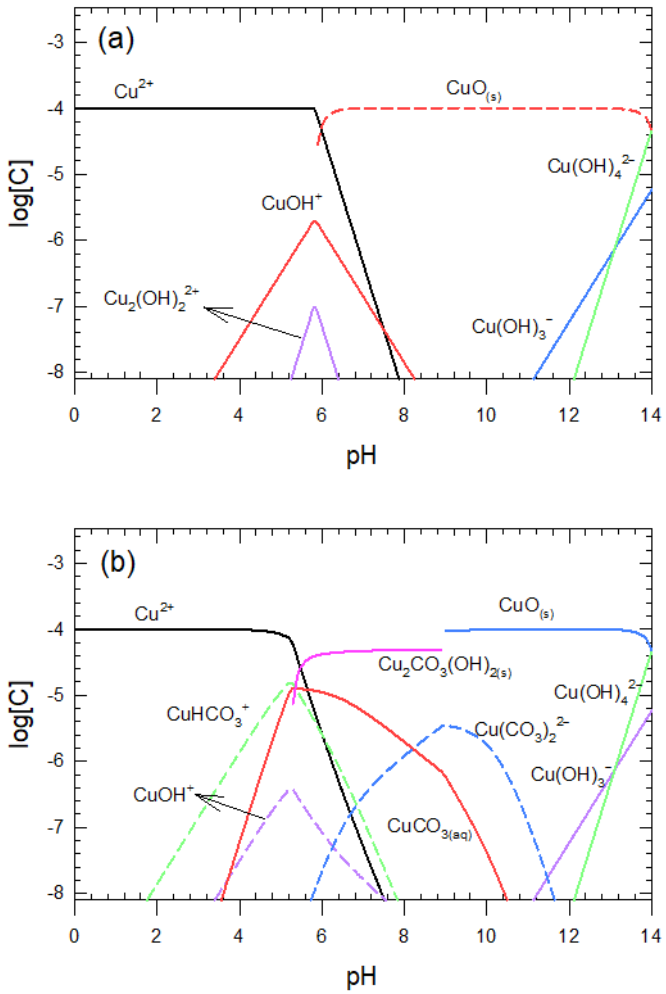

Figure 3.9. Speciation of Cu(II) in the absence (a) and presence (b) of HCO_3^-, calculated by MINEQL+ 4.6. ($[Cu(II)]_0$ = 0.1 mM; $[HCO_3^-]_0$ = 50 mM).

The addition of HCO_3^- can change the kinetics of the reaction of Cu(II) with H_2O_2 by forming Cu(II)-carbonate complexes. In the presence of HCO_3^- (50 mM), Cu(II)-carbonate complexes form in the pH range of 4–11 (Figure 3.9). These complexes are believed to have higher reactivity with H_2O_2 than those in the absence of HCO_3^- (e.g., Cu(II)-hydroxo complexes and Cu(II) oxide); the decomposition of H_2O_2 was indeed accelerated in the presence of HCO_3^- (Figure 3.1b). When strong Cu(II)-chelating agents, such as citrate, EDTA, and DMP, were added to the Cu(II)/HCO_3^-/H_2O_2 system (to replace Cu(II)-carbonate complexes with the Cu(II) complexes of added ligands), the phenol degradation was almost completely blocked (Figure 3.10), confirming the critical roles of Cu(II)-carbonate complexes.

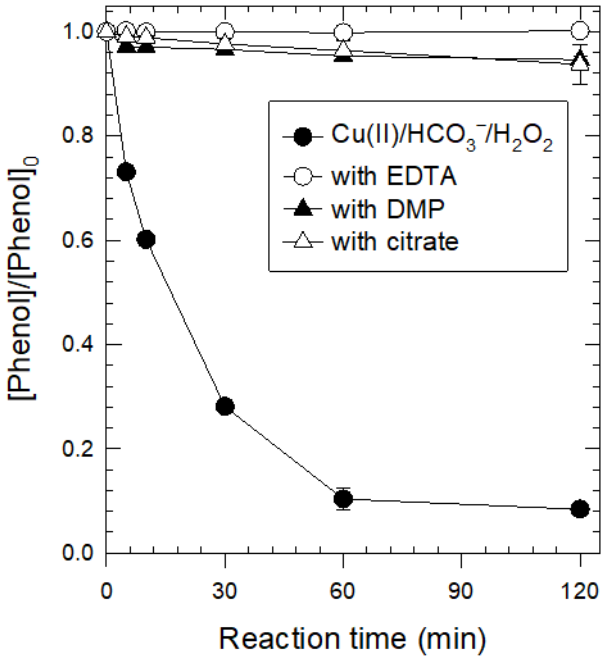

Figure 3.10. Effects of Cu(II)-chelating agents on phenol degradation by the Cu(II)/HCO_3^-/H_2O_2 system ($[Cu(II)]_0$ = 0.1 mM; $[EDTA]_0$ = $[DMP]_0$ = $[Citrate]_0$ =10 mM; $[H_2O_2]_0$ = 10 mM; $[HCO_3^-]_0$ = 50 mM; pH = 10.0).

On the other hand, it has been reported that HCO_3^- can directly react with H_2O_2 to produce peroxymonocarbonate (HCO_4^-) (Reaction 3.3) [84, 85]. HCO_4^- as a strong oxidant ($E^o[HCO_4^-/HCO_3^-] = 1.8\ V_{NHE}$ [84]) is known to oxidize sulfides [84], dyes, and 4-chlorophenol [85].

$$HCO_3^- + H_2O_2 \rightarrow HCO_4^- + H_2O \quad (3.3)$$

However, phenol degradation by the H_2O_2/HCO_3^- system was negligible under the conditions employed in this study (Figure 3.1). It appears that much higher concentrations of HCO_3^- and H_2O_2 may be required to generate a significant level of HCO_4^-.

Compared to the Co(II)/HCO_3^-/H_2O_2 system (a similar Fenton-like system [86, 87]), the Cu(II)/HCO_3^-/H_2O_2 system appears to have lower catalytic activity for decomposing H_2O_2 into reactive oxidants; the rates of both phenol degradation and H_2O_2 decomposition were lower (Figure 3.1). However, the Cu(II)/HCO_3^-/H_2O_2 system used H_2O_2 more efficiently (Figure 3.3), implying that the yields of reactive oxidants are higher or that reactive oxidants that are more selective toward the reaction with phenol are generated.

3.3.2. Nature of reactive oxidants

Earlier studies suggested that Cu(III) species are the major reactive oxidants produced by the Cu(II)/H_2O_2 system under neutral and alkaline pH conditions [40, 49, 83], and that •OH may be dominantly produced under lower pH conditions [40, 49]. However, more recently, Lee et al. suggested that Cu(III) species are dominantly produced regardless of pH in the Cu(II)/H_2O_2 system, and that they exhibit •OH-like reactivity [50].

In the Cu(II)/HCO_3^-/H_2O_2 system, discrepant views were presented about the identity of the reactive oxidants [54, 55]. Cheng et al. [54] and Peng et al. [55] suggested Cu(III) and •OH as the major reactive oxidants, respectively. This discrepancy appears to result mainly from different observations of the effects of radical scavengers, which did not inhibit the degradation of the target compound in Cheng et al.'s study, whereas Peng et al. observed significant inhibitory effects by radical scavengers. However, the inhibitory effects by typical •OH scavengers, such as 2-propanol and *tert*-butanol, do not necessarily identify •OH as the major reactive oxidant, because the •OH scavengers can also react with Cu(III) [50, 83]. Various Cu(III) species of different reactivity can exist, depending on their ligands, and some of them can have high reactivity with 2-propanol and *tert*-butanol.

Experimental results in this study present evidence against •OH, supporting the production of Cu(III) species as major reactive oxidants in the Cu(II)/HCO_3^-/H_2O_2 system. First, the failure of excess *tert*-butanol to quench the phenol degradation is not explained by the reaction of •OH (Figure 3.7); the rate of phenol degradation instead increased, for which no clear explanation can be provided. Although the addition of methanol somewhat inhibited the phenol degradation (Figure 3.7), the degree

of inhibition (40% decrease of k at 1 M methanol) is far from the observation anticipated from the reaction of $^{\bullet}OH$. The concentrations and second-order rate constants of the compounds present in the solution were as follows:

$[Phenol]_0 = 0.1$ mM, $k(^{\bullet}OH + phenol\ (at\ pH\ 10)) = 8.3 \times 10^9\ M^{-1}s^{-1}$;

$[H_2O_2]_0 = 10$ mM, $k(^{\bullet}OH + H_2O_2) = 3 \times 10^7\ M^{-1}s^{-1}$;

$[HCO_3^-]_0 = 50$ mM, $k(^{\bullet}OH + HCO_3^-/CO_3^{2-}\ (at\ pH\ 10)) = 1.4 \times 10^8\ M^{-1}s^{-1}$;

[Methanol] = 1 M, $k(^{\bullet}OH + methanol) = 9.7 \times 10^8\ M^{-1}s^{-1}$ [77]

Given these concentrations, almost complete quenching of $^{\bullet}OH$ by 1 M methanol would be anticipated. Second, the negligible degradation of benzoic acid (Figure 3.6) also weighs against the reaction of $^{\bullet}OH$; in fact, the second-order rate constant of benzoic acid (benzoate, $k(^{\bullet}OH + benzoate) = 5.9 \times 10^9\ M^{-1}s^{-1}$) is comparable to that of phenol ($k(^{\bullet}OH + phenol\ (at\ pH\ 10)) = 8.3 \times 10^9\ M^{-1}s^{-1}$) [77].

The reactivity of Cu(III) species (likely present as Cu(III) complexes) is believed to vary with the ligands coordinated to Cu(III). Different Cu(III) species including Cu(III)-carbonate complexes can be produced by the Cu(II)/HCO_3^-/H_2O_2 system, and the speciation of these Cu(III) complexes is determined by several parameters, such as pH and concentrations of Cu(III) and HCO_3^-. Therefore, the reactivity of Cu(III) species formed in the Cu(II)/HCO_3^-/H_2O_2 system can vary depending on these parameters.

The different trends in the pH-dependency of phenol and RB5 degradation by the Cu(II)/HCO_3^-/H_2O_2 system (Figures 3.5a and 3.5c) may be attributed to the pH-dependent Cu(III) speciation. At pH > 10, weaker oxidizing species (which can degrade RB5 but hardly phenol) appear to be formed; these species may be Cu(III)-hydroxo complexes with high coordination numbers, e.g., $Cu(OH)_3$, $Cu(OH)_4^-$, etc.

The discrepant effects of oxidant scavengers observed by previous studies [54, 55] are also likely due to the occurrence of Cu(III) species of different reactivities. Cheng et al. [54] used higher concentrations of Cu(II) and HCO_3^- than Peng et al. [55]; this difference may have affected the speciation of Cu(III), producing Cu(III) species of different reactivities with the oxidant scavengers.

3.3.3. Factors affecting the production of reactive oxidants

In the Cu(II)/HCO_3^-/H_2O_2 system, factors such as pH and doses of Cu(II), HCO_3^- and H_2O_2 affect the production of reactive oxidants and the resultant phenol degradation. Increasing doses of Cu(II) and HCO_3^- increased the rate of phenol degradation (Figure 3.4). The increase in the dose of Cu(II) (as a catalyst) accelerates the catalytic decomposition of H_2O_2 into reactive oxidants. In addition, the increase in the dose of HCO_3^- leads to increased formation of Cu(II)-carbonate complexes that are believed to have higher reactivity with H_2O_2 than those in the absence of HCO_3^- (e.g., Cu(II) oxide).

According to the calculation using MINEQL+ 4.6, more Cu(II)-carbonate complexes, such as $CuCO_3$ and $Cu(CO_3)_2^{2-}$, evolved under mild alkaline conditions when the dose of HCO_3^- increased from 1 mM to 100 mM (Figure 3.11).

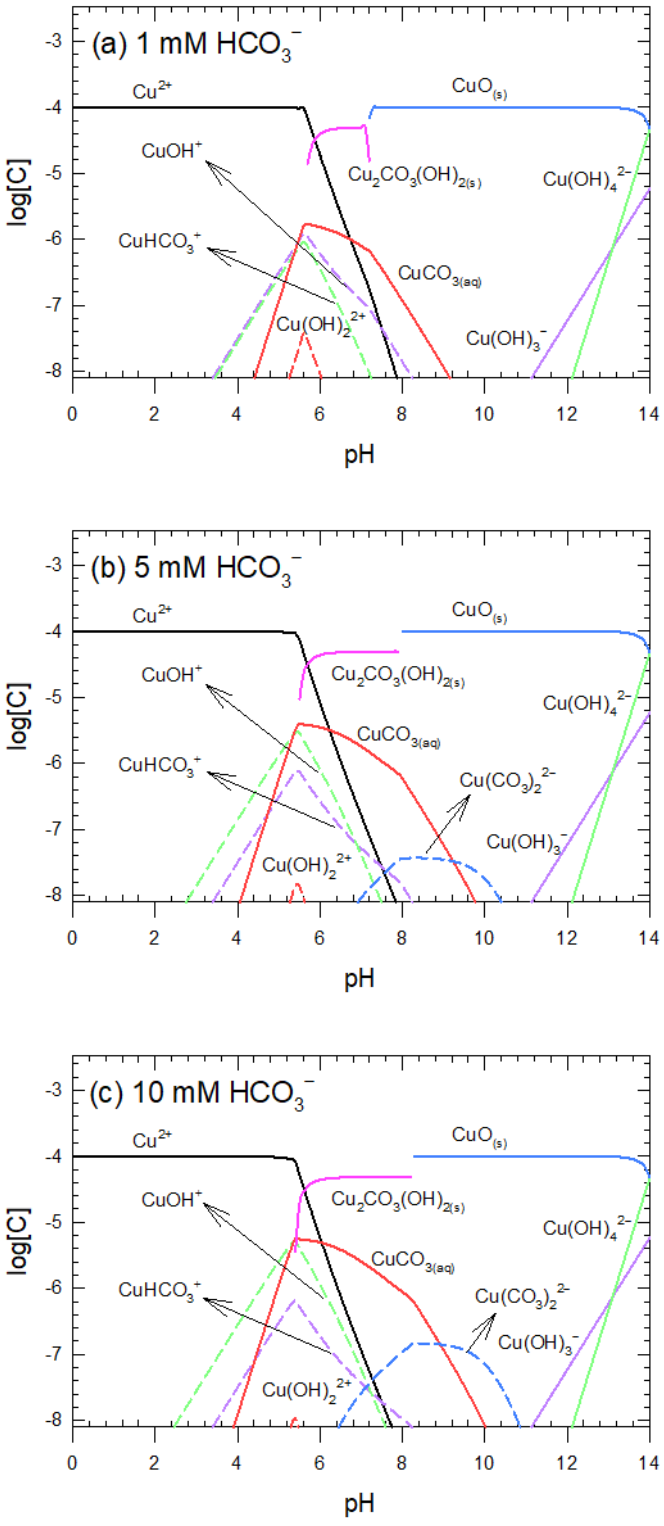

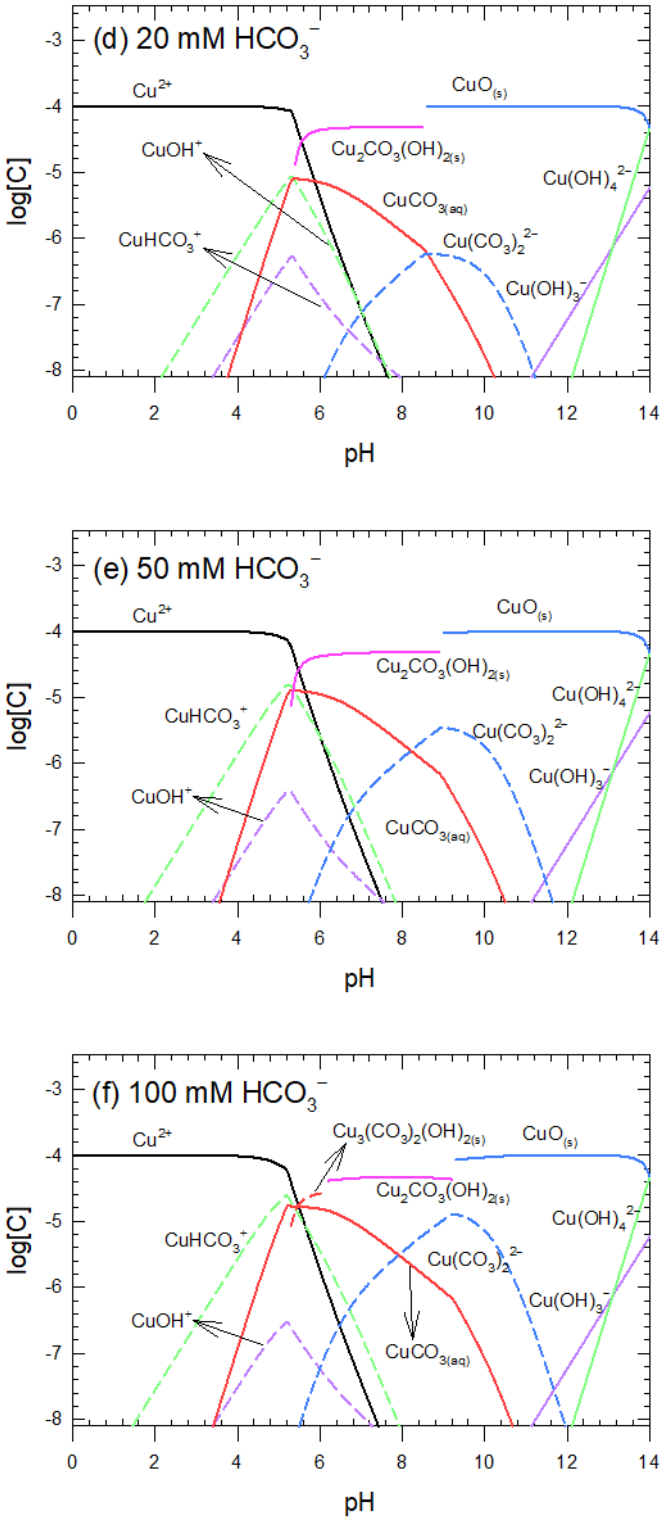

Figure 3.11. Speciation of Cu(II) in the presence of HCO_3^- with different concentrations, calculated by MINEQL+ 4.6 ($[Cu(II)]_0$ = 0.1 mM).

For the H_2O_2 dose, the rate of phenol degradation was maximized at 5 mM H_2O_2 (Figure 3.4). The inhibitory effect at $[H_2O_2] > 5$ mM is attributed to the scavenging of reactive oxidants by excess H_2O_2. Considering that the phenol degradation was not inhibited (or slowed down) by an excess amount of HCO_3^-, the reactions of reactive oxidants (likely Cu(III)-carbonate complexes) may be more selective to H_2O_2 than HCO_3^-. Note that, for $^{\bullet}OH$, the reaction with HCO_3^- is even faster than that with H_2O_2 (refer to $k(^{\bullet}OH + H_2O_2) = 3 \times 10^7\ M^{-1}s^{-1}$ and $k(^{\bullet}OH + HCO_3^-/CO_3^{2-}$ (at pH 10)) $= 1.4 \times 10^8\ M^{-1}s^{-1}$ [77]).

The phenol degradation was optimized at pH 10 (Figure 3.5a). The degradation of phenol at pH < 10 accelerates because the catalytic decomposition of H_2O_2 into reactive oxidants accelerates with increasing pH (Figure 3.5b). The reduction of Cu(II) by H_2O_2 (reaction 3.1, RDS) accelerates with increasing pH because the reaction proceeds via the complexation of Cu(II) with a deprotonated form of H_2O_2 (HO_2^-, pK_a of H_2O_2 = 11.75) as the primary step. As described in Section 3.3.2, at pH > 10, weaker Cu(III) species that hardly degrade phenol may arise.

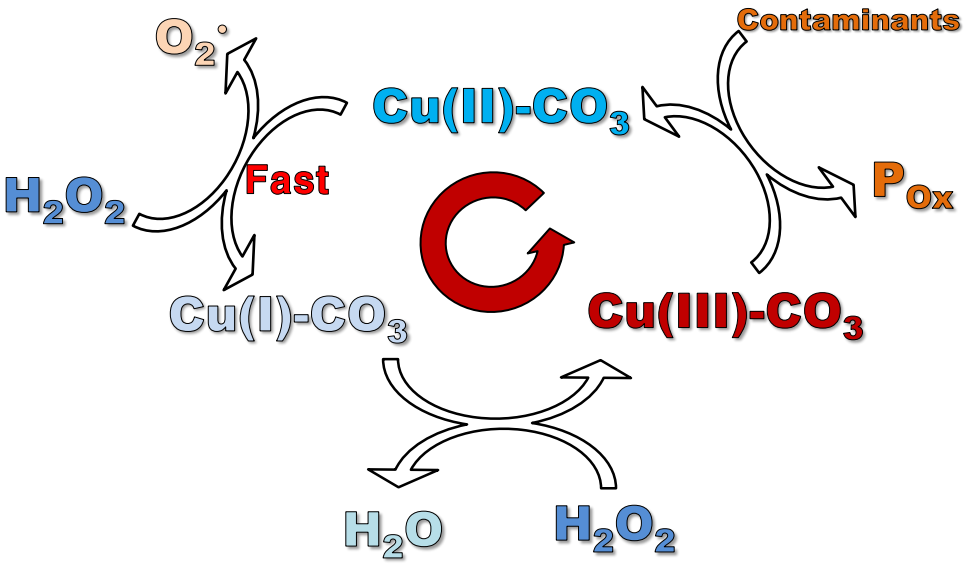

Scheme 3.1. Accelerated reaction kinetics by complexation between copper and carbonates.

3.3.4. Applications of the Cu(II)/HCO_3^-/H_2O_2 system

The Cu(II)/HCO_3^-/H_2O_2 system can potentially be used to oxidize refractory organic contaminants in water and wastewater. For practical application, Cu(II) needs to be immobilized in order to recycle the catalyst and minimize the (eco)toxic impacts of released copper ions. Particularly for treating drinking water, the concentration of released copper ions should be controlled at less than 1 mg/L; the regulation levels of copper in Korea and the United States are 1 mg/L (15.7 μM) and 1.3 mg/L (20.5

μM), respectively [88, 89].

In addition, as demonstrated in Figure 3.8, aeration by CO_2 gas is an effective alternative for supplying HCO_3^- into water to implement the Cu(II)/HCO_3^-/H_2O_2 system. When the Cu(II)/HCO_3^-/H_2O_2 system is used to treat industrial wastewater, waste CO_2 discharged by neighboring industries may be used for this purpose.

Chapter 4. Activation of Persulfates by NiO-NiC Nanocomposite: High-Valent Nickel Species for Removal of Organic Compounds

4.1. Materials and Methods

4.1.1. Reagents

All chemicals were of reagent grade and used without further purification. All chemicals used in this study obtained from Sigma–Aldrich Co., U.S.A. except acetonitrile (J.T. Baker Co., U.S.A.). All solutions were prepared in deionized (DI) water (18.2 MΩ·cm Milli–Q water, Millipore Co., U.S.A.). Stock solutions of acetaminophen (AAP, 1 mM), benzoic acid (BA, 10 mM), carbamazepine (CBZ, 0.125 mM), 4–chlorophenol (4-CP, 10 mM), furfuryl alcohol (FFA, 10 mM), PDS (100 mM) and phenol (10 mM) were prepared and stored at 4ºC until use.

4.1.2. Synthesis of NiOCs

The NiOC was synthesized by a ligand-assisted method [90]. The 50 mL of Nickel(II) nitrate solution ($Ni(NO_3)_2 \cdot 6H_2O$, 0.5 M) was chelated by dropwise addition of the 50 mL of sodium citrate solution (1.0 M) using a burette at the rate of 2 drops/s, where the mixture was well-stirred for 30 min at room temperature (22 ± 2°C). The resulting solution was evaporated by heating at 60°C for overnight (12 h), and subsequently gel-like mixture was transferred to crucible. Next, the mixture was sintered at 500ºC for 3 h to obtain the powdered sample. The final black powder product was washed three times with DI water and dried at 60°C for 4 h (denoted as NiOC or NiOC(500°C)). For the optimizing sintering temperature, another NiOCs were synthesized by the same method; all steps were identical, but sintered at 300°C and 700°C (denoted as NiOC(300°C) and NiOC(700°C), respectively). For some experiments, the synthetic NiOC was further treated with an excess amount of PDS solution (100 mM) in screw-capped scintillation vials during 72 h. The resulting PDS-treated NiOC powder was washed 3 times with deaerated DI water (N_2 sparged) and dried in the N_2 filled chamber for 48 h. The final PDS-treated NiOC powder was stored in Teflon®-sealed conical tube filled with pure N_2 gas until use.

4.1.3. Characterization

X–ray diffraction (XRD) patterns of the synthetic NiOCs and commercialized nickel oxides (i.e., micro NiO and nano NiO) were recorded using an X-ray diffractometer (D8 ADVANCE, Bruker AXS Inc., U.S.A.) with Cu–Kα radiation. A high–resolution transmission electron microscope, coupled with an energy dispersive X-ray spectrometer (HRTEM/EDS) (JEM–2100F, JEOL Co., Japan) was used to analyse morphology and surface elemental distribution with electron beam accelerated at 200 kV. A magnetic property measurement was performed using a physical property measurement system

(PPMS-14, Quantum Design Inc., U.S.A.) at 300 K. X-ray absorption near edge structure (XANES) spectra of the NiOC powders were recorded by an X-ray absorption spectrophotometer (R-XAS, Rigaku Co., Japan) in order to verify the valence oxidation state.

4.1.4. Experimental procedure

All experiments were performed by batch reaction in a 125 mL of Erlenmeyer flask at room temperature (22 ± 2°C). Most experiments were conducted with 100 mL of suspensions containing the NiOC powder (0.2 g/L), the target organic compounds (0.1 mM), and an aliquot of PDS stock solution. 50 mL of the reaction solution was used for few experiments including electrochemical measurements. Initial pH of the solution buffered by phosphates (phosphate buffer solution, PBS) was adjusted using NaOH (0.1 N) and $HClO_4$ (0.1 N) at 7.0, and the solution pH was varied by less than 0.2 units during the reaction. For initiating the reaction, the pre-weighed NiOC powder was injected into reaction solution. At predetermined time intervals, samples (1 mL) were withdrawn and immediately filtered using a 0.2 μm hydrophilic PTFE syringe filter (Advantec MFS Inc., U.S.A.) during the reaction. All experiments were performed at least in triplicates for each reaction conditions. Average values with standard deviations (error bars) were presented. For conducting the additional set of experiments, natural water catchments (ground, surface, and sea water) were used as after filtering with a 0.45 μm filter within 24 h after sampling and stored at 4°C until use.

4.1.5. EPR spectroscopy

The EPR spectra were recorded by an EPR spectrometer (JES-X310, JEOL Co., Japan). The 5,5-dimethyl-1-pyrroline N-oxide (DMPO, 10 mM) was used for spin-trapping agent in order to detect reactive species. For the EPR analysis, samples were withdrawn from the batch reactor, subsequently placed in a quartz flat cell and scanned EPR signals of the DMPO adducts under the following conditions: microwave frequency at 9.42 GHz, microwave power at 1.00 mW, modulation frequency at 100 kHz, and modulation amplitude at 2.0 G.

4.1.6. Linear sweep voltammetry

Linear sweep voltammetry (LSV) were carried out using potentiostat (VSP, BioLogic Science Instruments Ltd., France). The NiOC powder (10 mg) and carbon black (Vulcan® XC-72R, 5 mg) as a conducting material were firstly dispersed in 10% (w/w) polyvinylidene difluoride (PVDF)/dimethylacetamide (DMAc) solution. The mixture was well-spread on fluorine doped tin oxide (FTO) glass and dried for 30 min at 65°C. The reactor was equipped with the NiOC-coated FTO glass, a platinum plate (2.5 cm x 1.5 cm), and a saturated calomel electrode (SCE) serving as a working, counter, and reference electrode, respectively, and filled with $NaClO_4$ solution (0.1 M) as an electrolyte. The current at a working electrode was recorded with the potential increasing (20 mV/s

for scan rate) from 0.3 to 1.6 V.

4.1.7. Analytical methods

The concentrations of the organic compounds were determined by rapid separation liquid chromatography (RSLC, UltiMate™ 3000, Dionex Co., U.S.A.) with UV absorbance detection (at 241, 227, 285, 230, 220, and 277 nm for AAP, BA, CBZ, 4-CP, FFA, and phenol, respectively). Separation was performed on a 2.1 mm × 150 mm, 5 μm 120Å C18 column (Acclaim™ 120 C18 column, ThermoFisher Scientific Inc., U.S.A.). A binary mixture of phosphoric acid solution (0.1% v/v) and acetonitrile was used as the mobile phase at a flow rate of 0.8 mL/min except CBZ analysis (with phosphoric acid solution (0.1% v/v), methanol, and acetonitrile). The residual concentration of PDS was measured by a spectrophotometer (Lambda 465, Perkin-Elmer Inc., U.S.A.) using modified potassium iodide method, and detailed procedures are described elsewhere [58]. The concentration of total organic carbon (TOC) was measured by TOC analyser (TOC-V/CPH, Shimadzu Co., Japan). The RSLC system coupled with a quadrupole-Orbitrap mass spectrometer (Q Exactive™, ThermoFisher Scientific Inc., U.S.A.) (LC/MS) was used for the analyzing degradation products of 4-CP. Detailed analyzing conditions for the LC/MS are described elsewhere [91]. The concentration of total dissolved nickel (nickel leaching) was determined by an atomic absorption spectroscopy (AAS, AAnalyst 700, Perkin-Elmer Inc., U.S.A.) with Ni Lumina™ hollow cathode lamp at 232 nm.

4.2. Results

4.2.1. Characterization of NiOCs

The NiOC powder products were black precipitates and exhibited magnetic properties (Figures 4.1a and 4.2). XRD patterns of NiOCs and commercial NiOs recorded sharpen and well-crystallized peaks except for the NiOC(300°C) and the nano NiO which were shown broaden peaks with relatively poor crystallinity. The XRD patterns of NiOCs designated co-existence of nickel oxide (NiO, JCPDS # 01-078-0423) and nickel carbide (NiC, JCPDS # 00-014-0020) peaks except the NiOC(700°C) (Figure 4.1b). Sintering of the NiOCs at elevated temperatures can enhance the crystallinity evidenced by sharpen XRD patterns but appears to sudden elimination of nickel oxide at 700°C.

HRTEM images indicated that the NiOC forms agglomerates of broad size-distributed nanoparticles (10 ~ 100 nm) (Figure 4.3a), but relatively uniform-sized in commercial nano NiO (5 ~ 10 nm) (Figure 4.3b). Additionally, EDS mapping (eliminated the C portion of carbon-supports in a TEM grid) on C, Ni, O displayed that the surface on NiOC has atomic portions of carbon, nickel, and oxygen ratio (C:Ni:O = 6.6:51.5:41.9), (Figures 4.3c, 4.3d, and 4.3e); the atomic ratio of nano NiO has been analysed to be at 49.8:50.2 for Ni:O.

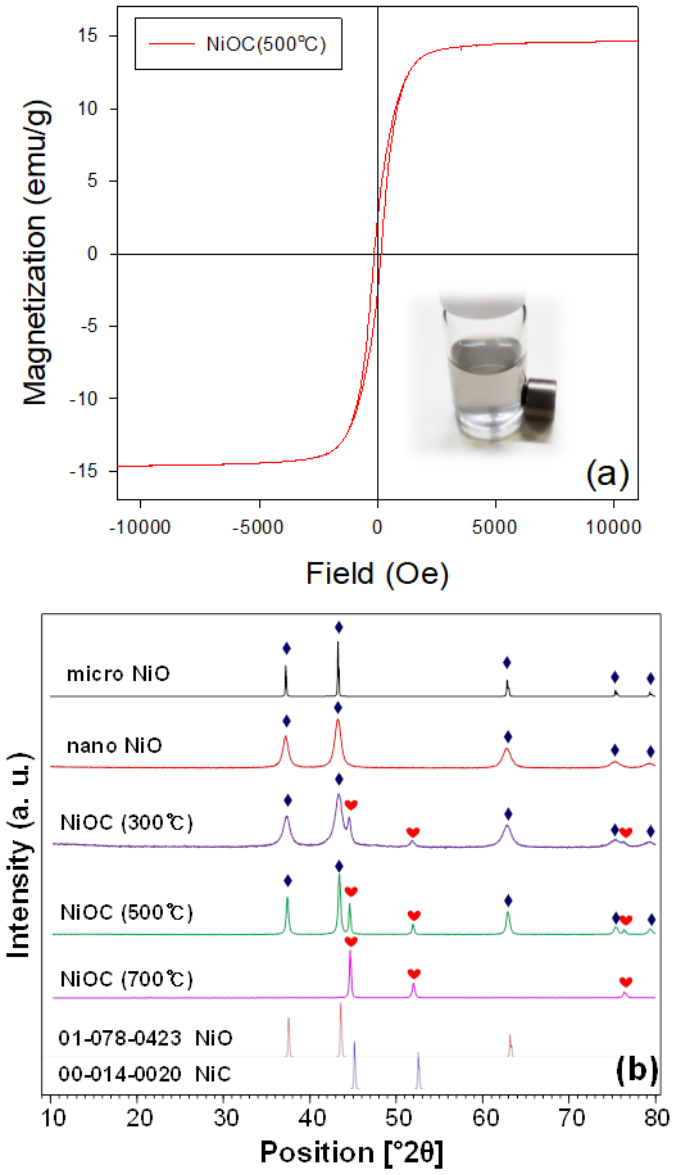

Figure 4.1. Hysteresis loop of the NiOC (a), and X-ray diffraction patterns of NiOCs and commercial NiOs (b).

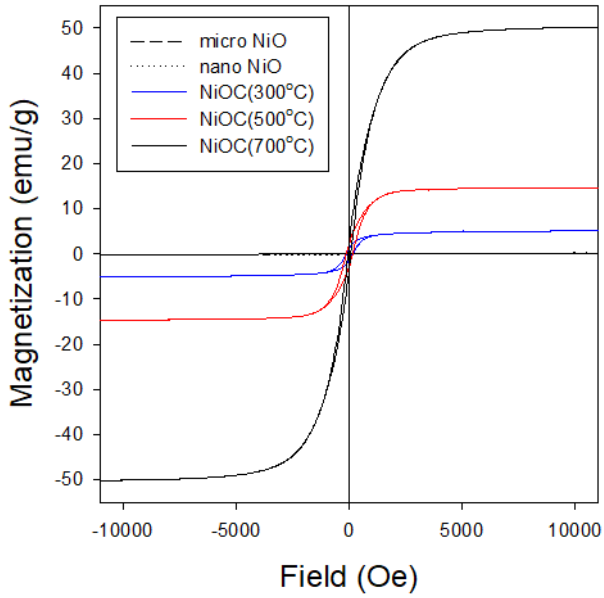

Figure 4.2. Hysteresis loop of NiOCs and NiOs.

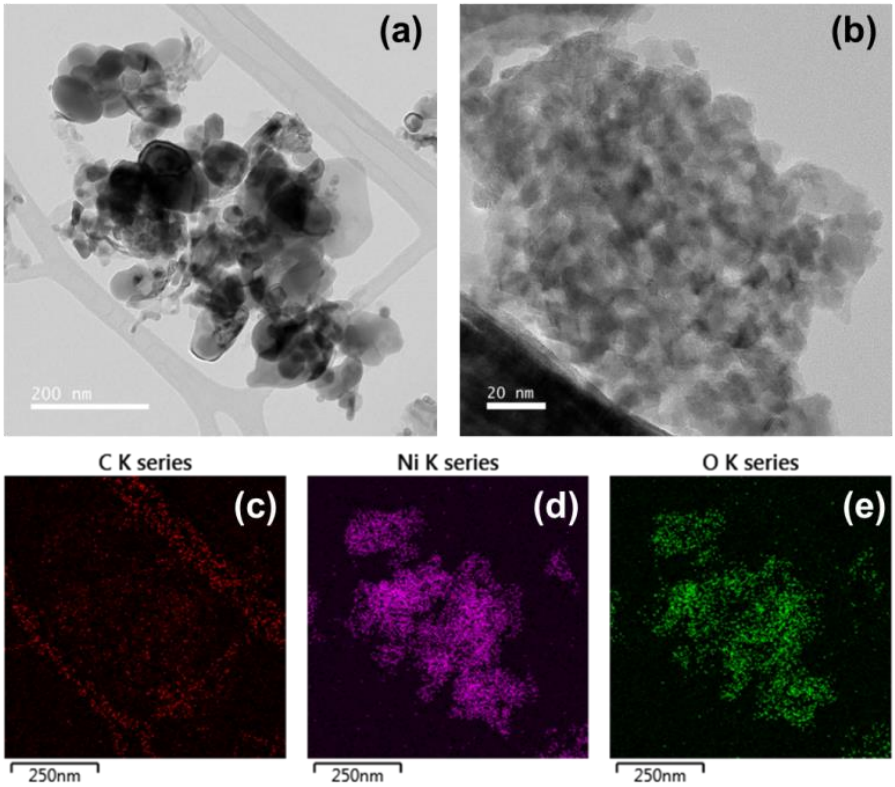

Figure 4.3. HRTEM images of the NiOC (a) and nano NiO (b) and EDS mappings (c for carbon), (d for nickel) and (e for oxygen) of the NiOC.

4.2.2. Degradation of organic compounds

The NiOC coupled with PDS and the respective sets of control reactions (i.e., the PDS only, the Ni(II) ion/PDS system, and the NiOC only) were examined for the degradation of 4-CP (Figure 4.4a). There was no significant degradation or adsorption of 4–CP for 60 min under the control reaction conditions. In contrast, the combination of NiOC and PDS can effectively degrade 4-CP (~ 99.7%) in 60 min. During the 4-CP degradation, approximately 58% of the degraded 4-CP was mineralized and 2.1 μM of the Ni(II) ion was leached in the NiOC/PDS system (Figures 4.5 and 4.6). And also, the degradation rate of 4-CP was gradually elevated approximately 0.011 min^{-1} to 0.068 min^{-1}, where the concentration of NiOC or PDS (i.e., 0.2 g/L for the NiOC and 0.2 mM of PDS, respectively) were fixed experimental sets (Figure 4.7). Notably, the NiOC combination with PDS can efficiently degraded 4-CP (50 ~ 55 % within 60 min) in natural water catchments including groundwater, surface water, and even chloride ion abundant seawater sample (known as an inhibitor of radical species) (Figure 4.8).

Degradation of select organic compounds (AAP, BA, CBZ, 4–CP, FFA, and phenol) was also examined in the NiOC/PDS suspension (Figure 4.4b). The degradation efficacies of phenolic compounds (i.e., phenol and 4-CP) were superior, which was followed by that of AAP. However, FFA hardly degraded and there was negligible degradation on BA and CBZ.

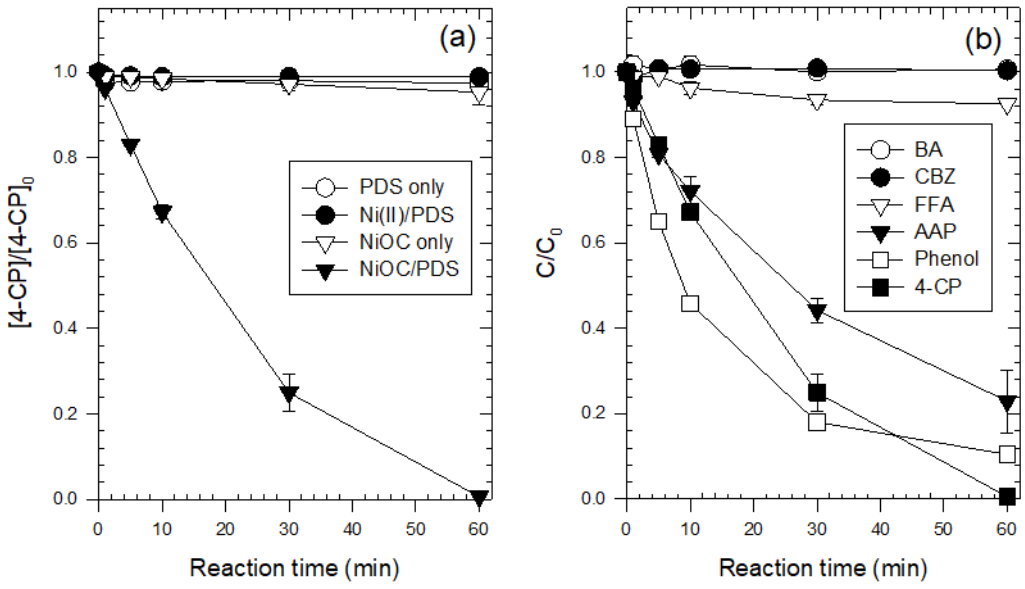

Figure 4.4. Degradation of 4-CP (a) and various organic compounds (b) by the NiOC/PDS system ($[NiOC]_0$ = 0.2 g/L, $[4\text{-CP}]_0$ = 0.1 mM, $[Ni(II)]_0$ = 0.1 mM, $[PDS]_0$ = 0.2 mM, $[PBS]_0$ = 1 mM, pH = 7.0 for (a); $[BA]_0 = [CBZ]_0 = [FFA]_0 = [Phenol]_0 = [4\text{-CP}]_0$ = 0.1 mM for (b)).

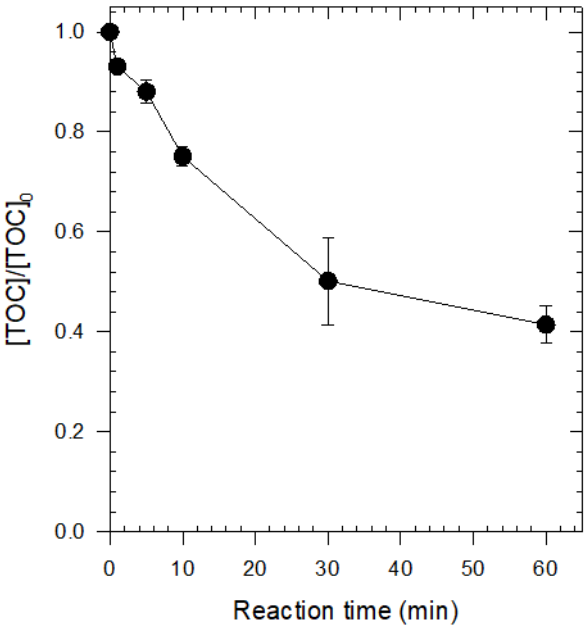

Figure 4.5. TOC removal during 4-CP oxidative degradation by NiOC/PDS system ($[NiOC]_0$ = 0.2 g/L, $[4\text{-CP}]_0$ = 0.1 mM, $[PDS]_0$ = 0.2 mM, $[PBS]_0$ = 1 mM, pH = 7.0).

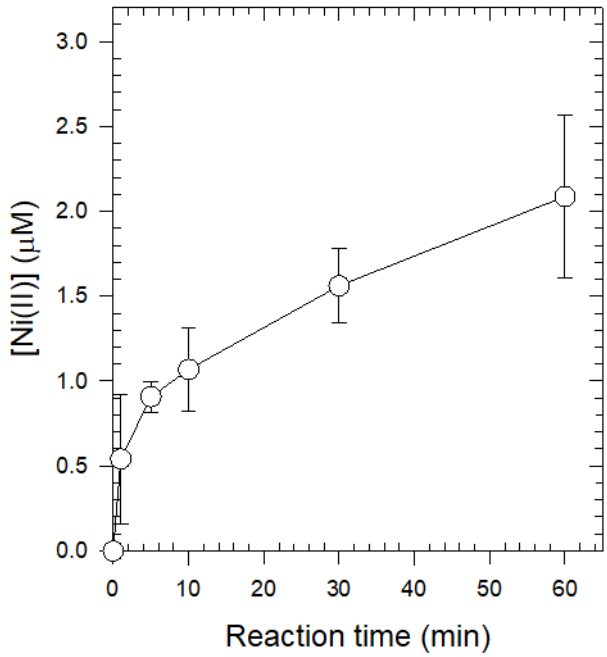

Figure 4.6. Leaching amount of Ni(II) in the NiOC/PDS system ($[NiOC]_0$ = 0.2 g/L, $[4\text{-CP}]_0$ = 0.1 mM, $[PDS]_0$ = 0.2 mM, $[PBS]_0$ = 1 mM, pH = 7.0).

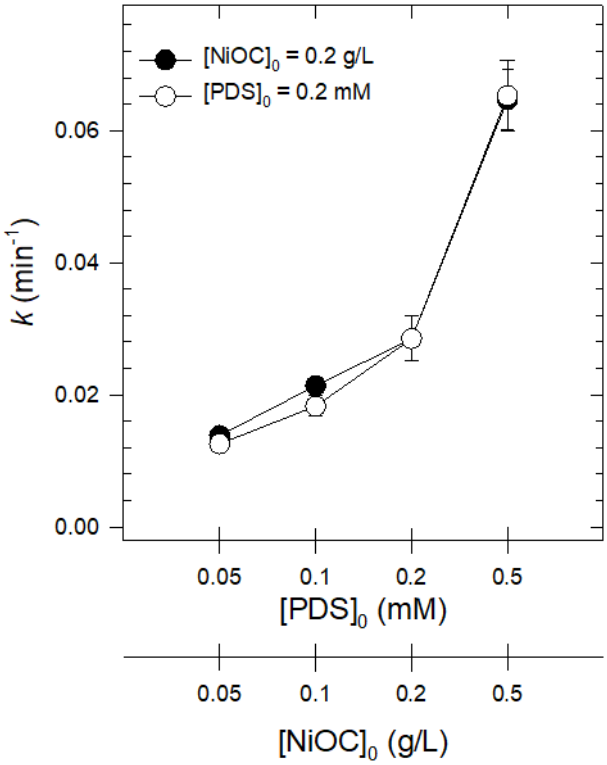

Figure 4.7. Effect of PDS and NiOC doses on degradation of 4-CP ($[4\text{-CP}]_0$ = 0.1 mM, $[PBS]_0$ = 1 mM, pH = 7.0, reaction time = 60 min).

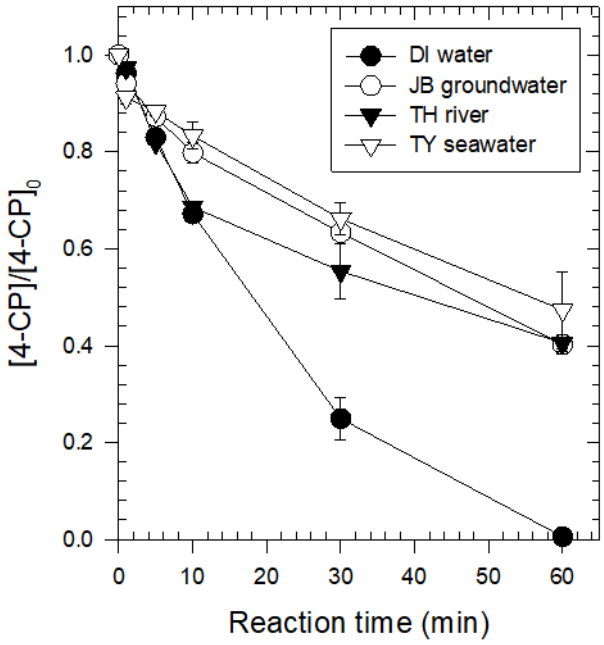

Figure 4.8. Degradation of 4-CP by NiOC/PDS system in natural waters ($[NiOC]_0$ = 0.2 g/L, $[4\text{-CP}]_0$ = 0.1 mM, $[PDS]_0$ = 0.2 mM, $[PBS]_0$ = 1 mM, pH = 7.0).

Additionally, in order to evaluate the reusability of NiOC, degradation of 4-CP was carried out repeatedly in the NiOC suspension coupled with PDS. Firstly, the NiOC was injected once at the initiating of the reaction, and subsequently added 4–CP (0.1 mM) and PDS (0.2 mM) for every 60 min (Figure 4.9). The degradation efficacy of 4-CP slightly decreased over the three reaction cycles (99.7%, 99%, and 95% at each cycle). The accumulated oxidation products (intermediates not fully mineralized) may be attributable to interference in the solution and on the NiOC surface decreasing 4-CP degradation efficacy.

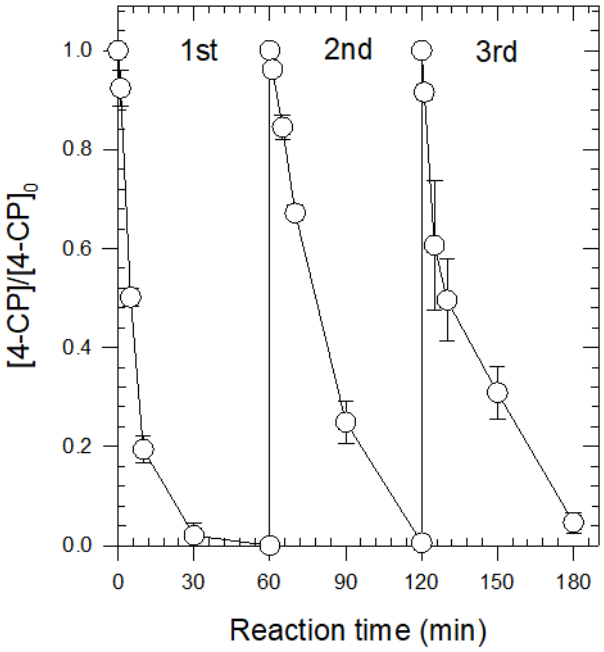

Figure 4.9. Repeated degradation of 4-CP by NiOC/PDS system ($[NiOC]_0$ = 0.2 g/L, $[4\text{-CP}]_0$ = 0.1 mM, $[PDS]_0$ = 0.2 mM, $[PBS]_0$ = 1 mM, pH = 7.0).

4.2.3. Catalytic performances of NiOCs and commercial NiOs

Catalytic performances of synthetic NiOCs and commercial NiOs were evaluated though the concept of PDS utilization efficiency (100*Δ[4-CP]/Δ[PDS] (%)) (Figures 4.10 and 4.11). The oxidative degradation of 4-CP was shown to be maximally accelerated by the NiOC(500°C) in the presence of PDS, which was followed by that of NiOC(300°C) (34%) and NiOC(700°C) (16%), respectively (Figure 4.10a). Same order on the decomposition of PDS was observed in Figure 4.10b. Collectively, PDS utilization efficiency was maximized in the NiOC(500°C) coupled with PDS system (Figure 4.10c).

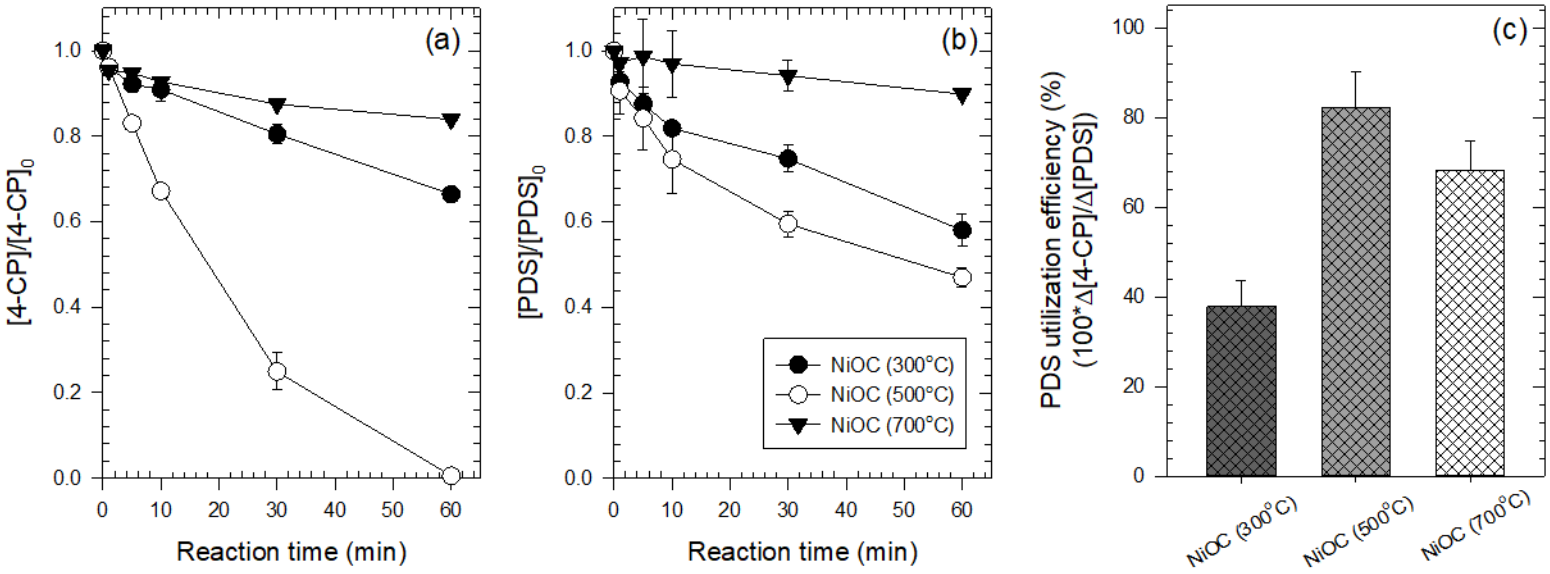

Figure 4.10. Effect of sintering temperature on degradation of 4-CP (a), decomposition of PDS (b) and PDS utilization efficiency (c) in the NiOC/PDS system ($[NiOC(300°C)]_0 = [NiOC(500°C)]_0 = [NiOC(700°C)]_0 = 0.2$ g/L, $[4\text{-CP}]_0 = 0.1$ mM, $[PDS]_0 = 0.2$ mM, $[PBS]_0 = 1$ mM, pH = 7.0).

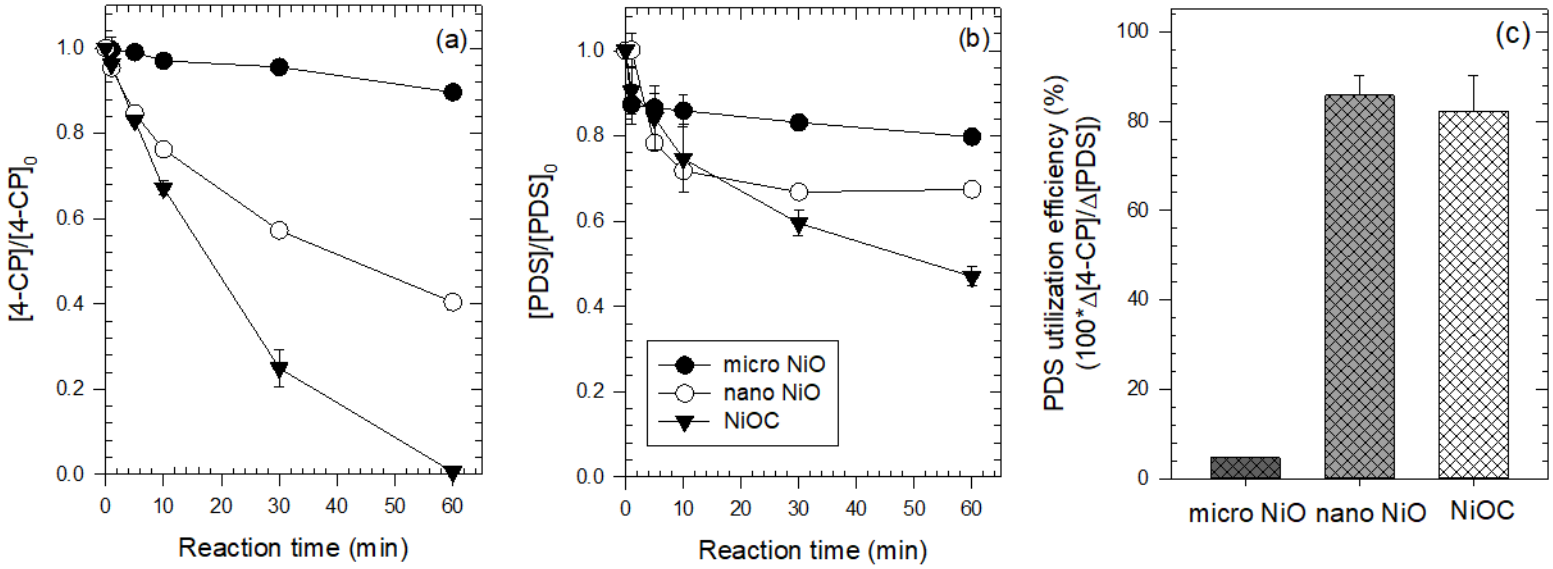

Figure 4.11. Comparison of the NiOC and commercial NiOs on degradation of 4-CP (a), decomposition of PDS (b) and PDS utilization efficiency (c) in the presence of PDS ($[NiOC]_0$ = $[micro\ NiO]_0$ = $[nano\ NiO]_0$ = 0.2 g/L, $[4\text{-}CP]_0$ = 0.1 mM, $[PDS]_0$ = 0.2 mM, $[PBS]_0$ = 1 mM, pH = 7.0).

As shown in Figure 4.11a, the 4-CP degradation capability of the combination of NiOC/PDS was superior, followed by the nano NiO/PDS system (approximately 60%), but no significant degradation was exhibited in the micro NiO/PDS system (10%). Also, the identical series on the decomposition of PDS was placed in Figure 4.11b. Notably, in Figure 4.11c, PDS utilization efficiency was close to 90% both the NiOC/PDS system and the nano NiO/PDS system. In contrast, PDS utilization efficiency was exhibited by less than 10 % in micro NiO/PDS system.

4.2.4. Decomposition of PDS and Linear sweep voltammetry

The decomposition of PDS in the NiOC/PDS system was measured in the presence of 4-CP and absence of 4-CP (Figure 4.12a). Interestingly, the noticeable decomposition of PDS was observed only in the presence of all reactants at once (i.e., the NiOC, PDS, and 4-CP). The other systems which had one missing reactants (i.e., the NiOC/PDS system and the PDS/4-CP system) were not shown to be significant decomposition of PDS.

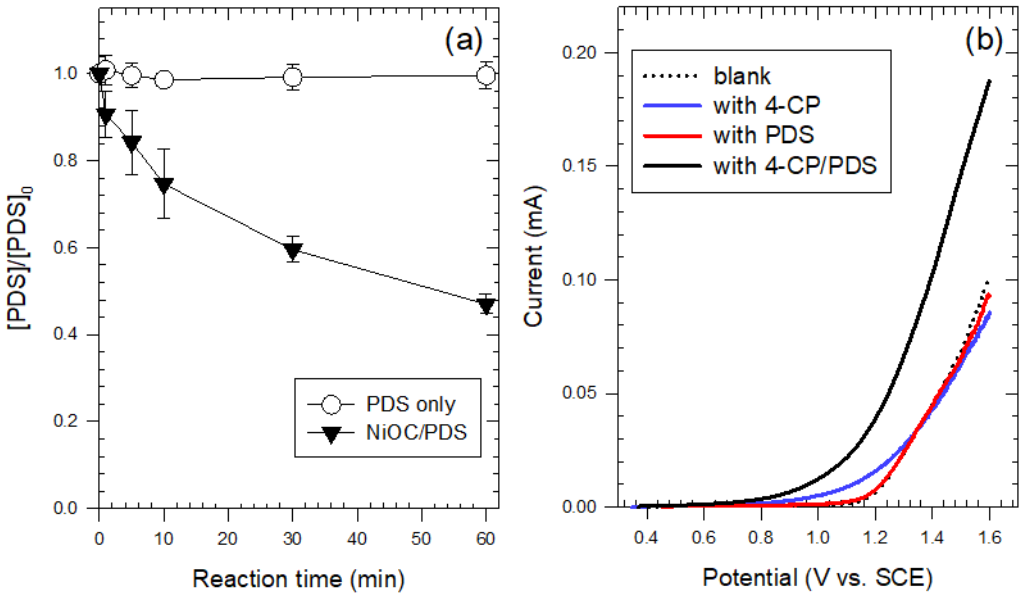

Figure 4.12. Decomposition of PDS (a) in the NiOC/PDS system and linear sweep voltammograms obtained (b) by the NiOC–FTO glass electrode in the presence of PDS and 4-CP ($[NiOC]_0$ = 0.2 g/L, $[4\text{-CP}]_0$ = 0.1 mM, $[PDS]_0$ = 0.2 mM, $[PBS]_0$ = 1 mM, pH = 7.0 for (a); [W. E.]: NiOC-FTO glass, [C. E.]: Pt plate, [R. E.]: SCE, $[NaClO_4]_0$ = 100 mM, $[4\text{-CP}]_0$ = 0.1 mM, $[PDS]_0$ = 0.2 mM, $[PBS]_0$ = 1 mM, pH = 7.0 for (b)).

Linear sweep voltammetry (LSV) were conducted in a reactor containing $NaClO_4$ electrolyte, 4-CP and PDS with a NiOC-coated FTO glass as the working electrode (Figure 4.12b). The current at a

working electrode was no noticeable increase in the voltage range (0.3 to 1.6 V) with phenol or PDS only added conditions compared to blank experimental set (electrolyte only). However, significant synergistic increase of the current was recorded in reactor set containing both 4-CP and PDS, where electron transfer reaction of reactants to the working electrode effectively.

4.2.5. Effect of methanol and EPR analysis

The effect of radical scavenger on the 4-CP degradation was examined (Figure 4.13); methanol was used as the radical (e.g., $^{\bullet}OH$, $SO_4^{\bullet-}$) scavenger. The methanol has been known to be scavenging both free $^{\bullet}OH$ and $SO_4^{\bullet-}$ in bulk phase and surface-bound $^{\bullet}OH$s [92]. As shown in Figures 4.13a and 4.13b, the addition of methanol did not much significantly affect inhibition on the both degradation rate of 4-CP and decomposition rate of PDS.

Additionally, the EPR analysis of the NiOC coupled with PDS was carried out in the presence of 4-CP and absence of 4-CP (Figure 4.14). There was no detection of DMPO spin adducts of $^{\bullet}OH$ or $SO_4^{\bullet-}$, while weak DMPOX signals were observed in 5 min and 10 min of samples, which were conducted in the absence of 4-CP (Figure 4.14a). Notably, no significant signal of DMPO adducts was shown in the presence of 4-CP (Figure 4.14b).

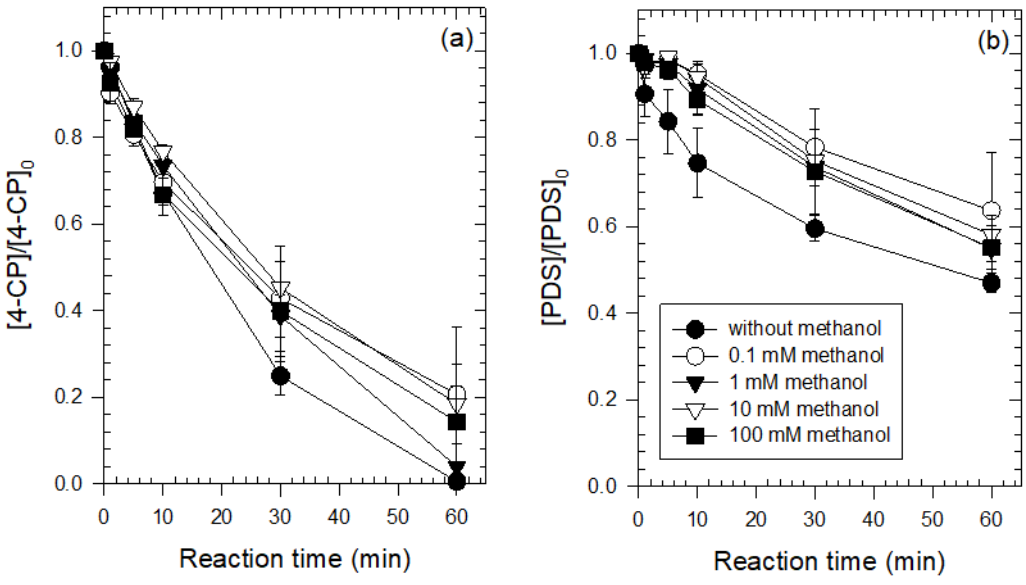

Figure 4.13. Effect of methanol doses on (a) degradation of 4-CP and (b) decomposition of PDS in the NiOC/PDS system ($[NiOC]_0$ = 0.2 g/L, $[4\text{-CP}]_0$ = 0.1 mM, $[PDS]_0$ = 0.2 mM, $[PBS]_0$ = 1 mM, pH = 7.0).

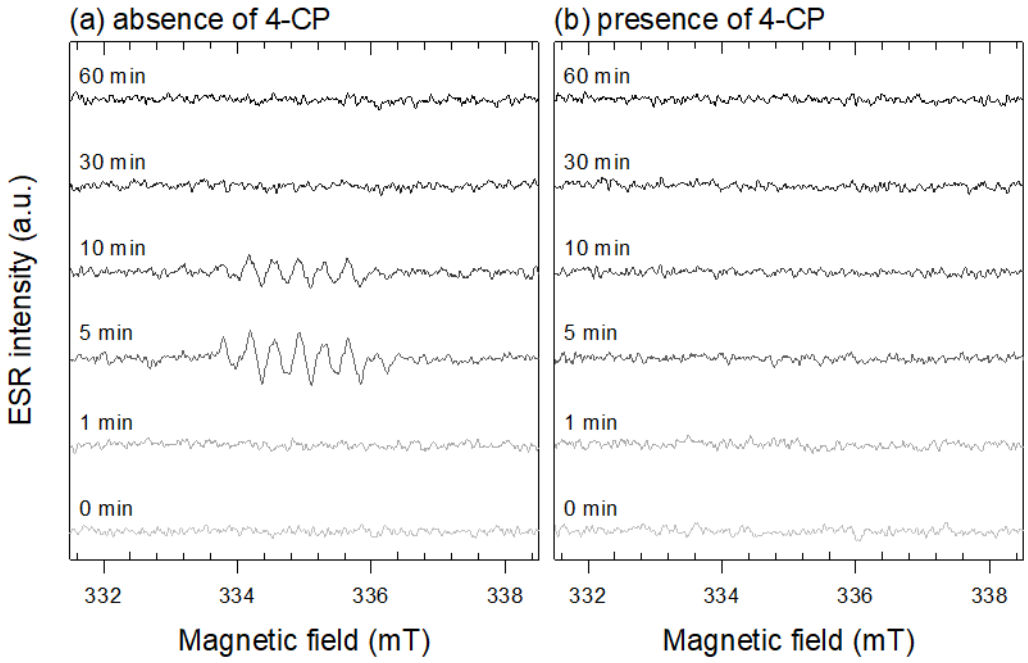

Figure 4.14. ESR spectra obtained by spin trapping with DMPO in the NiOC/PDS system: (a) Absence and (b) presence of 4-CP ($[DMPO]_0$ = 10 mM, $[NiOC]_0$ = 0.2 g/L, $[4\text{-CP}]_0$ = 0.1 mM, $[PDS]_0$ = 0.2 mM, $[PBS]_0$ = 1 mM, pH = 7.0).

4.2.6. The PDS-pretreated NiOC and XANES analysis

The NiOC pre-treated with PDS was used to examine the oxidizing power for 4-CP degradation in the absence of PDS (Figure 4.15a). In order to drastically display the oxidizing capacity of the PDS-treated NiOC, 10-fold higher concentration of material suspension was used and decreased initial concentration of 4-CP to 0.01 mM. Approximately, a quarter of 4-CP was degraded by the PDS-treated NiOC within 60 min.

The Ni K edge XANES spectrum of the PDS-treated NiOC (red line) was shifted to right side compared to pristine (black line), which right-shifted spectrum was known for an elevated oxidation state of valence (Figure 4.15b) [93]. The nickel atoms exposed on the surface of NiOC were converted to high-valent nickel state by the treatment of excess PDS.

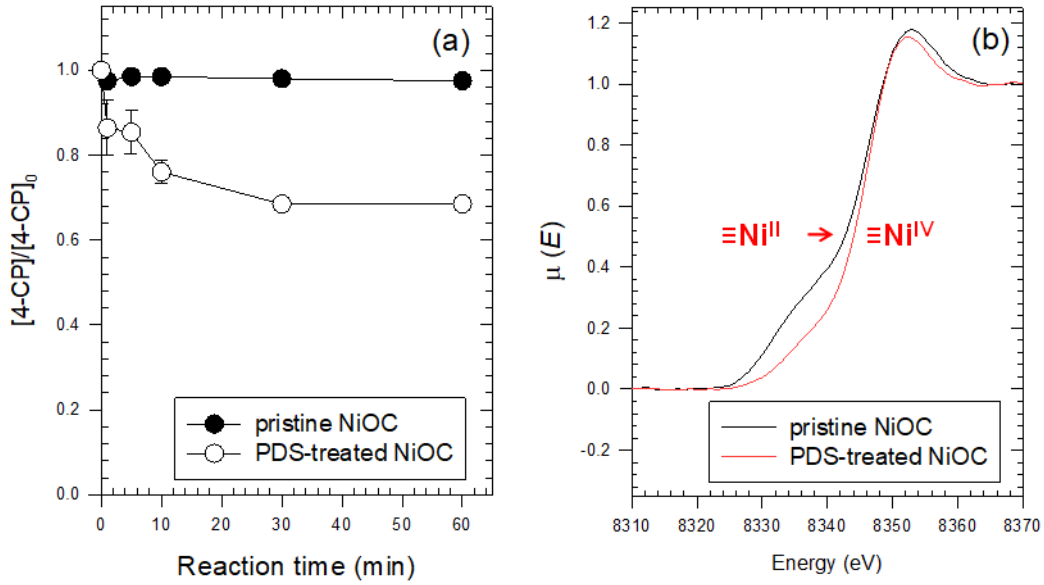

Figure 4.15. Degradation of 4-CP (a) by the PDS treated NiOC system and Ni K edge XANES for pristine (black) and PDS treated NiOC (red) (b) ($[PDS\text{-}treated\ NiOC]_0 = [NiOC]_0 = 2.0$ g/L, $[4\text{-}CP]_0 =$ 0.01 mM, $[PBS]_0 = 1$ mM, pH = 7.0 for (a)).

4.2.7. Oxidation products of 4-CP

9 products from the oxidative degradation of 4-CP by the NiOC suspension coupled with PDS were identified by RSLC and LC/MS analysis. The oxidation products listed in Table 4.1, their abundance and chromatograms for the products are presented by the time-dependent variations in Figures 4.16–4.18. Based on these results, the degradation pathways of 4-CP were depicted in Figure 4.19.

Hydroquinone (Product 1), benzoquinone (Product 2), and 4-chlorocatechol (Product 3) were the primary derivatives of the oxidation, which is consistently reported in previous studies about oxidative degradation of 4-CP using AOPs [94, 95]. Hydroquinone and benzoquinone were further oxidized to produce secondary derivatives such as hydroxybenzoquinone (Product 4), maleic acid (Product 5), and fumaric acid (Product 6). 4-Chlorocatechol was subsequently oxidized to 4-chloro-5-hydroxy-1,2-benzoquinone (Product 7). In addition, polyaromatic compounds (i.e., 5-chloro-2,4-dihydroxybiphenyl (Product 8) and 4-hydroxyphenylbenzoquinone (Product 9)) were also detected.

Table 4.1. Products of 4-CP degradation by the NiOC/PDS system identified by HPLC and LC/MS analysis.

Product No.	Compounds	Chemical formula	Theoretical m/z	Observed m/z	Δ (ppm)	Ionization form	Analysis method
1	Hydroquinone	$C_6H_6O_2$	109.0289	109.0284	4.58	$[M-H]^-$	HPLC&LC/MS
2	Benzoquinone	$C_6H_4O_2$	107.0138	107.0133	4.67	$[M-H]^-$	HPLC&LC/MS
3	4-Chlorocatechol	$C_6H_5ClO_2$	142.9905	142.9899	4.19	$[M-H]^-$	HPLC&LC/MS
4	Hydroxybenzoquinone	$C_6H_4O_3$	123.0087	123.0082	4.06	$[M-H]^-$	LC/MS
5	Maleic acid	$C_4H_4O_4$	115.0031	115.0034	-2.61	$[M-H]^-$	LC/MS
6	Fumaric acid	$C_4H_4O_4$	115.0031	115.0034	-2.61	$[M-H]^-$	LC/MS
7	4-Chloro-5-hydroxy-1,2,-benzoquinone	$C_6H_3ClO_3$	156.9697	156.9692	3.19	$[M-H]^-$	LC/MS
8	4-Hydroxyphenylbenzoquinone	$C_{12}H_8O_3$	199.0411	199.0400	5.52	$[M-H]^-$	LC/MS
9	5-Chloro-2,4-dihydroxybiphenyl	$C_{12}H_9ClO_2$	219.0207	219.0199	3.65	$[M-H]^-$	LC/MS

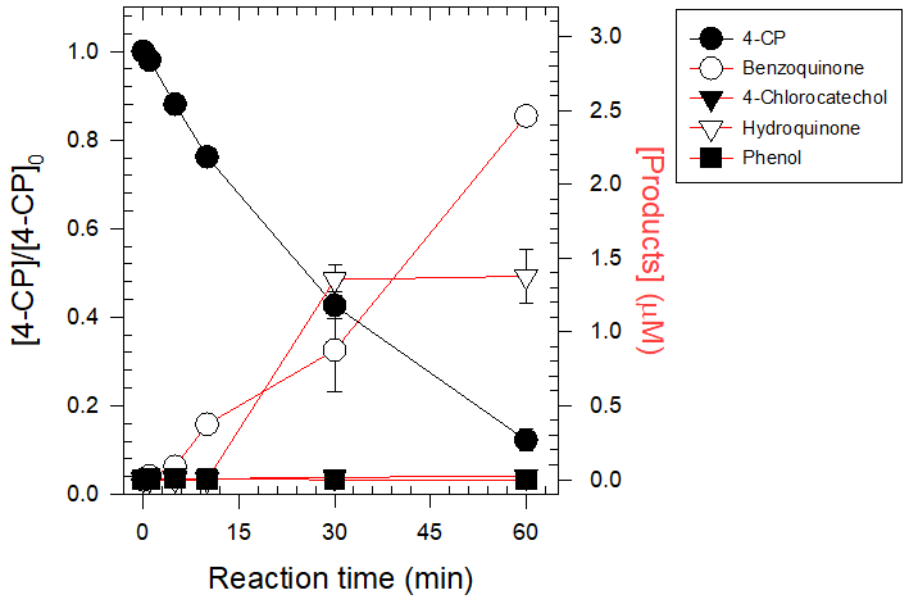

Figure 4.16. Formation of oxidation products during 4-CP degradation by the NiOC/PDS system analysed by HPLC ($[NiOC]_0$ = 0.2 g/L, $[4\text{-CP}]_0$ = 0.1 mM, $[PDS]_0$ = 0.2 mM, $[PBS]_0$ = 1 mM, pH = 7.0).

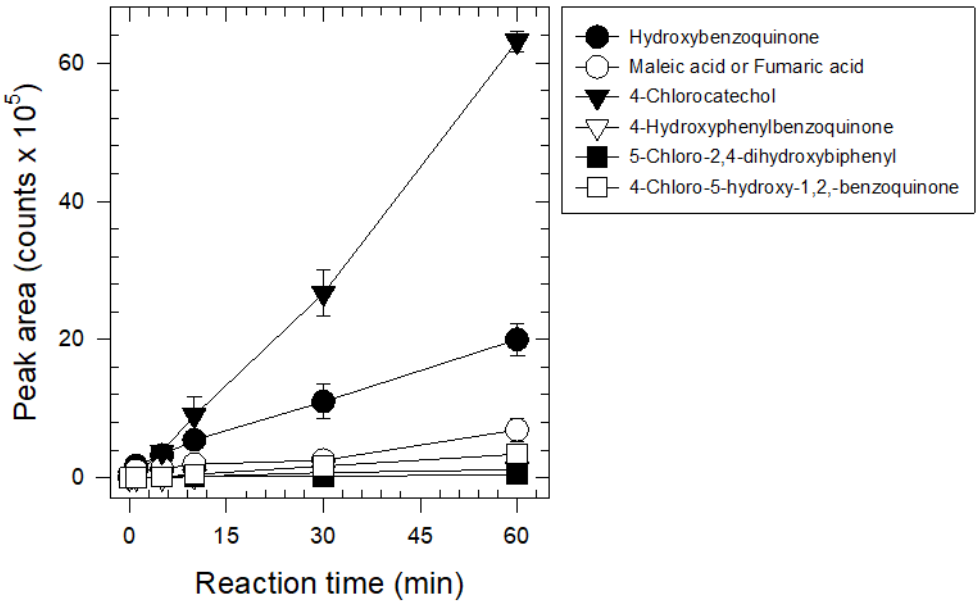

Figure 4.17. Formation of oxidation products during 4-CP degradation by the NiOC/PDS system analysed by LC/MS ($[NiOC]_0$ = 0.2 g/L, $[4\text{-CP}]_0$ = 0.1 mM, $[PDS]_0$ = 0.2 mM, $[PBS]_0$ = 1 mM, pH = 7.0).

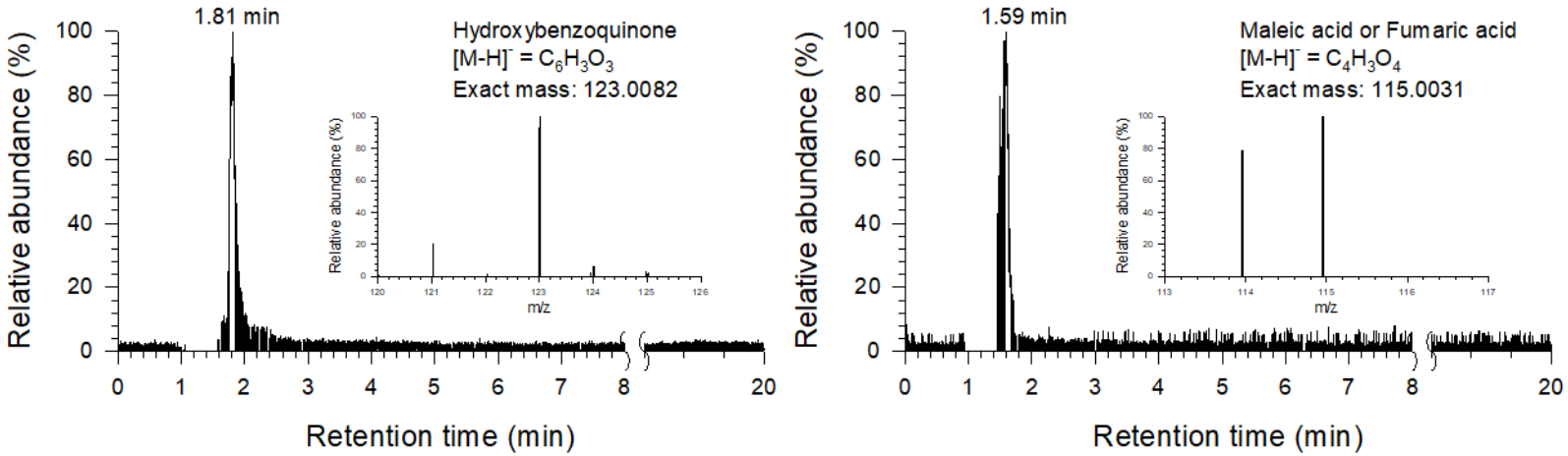

Figure 4.18a. Formation of oxidation products during 4-CP degradation by the NiOC/PDS system: chromatograms of oxidation products at 60 min with mass spectra ($[NiOC]_0$ = 0.2 g/L, $[4\text{-CP}]_0$ = 0.1 mM, $[PDS]_0$ = 0.2 mM, $[PBS]_0$ = 1 mM, pH = 7.0).

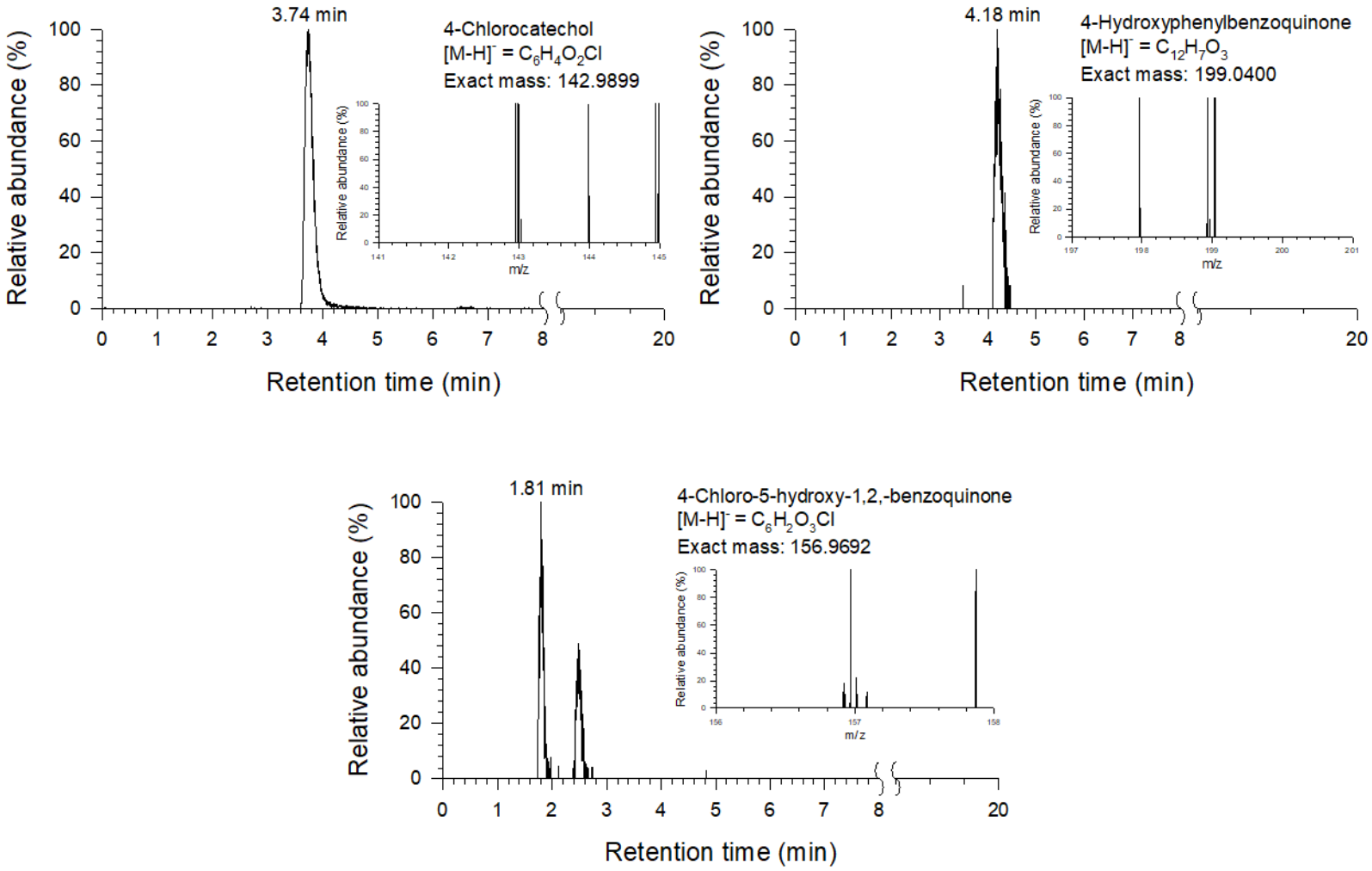

Figure 4.18b. Formation of oxidation products during 4-CP degradation by the NiOC/PDS system: chromatograms of oxidation products at 60 min with mass spectra ($[NiOC]_0$ = 0.2 g/L, $[4\text{-CP}]_0$ = 0.1 mM, $[PDS]_0$ = 0.2 mM, $[PBS]_0$ = 1 mM, pH = 7.0).

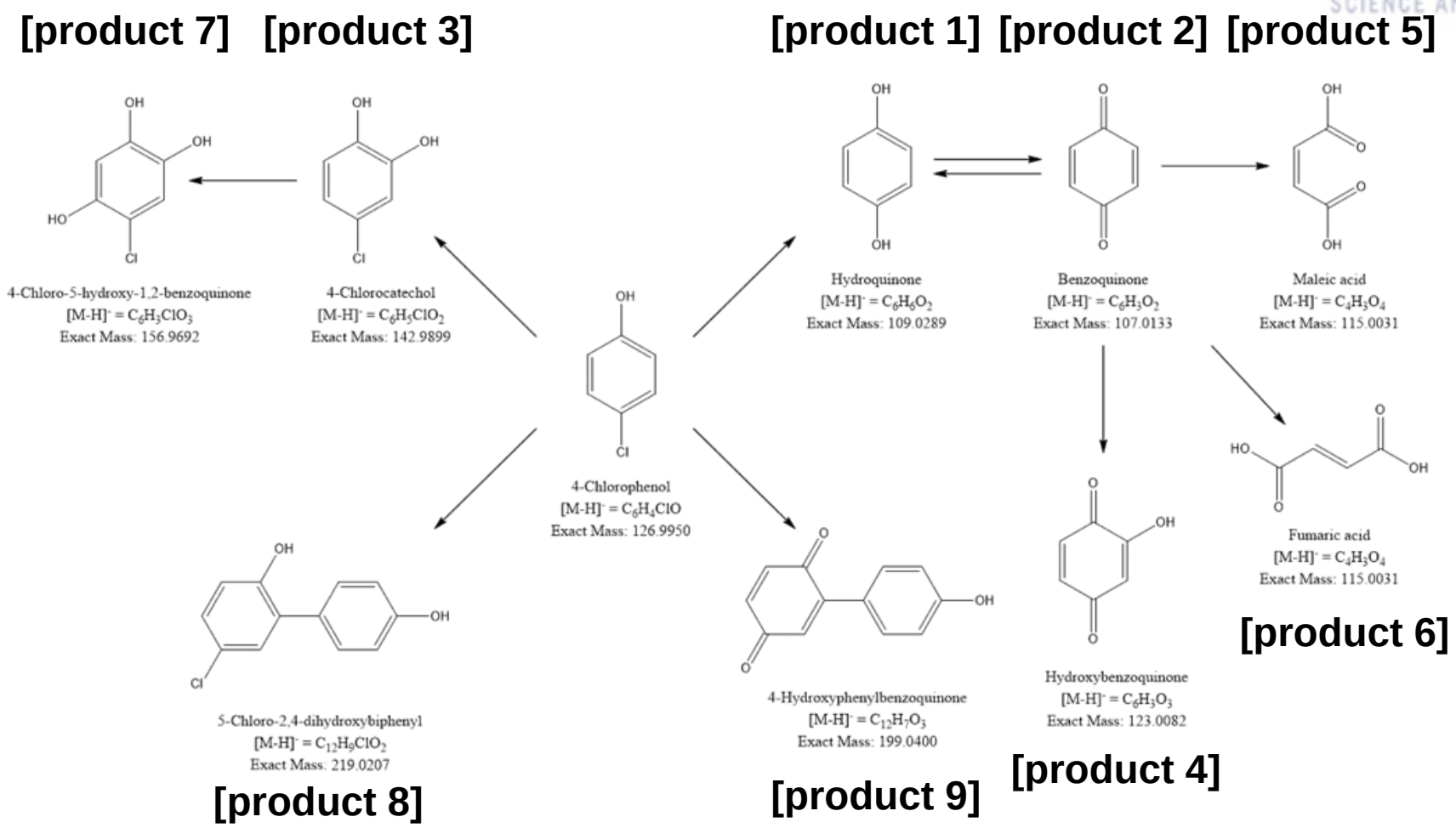

Figure 4.19. Pathways depicting oxidative degradation of 4-CP by the NiOC/PDS system.

4.3. Discussion

4.3.1. Effects of crystallinity and size

It has been found that both crystallinity and size of the catalyst were important factors on the accelerating degradation rate of 4-CP (Figures 4.10 and 4.11). Magnetic properties and crystallinities of the NiOCs were drastically multiplied simultaneously as elevating sintering temperature (Figures 4.1b and 4.2). However, refers to section 3.3, the degradation efficacies of the NiOCs coupled with PDS were shown maximized catalytic performance at 500 °C sintered powder. The NiOC(700°C), which was composed of NiC only, hardly activates PDS for the 4-CP degradation although it appears strongest magnetic performance (Figure 4.10). In conclusion, those indicate the NiO and NiC, which were constituents of the NiOC, exhibited different properties. The NiO has a role of catalyst on the degradation of organic compounds, and the NiC shows magnetic performance in the NiOC.

In order to evaluate the aforementioned catalytic property of the NiOC, the degradation efficacy of the PDS activated by the NiOC was compared to those of commercial NiOs coupled with PDS (Figure 4.11). Also, refers to section 3.3, the degradation efficacies of the NiOC suspension combined with PDS appeared superior catalytic performance compared with other commercial NiOs. Although the micro NiO (~ 325 meshed) exhibited sharpen and well-crystallized peaks in the recorded XRD pattern, the surface area in order to activate PDS was extremely low compared to the nano NiO or the NiOC. On the contrary, a quite acceptable degradation capability was elicited from PDS activated by the nano NiO, but not fully reached to the maximized performance because of relatively poor crystallinity compared to the NiOC. In summarize, it might be maximized acceleration of the degradation rate when PDS activated with precisely size-controlled and well-crystallized NiO-based catalyst.

4.3.2. Possible reactions in the NiOC/PDS system

Possible reactions in the combination of NiOC and PDS can be proposed in both radical and nonradical mechanisms via reactions 4.1–4.3, 4.4–4.5 or 4.6–4.7. When Ni(II) atoms on the NiOC surface oxidized by persulfates, an electron transfers to the persulfates, generating an $SO_4^{\bullet-}$ (or $^{\bullet}OH$; further reacted with H_2O) (reaction 4.1). In contrast, when Ni(III) atoms on the NiOC surface reduced by persulfates, an electron transfers to the Ni(III) atoms, generating an $S_2O_8^{\bullet-}$ (or $SO_5^{\bullet-}$) (reaction 4.2). Generated radical species can oxidize organic compounds, further react the series of oxidation to be mineralized finally. Both reaction 4.1 and 4.2 catalytically proceed with surface Ni atoms through radical mechanism:

$$\equiv Ni^{II} + S_2O_8^{2-} \text{ (or } HSO_5^-) \rightarrow \equiv Ni^{III} + SO_4^{\bullet-} + SO_4^{2-} \text{ (or } SO_4^{\bullet-} + OH^-) \quad (4.1)$$

$$\equiv Ni^{III} + S_2O_8^{2-} \text{ (or } HSO_5^-) \rightarrow \equiv Ni^{II} + S_2O_8^{\bullet-} \text{ (or } SO_5^{\bullet-} + H^+) \quad (4.2)$$

$$\text{Organic compounds} + SO_4^{\bullet-} \text{ (or } {}^{\bullet}OH) \rightarrow P_{oxi} \text{ (oxidized products)} + SO_4^{2-} \text{ (or } OH^-) \quad (4.3)$$

Alternatively, the NiOC/PDS system has possibility to generate nickel-persulfate intermediates on

the surface of NiOC to be analogous on reactive complexes of carbonaceous materials (reaction 4.4) [58, 62, 63, 96]. Subsequently, electrons were abstracted from the organic compounds to the surface the nickel-persulfate intermediates, lastly, the intermediates decompose to the pristine NiOC and molecular ions (reaction 4.5). Overall reactions are described as follows through nonradical mechanism:

$$\equiv Ni^{II} + S_2O_8^{2-} \text{ (or } HSO_5^-) \rightarrow \equiv Ni^{II}\cdots S_2O_8^{2-} \text{ (or } \equiv Ni^{II}\cdots HSO_5^-) \text{ (reactive complexes)} \quad (4.4)$$

$$\text{Organic compounds} + \equiv Ni^{II}\cdots S_2O_8^{2-} \text{ (or } \equiv Ni^{II}\cdots HSO_5^-) \rightarrow P_{oxi} + \equiv Ni^{II} + 2SO_4^{2-} \text{ (or } SO_4^{2-} + OH^-) \quad (4.5)$$

On the other hands, there is another possible explanation for the NiOC/PDS system to generate high-valent nickel species (likely Ni^{IV}) on the surface of NiOC via 2 electron-transfer reactions, firstly, which was similarly proposed reactive species from previous studies (reaction 4.6) [97, 98, 99]. And also, the organic compounds can be degraded by generated high-valent nickel species, secondly (reaction 4.7). Catalytic generation of high-valent nickel species can be described by following reactions through nonradical mechanism:

$$\equiv Ni^{II} + S_2O_8^{2-} \text{ (or } HSO_5^-) \rightarrow \equiv Ni^{IV} + 2SO_4^{2-} \text{ (or } SO_4^{2-} + OH^-) \quad (4.6)$$

$$\text{Organic compounds} + \equiv Ni^{IV} \rightarrow P_{oxi} + \equiv Ni^{II} \quad (4.7)$$

4.3.3. A proposed mechanism of organic compound degradation by the NiOC/PDS system

Among the aforementioned mechanisms, the generated high-valent nickel species (likely Ni(IV)) on the NiOC surface are suggested to be responsible for the oxidative degradation of organic compounds (Scheme 4.1). For elucidating this suggestion, different experimental approaches (i.e., LSV, radical scavenger, EPR, and XANES analysis) were carried out (Figures 4.12, 4.13, 4.14, and 4.15, respectively). Refers to section 4.2.4 and 4.2.5, the nonradical mechanisms (reaction 4.4–4.5 or 4.6–4.7) are well-corresponded to be evidenced by the aforementioned results, but hard to be explained with acts of the radical mechanism. If the system acts like radical mechanism, should have characteristics that decompose PDS by the NiOC without organic compounds, be inhibited by methanol and be detected radical adducts in EPR analysis [18, 19, 20].

Importantly, the only explanation in order to distinguish the generation of reactive intermediates or high-valent nickel species is possible by results from 4-CP degradation by the PDS-treated NiOC and XANES analysis (Figure 4.15). The PDS-treated NiOC exhibited certain degradation capacity when injected alone in the 4-CP solution, and also the pre-treated NiOC appeared to higher oxidation state in the XANES spectra compared to that of the pristine NiOC (refers to section 4.2.6). Those results were evidences for the generation of high-valent nickel species, which are the nature of dominant oxidants in the NiOC/PDS system. If the NiOC in combination with PDS just forms reactive complexes as an oxidant, XANES spectra would not be shifted because of same oxidation

state in the NiOC and complexes.

Lastly, in order to further investigate the nature of oxidant, LC/MS analysis was conducted about the oxidized products of 4-CP depicted in Figure 4.19. Most detected products can be explained by electron abstraction or hydroxylation of the 4-CP [91]. High-valent nickel-(hydr)oxo complexes (e.g., $[\equiv Ni^{IV}=O]^{2+}$ and $[\equiv Ni^{IV}–(OH)_2]^{2+}$) are considered as possible species formed on the NiOC surface oxidized by PDS, which may be interconvertible by (de)hydration in the equilibrium analogous to the act of ferryl species (reaction 4.8) [78, 79]. Those oxidants are believed to exhibit similar property to surface-bound •OH, and also appear oxidizing capacity for specific organic compounds (e.g., 4-CP) via an electron abstraction or hydroxylation mechanism [100].

$$[\equiv Ni^{IV}=O]^{2+} + H_2O \quad \leftrightarrow \quad [\equiv Ni^{IV}–(OH)_2]^{2+} \qquad (4.8)$$

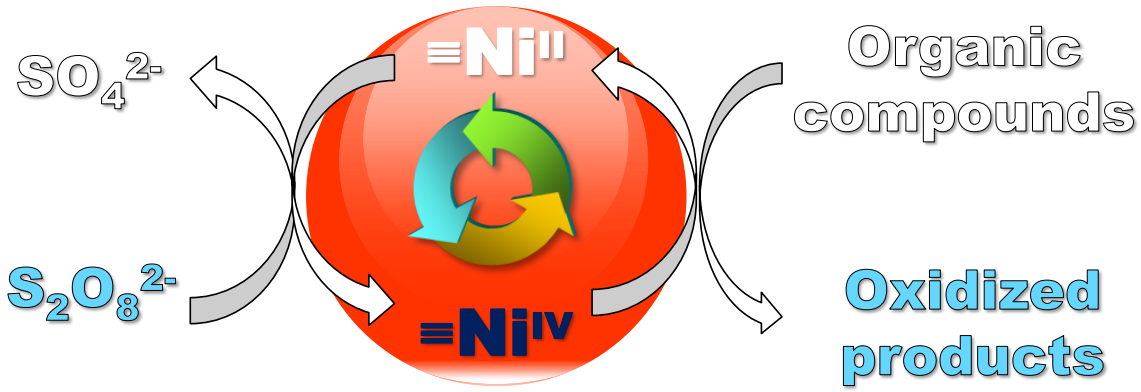

Scheme 4.1. Generated high-valent nickel species on the NiOC surface for oxidative degradation of organic compounds by catalytic decomposition of PDS.

Chapter 5. Conclusions

In this dissertation, several Fenton(-like) systems which produce high-valent metal species (i.e., Fe(IV), Cu(III), and Ni(IV)) were proposed for degrading recalcitrant organic contaminants. Further, oxidizing capabilities of reactive species were assessed and also the nature of oxidants was elucidated. Major conclusions of respective chapters are summarized as follows.

1. In the chapter 2, The nZVI/TPP/O_2 and Fe(II)/TPP/O_2 systems had similar levels of oxidant yields and degradation efficacies with organic compounds, indicating that nZVI mainly plays a role as a Fe(II)-releasing agent. The high oxidant yield from the Fe(II)/TPP/O_2 system (Δ[HCHO]/Δ[Fe(II)] = 70%) could not be explained by the known chemistry for Fe(II) oxidation by oxygen (i.e., a series of one-electron transfer reactions), suggesting that a more direct pathway to produce reactive oxidants may exist (e.g., two-electron oxidation of Fe(II) into Fe(IV) by oxygen). Both $^{\bullet}$OH and Fe(IV) are believed to be produced by the Fe(II)/TPP/O_2 system, but the low yields of hydroxylated products compared to other ligand-enhanced Fe(II)/O_2 systems suggests that the production of Fe(IV) is more important. The pH-dependence of CBZ and RB5 degradation appears to be attributed to the speciation of Fe(IV)-TPP complexes with different reactivities. The Fe(II)/TPP/O_2 system can be applied to the treatment of refractory organic contaminants in water and wastewater. For the ISCO application, there is no advantage to using nZVI instead of Fe(II). However, a sequential reduction-oxidation treatment for groundwater containing multiple organic pollutants can be a potential application of nZVI together with TPP.

2. In the chapter 3, The Cu(II)/HCO_3^-/H_2O_2 system was shown to effectively degrade phenolic compounds, better than the Cu(II)/H_2O_2 system. Cu(II)-carbonate complexes formed in the presence of HCO_3^- appear to have higher catalytic activity for decomposing H_2O_2 into reactive oxidants. Cu(III) species (likely complexed forms with carbonate) may be the major reactive oxidants responsible for the phenol degradation. Several parameters, such as pH and doses of Cu(II), HCO_3^-, and H_2O_2, influenced the rate of phenol degradation by affecting the generation and consumption of reactive oxidants as well as their speciation. The Cu(II)/HCO_3^-/H_2O_2 system can be used to treat water and wastewater after addressing such issues as the immobilization and long-term stability of the catalyst, environmental impacts of released copper ions, and economic feasibility.

3. In the chapter 4, a novel persulfate activator (NiOC) working at the neutral pH region was synthesized by a ligand-assisted method using nickel precursor and citrate as a chelating agent. The NiOC was found to spherical nanocomposite of nickel oxide and nickel carbide,

which possesses both catalytic and magnetic properties allowed magnetically recoverable for reuse. The certain sintering temperature (500°C) on the NiOC synthesis was exhibited to be maximized catalytic performance such as degradation rate of 4-CP and PDS utilization efficiency, simultaneously. The NiOC coupled with PDS exhibited superior but relatively selective activity for degrading specific organic compounds. Although the spectrum of degradable target contaminants may be limited by such reaction selectivity, it can minimize unexpected consumption of oxidant reacted with natural background substances, which can be evidenced to effectively degrading 4-CP in select natural water samples. Notably, the activation of persulfates was elucidated by a nonradical mechanism via the catalytic 2-electron transfer reaction on the NiOC surface. Generated reactive species on the NiOC surface (i.e., $\equiv Ni^{IV}$) may be responsible for the nature of oxidant on the degradation of select organic compounds. These high-valent nickel species are assumed to be capable of oxidizing 4-CP via a series of electron abstraction and hydroxylation reactions.

References

[1] S.K. Khetan, T.J. Collins, Human pharmaceuticals in the aquatic environment: A challenge to green chemistry, Chem. Rev., 107 (2007) 2319-2364.

[2] T. Shioiri, K. Izawa, T. Konoike, *Pharmaceutical process chemistry*, Wiley-VCH, Weinheim, Germany, (2011).

[3] T. Heberer, Occurrence, fate, and removal of pharmaceutical residues in the aquatic environment: a review of recent research data, Toxicol. Lett., 131 (2002) 5-17.

[4] D.W. Kolpin, E.T. Furlong, M.T. Meyer, E.M. Thurman, S.D. Zaugg, L.B. Barber, H.T. Buxton, Pharmaceuticals, hormones, and other organic wastewater contaminants in US streams, 1999-2000: A national reconnaissance, Environ. Sci. Technol., 36 (2002) 1202-1211.

[5] The Ministry of environment, Annual report, *'2017 Occurrence and treatment of industrial wastewater in Korea'*, Republic of Korea, (2017) 11-1480000-001452-10.

[6] The Ministry of environment, Water quality protection law: Article 34, *'Emission criteria of water pollution substances'*, Republic of Korea, (2018).

[7] J.J. Pignatello, E. Oliveros, A. MacKay, Advanced oxidation processes for organic contaminant destruction based on the Fenton reaction and related chemistry, Crit. Rev. Environ. Sci. Technol., 36 (2006) 1-84.

[8] A.J. Bard, R. Parsons, J. Jordan, *Standard Potentials in Aqueous Solution*, 1st ed., M. Dekker, New York, (1985).

[9] M.A. Oturan, J.J. Aaron, Advanced oxidation processes in water/wastewater treatment: Principles and applications. A review, Crit. Rev. Environ. Sci. Technol., 44 (2014) 2577-2641.

[10] C. Walling, A. Goosen, Mechanism of ferric ion catalyzed decomposition of hydrogen peroxide. Effect of organic substrates, J. Am. Chem. Soc., 95 (1973) 2987-2991.

[11] C.R. Keenan, D.L. Sedlak, Factors affecting the yield of oxidants from the reaction of manoparticulate zero-valent iron and oxygen, Environ. Sci. Technol., 42 (2008) 1262-1267.

[12] S.H. Joo, A.J. Feitz, T.D. Waite, Oxidative degradation of the carbothioate herbicide, molinate, using nanoscale zero-valent iron, Environ. Sci. Technol. 38 (2004), 2242-2247.

[13] A.J. Feitz, S.H. Joo, J. Guan, Q. Sun, D.L. Sedlak, T.D. Waite, Oxidative transformation of

contaminants using colloidal zero-valent iron, Colloids Surf., A 265 (2005), 88-94.

[14] S.H. Joo, A.J. Feitz, D.L. Sedlak, T.D. Waite, Quantification of the oxidizing capacity of nanoparticulate zero-valent iron, Environ. Sci. Technol. 39 (2005), 1263-1268.

[15] I.A. Katsoyiannis, T. Ruettimann, S.J. Hug, pH Dependence of Fenton reagent generation and As(III) oxidation and removal by corrosion of zero valent iron in aerated water, Environ. Sci. Technol. 42 (2008), 7424-7430.

[16] H. Lee, H.-J. Lee, H.-E. Kim, J. Kweon, B.-D. Lee, C. Lee, Oxidant production from corrosion of nano- and microparticulate zero-valent iron in the presence of oxygen: A comparative study, J. Hazard. Mater. 265 (2014), 201-207.

[17] A. Tsitonaki, B. Petri, M. Crimi, H. Mosbaek, R.L. Siegrist, P.L. Bjerg, In situ chemical oxidation of contaminated soil and groundwater using persulfate: A review, Crit. Rev. Environ. Sci. Technol, 40 (2010) 55-91.

[18] G.P. Anipsitakis, D.D. Dionysiou, Degradation of organic contaminants in water with sulfate radicals generated by the conjunction of peroxymonosulfate with cobalt, Environ. Sci. Technol., 37 (2003) 4790-4797.

[19] G.P. Anipsitakis, D.D. Dionysiou, Radical generation by the interaction of transition metals with common oxidants, Environ. Sci. Technol., 38 (2004) 3705-3712.

[20] G.P. Anipsitakis, D.D. Dionysiou, M.A. Gonzalez, Cobalt-mediated activation of peroxymonosulfate and sulfate radical attack on phenolic compounds. Implications of chloride ions, Environ. Sci. Technol., 40 (2006) 1000-1007.

[21] S. Wacławek, H.V. Lutze, K. Grubel, V.V.T. Padil, M. Cernik, D.D. Dionysiou, Chemistry of persulfates in water and wastewater treatment: A review, Chem. Eng. J., 330 (2017) 44-62.

[22] M. Spiro, Standard potential of the peroxosulfate-sulfate couple, Electrochim. Acta, 24 (1979) 313-314.

[23] P. Neta, R.E. Huie, A.B. Ross, Rate constants for reactions of inorganic radicals in aqueous-solution, J. Phys. Chem. Ref. Data, 17 (1988) 1027-1284.

[24] J. Du, J. Bao, Y. Liu, H. Ling, H. Zheng, S.H. Kim, D.D. Dionysiou, Efficient activation of peroxymonosulfate by magnetic Mn-MGO for degradation of bisphenol A, J. Hazard. Mater., 320 (2016) 150-159.

[25] Y.C. Lee, S.L. Lo, P.T. Chiueh, Y.H. Liou, M.L. Chen, Microwave-hydrothermal decomposition

of perfluorooctanoic acid in water by iron-activated persulfate oxidation, Water Res., 44 (2010) 886-892.

[26] J.M. Monteagudo, A. Duran, R. Gonzalez, A.J. Exposito, In situ chemical oxidation of carbamazepine solutions using persulfate simultaneously activated by heat energy, UV light, Fe^{2+} ions, and H_2O_2, Appl. Catal. B: Environ., 176 (2015) 120-129.

[27] S.Y. Yang, P. Wang, X. Yang, L. Shan, W.Y. Zhang, X.T. Shao, R. Niu, Degradation efficiencies of azo dye Acid Orange 7 by the interaction of heat, UV and anions with common oxidants: Persulfate, peroxymonosulfate and hydrogen peroxide, J. Hazard. Mater., 179 (2010) 552-558.

[28] Y.H. Guan, J. Ma, X.C. Li, J.Y. Fang, L.W. Chen, Influence of pH on the formation of sulfate and hydroxyl radicals in the UV/peroxymonosulfate system, Environ. Sci. Technol., 45 (2011) 9308-9314.

[29] O.S. Furman, A.L. Teel, R.J. Watts, Mechanism of base activation of persulfate, Environ. Sci. Technol., 44 (2010) 6423-6428.

[30] G. Fang, J. Gao, D.D. Dionysiou, C. Liu, D. Zhou, Activation of persulfate by quinones: Free radical reactions and implication for the degradation of PCBs, Environ. Sci. Technol., 47 (2013) 4605-4611.

[31] M. Ahmad, A.L. Teel, R.J. Watts, Mechanism of persulfate activation by phenols, Environ. Sci. Technol., 47 (2013) 5864-5871.

[32] C.S. Liu, K. Shih, C.X. Sun, F. Wang, Oxidative degradation of propachlor by ferrous and copper ion activated persulfate, Sci. Total Environ., 416 (2012) 507-512.

[33] W.H. Koppenol, J.F. Liebman, The oxidizing nature of the hydroxyl radical. A comparison with the ferryl ion (FeO^{2+}), J. Phys. Chem., 88 (1984) 99-101.

[34] H.A. Schwarz, R.W. Dodson, Equilibrium between hydroxyl radicals and thallium(II) and the oxidation potential of OH(aq), J. Phys. Chem., 88 (1984) 3643-3647.

[35] U.K. Klaning, K. Sehested, J. Holcman, Standard Gibbs energy of formation of the hydroxyl radical in aqueous solution. Rate constants for the reaction $ClO_2^- + O_3 \leftrightarrow O_3^- + ClO_2$, J. Phys. Chem., 89 (1985) 760-763.

[36] R.E. Huie, C.L. Clifton, P. Neta, Electron transfer reaction rates and equilibria of the carbonate and sulfate radical anions, Radiat. Phys. Chem., 38 (1991) 477-481.

[37] L. Eberson, Electron transfer reactions in organic chemistry, Adv. Phys. Org. Chem., 18 (1982) 79-185.

[38] R.E. Huie, P. Neta, Chemical behavior of SO_3^- and SO_5^- radicals in aqueous solutions, J. Phys. Chem., 88 (1984) 5665-5669.

[39] W.V. Steele, E.H. Appelman, The standard enthalpy of formation of peroxymonosulfate (HSO_5^-) and the standard electrode potential of the peroxymonosulfate-bisulfate couple, J. Chem. Thermodyn., 14 (1982) 337-344.

[40] H. Lee, H.J. Lee, D.L. Sedlak, C. Lee, pH-Dependent reactivity of oxidants formed by iron and copper-catalyzed decomposition of hydrogen peroxide, Chemosphere, 92 (2013) 652-658.

[41] S. Seibig, R. van Eldik, Kinetics of [Fe^{II}(EDTA)] oxidation by molecular oxygen revisited. New evidence for a multistep mechanism, Inorg. Chem. 36 (1997), 4115-4120.

[42] C.R. Keenan, D.L. Sedlak, Ligand-enhanced reactive oxidant generation by nanoparticulate zero-valent iron and oxygen, Environ. Sci. Technol. 42 (2008), 6936-6941.

[43] P. Belanzoni, L. Bernasconi, E.J. Baerends, O_2 Activation in a dinuclear Fe(II)/EDTA complex: Spin surface crossing as a route to highly reactive Fe(IV) oxo species, J. Phys. Chem. A 113 (2009), 11926-11937.

[44] C. Lee, C.R. Keenan, D.L. Sedlak, Polyoxometalate-enhanced oxidation of organic compounds by nanoparticulate zero-valent iron and ferrous ion in the presence of oxygen, Environ. Sci. Technol. 42 (2008), 4921-4926.

[45] J.H. Kyle, Kinetics of the base decomposition of dodecatungstophosphate(3-) in weakly alkaline solutions, J. Chem. Soc., Dalton Trans. 1 (1983), 2609-2612.

[46] A. Jürgensen, J.B. Moffat, The stability of 12-molybdosilicic, 12-tungstosilicic, 12-molybdophosphoric and 12-tungstophosphoric acids in aqueous solution at various pH, Catal. Lett. 34 (1995), 237-244.

[47] L. Wang, F. Wang, P.N. Li, L.Z. Zhang, Ferrous-tetrapolyphosphate complex induced dioxygen activation for toxic organic pollutants degradation, Sep. Purif. Technol. 120 (2013), 148-155.

[48] L. Wang, M.H. Cao, Z.H. Ai, L.Z. Zhang, Dramatically enhanced aerobic atrazine degradation with Fe@Fe_2O_3 core-shell nanowires by tetrapolyphosphate, Environ. Sci. Technol. 48 (2014), 3354-3362.

[49] H.-J. Lee, H. Lee, C. Lee, Degradation of diclofenac and carbamazepine by the copper(II)-

catalyzed dark and photo-assisted Fenton-like systems, Chem. Eng. J., 245 (2014) 258-264.

[50] H. Lee, H.-J. Lee, J. Seo, H.-E. Kim, Y.K. Shin, J.-H. Kim, C. Lee, Activation of oxygen and hydrogen peroxide by copper(II) coupled with hydroxylamine for oxidation of organic contaminants, Environ. Sci. Technol., 50 (2016) 8231-8238.

[51] T.T.M. Nguyen, H.-J. Park, J.Y. Kim, H.-E. Kim, H. Lee, J. Yoon, C. Lee, Microbial inactivation by cupric ion in combination with H_2O_2: Role of reactive oxidants, Environ. Sci. Technol., 47 (2013) 13661-13667.

[52] H.-E. Kim, T.T.M. Nguyen, H. Lee, C. Lee, Enhanced Inactivation of *Escherichia coli* and MS2 coliphage by cupric ion in the presence of hydroxylamine: Dual microbicidal effects, Environ. Sci. Technol., 49 (2015) 14416-14423.

[53] H.-J. Lee, H.-E. Kim, C. Lee, Combination of cupric ion with hydroxylamine and hydrogen peroxide for the control of bacterial biofilms on RO membranes, Water Res., 110 (2017) 83-90.

[54] L. Cheng, M. Wei, L. Huang, F. Pan, D. Xia, X. Li, A. Xu, Efficient H_2O_2 Oxidation of organic dyes catalyzed by simple copper(II) ions in bicarbonate aqueous solution, Ind. Eng. Chem. Res., 53 (2014) 3478-3485.

[55] J. Peng, H. Shi, J. Li, L. Wang, Z. Wang, S. Gao, Bicarbonate enhanced removal of triclosan by copper(II) catalyzed Fenton-like reaction in aqueous solution, Chem. Eng. J., 306 (2016) 484-491.

[56] T. Zhang, Y. Chen, Y.R. Wang, J. Le Roux, Y. Yang, J.P. Croue, Efficient peroxydisulfate activation process not relying on sulfate radical generation for water pollutant degradation, Environ. Sci. Technol., 48 (2014) 5868-5875.

[57] X. Duan, Z. Ao, H. Sun, L. Zhou, G. Wang, S. Wang, Insights into N-doping in single-walled carbon nanotubes for enhanced activation of superoxides: A mechanistic study, Chem. Commun., 51 (2015) 15249-15252.

[58] H. Lee, H.-J. Lee, J. Jeong, J. Lee, N.-B. Park, C. Lee, Activation of persulfates by carbon nanotubes: Oxidation of organic compounds by nonradical mechanism, Chem. Eng. J., 266 (2015) 28-33.

[59] H. Sun, Y. Wang, S. Liu, L. Ge, L. Wang, Z. Zhu, S. Wang, Facile synthesis of nitrogen doped reduced graphene oxide as a superior metal-free catalyst for oxidation, Chem Commun, 49 (2013) 9914-9916.

[60] X. Duan, H. Sun, J. Kang, Y. Wang, S. Indrawirawan, S. Wang, Insights into heterogeneous

catalysis of persulfate activation on dimensional-structured nanocarbons, ACS Catal., 5 (2015) 4629-4636.

[61] G. Fang, C. Liu, J. Gao, D.D. Dionysiou, D. Zhou, Manipulation of persistent free radicals in biochar to activate persulfate for contaminant degradation, Environ. Sci. Technol., 49 (2015) 5645-5653.

[62] H. Lee, H.-I. Kim, S. Weon, W. Choi, Y.-S. Hwang, J. Seo, C. Lee, J.-H. Kim, Activation of persulfates by graphitized nanodiamonds for removal of organic compounds, Environ. Sci. Technol., 50 (2016) 10134-10142.

[63] E.-T. Yun, G.-H. Moon, H. Lee, T.H. Jeon, C. Lee, W. Choi, J. Lee, Oxidation of organic pollutants by peroxymonosulfate activated with low-temperature-modified nanodiamonds: Understanding the reaction kinetics and mechanism, Appl. Catal. B: Environ., 237 (2018) 432-441.

[64] C. Lee, J.Y. Kim, W.I. Lee, K.L. Nelson, J. Yoon, D.L. Sedlak, Bactericidal effect of zero-valent iron nanoparticles on *Escherichia coli*, Environ. Sci. Technol. 42 (2008), 4927-4933.

[65] G. Louit, S. Foley, J. Cabillic, H. Coffigny, F. Taran, A. Valleix, J.P. Renault, S. Pin, The reaction of coumarin with the OH radical revisited: Hydroxylation product analysis determined by fluorescence and chromatography, Radiat. Phys. Chem. 72 (2005), 119-124.

[66] X.L. Zhou, K. Mopper, Determination of photochemically produced hydroxyl radicals in seawater and fresh-water, Mar. Chem. 30 (1990), 71-88.

[67] H. Tamura, K. Goto, T. Yotsuyanagi, M. Nagayama, Spectrophotometric determination of iron(II) with 1,10-phenanthroline in presence of large amounts of iron(III), Talanta 21 (1974), 314-318.

[68] S. Zecevic, D.M. Drazic, S. Gojkovic, Oxygen reduction on iron. Part III. An analysis of the rotating disk-ring electrode measurements in near neutral solutions, J. Electroanal. Chem. 265 (1989), 179-193.

[69] S. Zecevic, D.M. Drazic, S. Gojkovic, Oxygen reduction on iron. Part IV. The reduction of hydrogen peroxide as the intermediate in oxygen reduction reaction in alkaline solutions, Electrochim. Acta 36 (1991), 5-14.

[70] W. Stumm, G.F. Lee, Oxygenation of ferrous iron, Ind. Eng. Chem. 53 (1961), 143-146.

[71] F.J. Millero, M. Izaguirre, Effect of ionic strength and ionic interactions on the oxidation of Fe(II), J. Solution Chem. 18 (1989), 585-599.

[72] D.W. King, H.A. Lounsbury, F.J. Millero, Rates and mechanism of Fe(II) oxidation at nanomolar total iron concentrations, Environ. Sci. Technol. 29 (1995), 818-824.

[73] A.L.T. Pham, C. Lee, F.M. Doyle, D.L. Sedlak, A silica-supported iron oxide catalyst capable of activating hydrogen peroxide at neutral pH values, Environ. Sci. Technol. 43 (2009), 8930-8935.

[74] L. Bernasconi, E.J. Baerends, Generation of ferryl species through dioxygen activation in iron/EDTA systems: a computational study, Inorg. Chem. 48 (2009), 527-540.

[75] S.J. Hug, O. Leupin, Iron-catalyzed oxidation of arsenic(III) by oxygen and by hydrogen peroxide: pH-dependent formation of oxidants in the Fenton reaction, Environ. Sci. Technol. 37 (2003), 2734-2742.

[76] G.W. Klein, K. Bhatia, V. Madhavan, R.H. Schuler, Reaction of •OH with benzoic acid: Isomer distribution in radical intermediates, J. Phys. Chem. 79 (1975), 1767-1774.

[77] G.V. Buxton, C.L. Greenstock, W.P. Helman, A.B. Ross, Critical review of rate constants for reactions of hydrated electrons, hydrogen atoms and hydroxyl radicals (•OH/•O⁻) in aqueous solution, J. Phys. Chem. Ref. Data 17 (1988), 513-886.

[78] O. Pestovsky, A. Bakac, Reactivity of aqueous Fe(IV) in hydride and hydrogen atom transfer reactions, J. Am. Chem. Soc. 126 (2004), 13757-13764.

[79] O. Pestovsky, A. Bakac, Aqueous ferryl(IV) ion: Kinetics of oxygen atom transfer to substrates and oxo exchange with solvent water. Inorg. Chem. 45 (2006), 814-820.

[80] B.-C. Jeon, S.-Y. Nam, Y.-K. Kim, Treatment of pharmaceutical wastewaters by hydrogen peroxide and zerovalent iron, Environ. Eng. Res. 19 (2014), 9-14

[81] G.M. Eisenberg, Colorimetric determination of hydrogen peroxide, Ind. Eng. Chem. Anal. Ed, 15 (1943) 327-328.

[82] J.W. Moffett, R.G. Zika, Reaction kinetics of hydrogen peroxide with copper and iron in seawater, Environ. Sci. Technol., 21 (1987) 804-810.

[83] A.N. Pham, G.W. Xing, C.J. Miller, T.D. Waite, Fenton-like copper redox chemistry revisited: Hydrogen peroxide and superoxide mediation of copper-catalyzed oxidant production, J Catal, 301 (2013) 54-64.

[84] D.E. Richardson, H.R. Yao, K.M. Frank, D.A. Bennett, Equilibria, kinetics, and mechanism in the bicarbonate activation of hydrogen peroxide: Oxidation of sulfides by peroxymonocarbonate,

J. Am. Chem. Soc., 122 (2000) 1729-1739.

[85] A. Xu, X. Li, H. Xiong, G. Yin, Efficient degradation of organic pollutants in aqueous solution with bicarbonate-activated hydrogen peroxide, Chemosphere, 82 (2011) 1190-1195.

[86] A. Xu, X. Li, S. Ye, G. Yin, Q. Zeng, Catalyzed oxidative degradation of methylene blue by in situ generated cobalt (II)-bicarbonate complexes with hydrogen peroxide, Appl. Catal. B: Environ., 102 (2011) 37-43.

[87] X. Li, Z. Xiong, X. Ruan, D. Xia, Q. Zeng, A. Xu, Kinetics and mechanism of organic pollutants degradation with cobalt-bicarbonate-hydrogen peroxide system: Investigation of the role of substrates, Appl. Cat. A: General, 411 (2012) 24-30.

[88] The Ministry of Environment, *Drinking water quality standard and test*, Republic of Korea, (2014).

[89] U. S. Environmental Protection Agency. *National primary drinking water regulations*, United States, (2009).

[90] E.N. Baker, H.M. Baker, B.F. Anderson, R.D. Reeves, Chelation of nickel(II) by citrate. The crystal structure of a nickel-citrate complex, $K_2[Ni(C_6H_5O_7)(H_2O)_2]_2 \cdot 4H_2O$, Inorg. Chim. Acta, 78 (1983) 281-285.

[91] J. Seo, H. Lee, H.-J. Lee, M.S. Kim, S.W. Hong, J. Lee, K. Cho, W. Choi, C. Lee, Visible light-photosensitized oxidation of organic pollutants using amorphous peroxo-titania, Appl. Catal. B: Environ., 225 (2018) 487-495.

[92] M. Cho, H. Chung, W. Choi, J. Yoon, Different inactivation behaviors of MS-2 phage and *Escherichia coli* in TiO_2 photocatalytic disinfection, Appl. Environ. Microbiol., 71 (2005) 270-275.

[93] S.K. Padamati, D. Anielone, A. Draksharapu, G. Primi, D.J. Martin, M. Tromp, M. Swart, W.R. Browne, Transient formation and reactivity of a high-valent nickel(IV) oxido complex, J. Am. Chem. Soc., 139 (2017) 8718-8724.

[94] X. Li, J.W. Cubbage, T.A. Tetzlaff, W.S. Jenks, Photocatalytic degradation of 4-chlorophenol. 1. The hydroquinone pathway, J. Org. Chem., 64 (1999) 8509-8524.

[95] X. Li, J.W. Cubbage, W.S. Jenks, Photocatalytic degradation of 4-chlorophenol. 2. The 4-chlorocatechol pathway, J. Org. Chem., 64 (1999) 8525-8536.

[96] X. Du, Y. Zhang, F. Si, C. Yao, M. Du, I. Hussain, H. Kim, S. Huang, Z. Lin, W. Hayat,

Persulfate non-radical activation by nano-CuO for efficient removal of chlorinated organic compounds: Reduced graphene oxide-assisted and CuO (001) facet-dependent, Chem. Eng. J., 356 (2019) 178-189.

[97] Y. Feng, C. Liao, L. Kong, D. Wu, Y. Liu, P.H. Lee, K. Shih, Facile synthesis of highly reactive and stable Fe-doped g-C_3N_4 composites for peroxymonosulfate activation: A novel nonradical oxidation process, J. Hazard. Mater., 354 (2018) 63-71.

[98] H. Li, C. Shan, B. Pan, Fe(III)-Doped g-C_3N_4 mediated peroxymonosulfate activation for selective degradation of phenolic compounds via high-valent iron-oxo species, Environ. Sci. Technol., 52 (2018) 2197-2205.

[99] Z. Wang, J. Jiang, S. Pang, Y. Zhou, C. Guan, Y. Gao, J. Li, Y. Yang, W. Qu, C. Jiang, Is sulfate radical really generated from peroxydisulfate activated by iron(II) for environmental decontamination?, Environ. Sci. Technol., 52 (2018) 11276-11284.

[100] A.Y. Sychev, V.G. Isak, Iron compounds and the mechanisms of the homogeneous catalysis of the activation of O_2 and H_2O_2 and of the oxidation of organic substrates, Russ. Chem. Rev. 64 (1995) 1105-1129.